PHD THESIS

Analysis of the Haemodynamic and Biomechanical Properties of the Lumina in Aortic Dissections Using an Integrated Approach Focussing on the Complementary Value of In-silico, In-vitro and In-vivo Assessments

Paula Andrea RUDENICK

UNIVERSIDAD AUTÒNOMA DE BARCELONA
Departamento de Medicina
2014

Supervisors
Dr. Arturo EVANGELISTA MASIP
Dr. Bart Hendrik BIJNENS

Tutor
Dr. David GARCÍA-DORADO

Science seldom proceeds in the straightforward logical manner imagined by outsiders. Instead, its steps forward (and sometimes backward) are often very human events in which personalities and cultural traditions play major roles.

James D. Watson – "The Double Helix"

Acknowledgments

It seems like yesterday when I started my PhD programme...Yes, time passed too fast and the overall process was not as painful as many people used to claim, and so I would like to thank all the people that made this period so enjoyable and fruitful instead.

First of all, a very special thanks to my supervisors: Dr. Arturo Evangelista, Dr. Bart Bijnens and Dr. David García-Dorado, for the constant and patient support given, and most important, for challenging me all these years, making me think and improve, both personally and professionally. Thanks!

To the nice group of people from the Institut de Recerca Vall d'Hebron. My loved "Cardio constellation", who created a very friendly atmosphere and provided me the unique and wonderful opportunity of working in a multidisciplinary environment. I had a lot of fun and I am very grateful for knowing you all.

To the people from bioMMeda in Ghent and especially to Prof. Patrick Segers (one of my heroes :-)) for accepting me as an additional member of his group for 6 months. It was a very productive and enriching stay and it was a pleasure to do part of my PhD there.

Also to people from UPF that helped and supported me a lot during these last 2 months of my thesis.

To my great group of friends all over the world that, even when they are so far away in some cases, are very close to me at the same time: Agus, Babi, Barbara, Beto, Cuchi, Ele, Estefo, Hrvy, Ile, Juana, Kita, Kaushik, Majo, Matías, Ross, Sergiete.

Y finalmente, muchísimas gracias a mi hermosa y amada familia: mis padres Angélica y Federico, mis hermanos Leopoldo y Emiliano y mi abuela Betty. Gracias por todas las oportunidades dadas y en apostar siempre por mi, ya que sin vuestro apoyo y amor nada de esto sería posible. Además, gracias por escucharme siempre durante la elaboración de esta tesis y por todas las buenas intenciones en ayudarme siempre que era posible, convirtiéndose también en expertos en disecciones aórticas. Los quiero muchísimo!!!!!!!!!

Barcelona, March 2014

Contents

List of Figures

List of Tables

Nomenclature

AbAo	Abdominal Aorta
AD	Aortic dissection
C	Capacitor
CAD	Computer-aided design
CFD	Computational Fluid Dynamics
$C_{\text{proximal size, distal size}}$	Dissection configuration with proximal tear of *proximal size* and distal tear of *distal size*
CT	Computed Tomography
DP	Diastolic pressure
DT	Distal tear
E	Young's modulus
FL	False lumen
$FPI_{\text{diastolic}}\%$	FL diastolic pressure index
$FPI_{\text{mean}}\%$	FL mean pressure index
$FPI_{\text{systolic}}\%$	FL systolic pressure index
FSI	Fluid Structure Interaction
L	Inductance
MRI	Magnetic Resonance Imaging
PH	Peripheral
PP	Pulse pressure
PT	Proximal tear
PVC	Polyvinyl chloride
Q	Flow
R	Resistance
RDF	Retrograde diastolic flow
ROI	Region of interest
rRMSE	Relative root square mean error
RSF	Retrograde systolic flow
RTV	Room-temperature vulcanising silicone elastomer
SD	Standard deviation
SP	Systolic pressure
TBAD	Type B aortic dissection
TEE	Transoesophageal echocardiography
ThAo	Thoracic Aorta
TL	True lumen
TTE	Transthoracic echocardiography
TVF	Total volume flow
V_{in}	Incoming volume
V_{out}	Outgoing volume

WSS	Wall shear stress
Zin	Input impedance
μ	Dynamic viscosity
σ	Density

Abstract

The follow-up and management of chronic type B aortic dissections continue being highly challenging in clinical practice. In the acute phase, an acute type B aortic dissection is in general less lethal than a type A dissection and medically treated. However, a type A dissection usually converts into a type B dissection in more than 70% of cases after overcoming its acute phase and patients with type B aortic dissection have high mortality during the chronic phase (30-50% at 5 years), mainly due to the progressive dilatation of the aorta, potentially resulting in aortic rupture.

Currently, image-based and clinical assessment and follow-up (mainly quantifying changes in diameters) have serious limitations for optimal management, adding to the fact that individual patients show considerable difference in the disease evolution and thus prognosis. Additionally, open surgery or endovascular treatment has shown to be not optimal in each individual due to the additional interventional risks. Therefore, in spite of important advances in image-based diagnosis of this disease, it remains difficult to perform individual risk stratification, balancing medical and surgical strategies to optimise the outcome in a given patient. Consequently, it is crucial to quantify the markers that will determine progressive aortic dilatation and further rupture, thus identifying patients that pose low risks on medical treatment and recognise individuals that will benefit from an intervention despite the risks associated with the procedure.

This thesis builds upon the hypothesis that progressive aortic dilatation in patients with chronic aortic dissections is determined by anatomic-geometrical configurations, such as interluminal communication and incidence of side branches in the false lumen; biomechanical factors, such as wall compliance; and mechanical stimuli, such as intraluminal pressures and flows.

Hence, the main contribution of this thesis is the proposal of an integrated approach to understand aortic dilatation and the associated complex flow phenomena in the setting of chronic aortic dissections, focussing on the complementary information and knowledge that can be obtained by combining in-vitro, in-silico and in-vivo data.

These different approaches are used to:

1) Gain insight into the relationship between the potential geometrical (tear size, number and location and incidence of visceral side branches originating from the false lumen) and biomechanical (wall compliance) parameters of severe aortic enlargement and the induced intraluminal flows and pressures.

2) Characterize intraluminal haemodynamic in aortic dissections.

3) Better understand the mechanisms underlying haemodynamic phenomena in aortic dissections.

Resumen

El seguimiento y el manejo de disecciones aórticas de tipo B siguen siendo un gran reto en la práctica clínica. En la fase aguda, la disección aórtica de tipo B es en general menos letal que la disección de tipo A y es tratada médicamente. Sin embargo, una disección de tipo A generalmente persiste en una de tipo B en más del 70% de los casos después de superar la fase aguda y los pacientes con disección aórtica de tipo B tienen una alta mortalidad durante la fase crónica (30-50% a los 5 años), principalmente debido a la dilatación progresiva de la aorta y subsecuente ruptura aórtica.

Actualmente, la evaluación y el seguimiento clínicos por imagen (sobre todo basados en la cuantificación de los cambios del diámetro aórtico) presentan serias limitaciones para un manejo óptimo, sumado al hecho de que cada paciente muestra diferencias considerables en la evolución de la enfermedad y por lo tanto, en el pronóstico. Además, la cirugía abierta o endovascular han demostrado no ser óptimas en todos los pacientes, debido a los riesgos adicionales de intervención. Por lo tanto, a pesar de los importantes avances en el diagnóstico por imagen, aún sigue siendo difícil de realizar la estratificación individual de riesgo, encontrando un balance entre el tratamiento médico y quirúrgico para optimizar los resultados en un paciente específico. Por lo tanto, es crucial la cuantificación de marcadores que determinarán la dilatación aórtica progresiva y posterior ruptura, identificando así los pacientes que presentan un bajo riesgo para ser tratados médicamente y reconocer a aquellos que se beneficiarán de una intervención quirúrgica a pesar de los riesgos asociados con el procedimiento.

La realización de esta tesis se basa en la hipótesis de que la dilatación aórtica progresiva, en pacientes con disecciones aórticas crónicas, está determinada por factores anatómicos, tales como la comunicación interluminal y la incidencia de ramas laterales en la luz falsa; factores biomecánicos, como la elasticidad de la pared aórtica; y estímulos mecánicos, tales como las presiones y los flujos intraluminales.

Por lo tanto, la contribución principal de esta tesis es la propuesta de un enfoque integrado para comprender, en el ámbito de las disecciones aórticas crónicas, la dilatación aórtica y los fenómenos complejos de flujo, centrándose en la información y el conocimiento complementarios que es posible obtener mediante la combinación de enfoques in-vivo, in-vitro e in-silico.

Los diferentes enfoques son utilizados para:

1) Determinar la relación existente entre los parámetros geométricos (tamaño, número y localización de las puertas de comunicación e incidencia de ramas laterales comunicantes con la luz falsa) y biomédicos (elasticidad de la pared) potencialmente relacionados con la dilatación aórtica severa y la determinación de flujos y presiones intraluminales resultantes;

2) Caracterizar la hemodinámica intraluminal en disecciones aórticas;

3) Comprender los mecanismos subyacentes en el fenómeno hemodinámico en disecciones aórticas.

CHAPTER 1

Introduction

1.1 Motivation

Cardiovascular pathologies are one of the major causes of death worldwide (Sans et al. 1997) and aortic diseases, in particular aortic dissections, contribute to this overall mortality. Aortic dissection, in contrast with other diseases, is not very symptomatic but it is linked with a very high morbidity and mortality. The most common cause of death in long-term patients of aortic dissections is the aortic rupture as a consequence of uncontrolled aortic aneurismal growth.

From the experience of our group, patients with aortic dissection can show considerable difference in the disease evolution and thus prognosis. Despite the important advances in the image-based diagnosis of aortic dissections, it remains difficult to perform risk stratification in these patients and initiate a more aggressive therapeutic strategy to those in greater risk. Currently, there is poor knowledge about the clinical morphological, haemodynamic and biomechanical variables, derived from imaging techniques that influence on progressive aortic enlargement and eventual rupture and could predict the need for endovascular or open repair treatment because of re-dissection or aortic aneurismal growth.

In daily clinical practice, aortic dissection is primarily managed based on maximum aortic diameter measured by computed tomography (CT), transthoracic (TTE) or transoesophageal (TEE) echocardiography or, by magnetic resonance imaging (MRI). These individual measurements are reported, compared to guidelines and integrated in the mind of the cardiologist to decide for the best therapeutic approach. However, this ad-hoc approach has important limitations. The individual geometrical measurements do not provide a full description of the whole aortic morphology and are operator dependent; the relation between single geometry measurements and clinical risk is not straightforward; several potentially relevant parameters analysing biophysical properties of the aorta, such as wall stiffness, wall stress and abnormal flow dynamics, are not taken into account; follow-up measurements in patients with evolving aortic dissections are difficult to standardise and the quantification of their evolution is not straightforward.

Thus, a combined morphologic, biomechanical and hemodynamic assessment in chronic aortic dissections will improve the prediction for aortic enlargement and rupture and hence, the therapeutic management of patients.

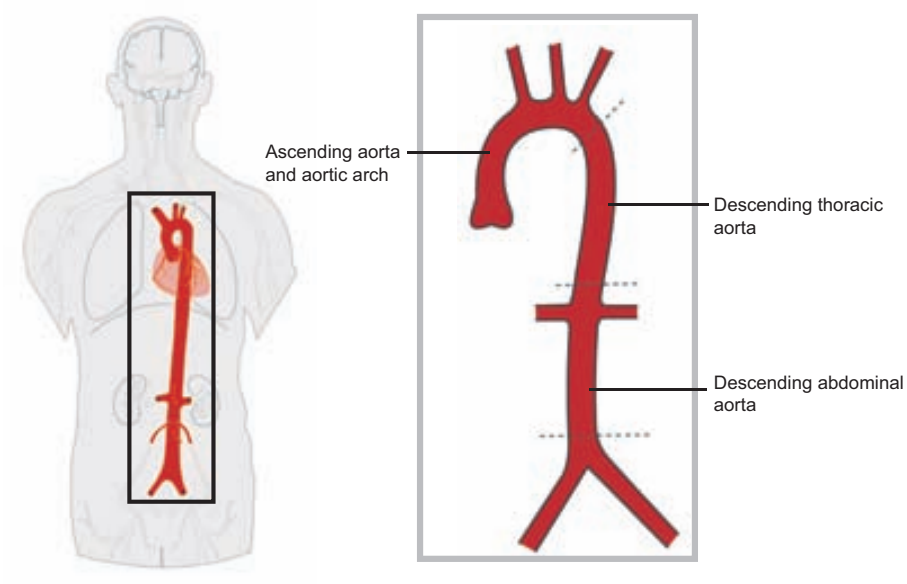

Figure 1.1: The aorta extends from the left ventricle of the heart down the abdomen. The aorta is divided into 3 main sections: the ascending aorta and the aortic arch, the descending thoracic aorta and the descending abdominal aorta, depending on their location and geometrical and compositional characteristics. Adapted from (Wikipedia website) and (Westerhof et al. 2010).

1.2 Anatomy and Physiology of the Aorta

The aorta is the largest artery in the body (Fig. 1.1). It is often described as the fifth chamber of the heart due to its very relevant cardiovascular function of distributing blood from the left ventricle of the heart to the rest of the body through the systemic circulation while buffering/dampening the pulsatile cardiac output to reduce the pressure load on the vascular tree.

Three major sections identify the aorta: the ascending aorta and aortic arch, the descending thoracic aorta and the descending abdominal aorta. The ascending aorta and the aortic arch rise up from the heart and curves over it; the descending thoracic aorta travels down from the end of the left subclavian artery up to the diaphragm; and the descending abdominal artery begins at the diaphragm and at the end splits to become the paired iliac arteries in the lower abdomen.

The aortic wall is composed by three layers (from inside to outside): the intima, media and adventitia. These layers are made up of connective tissue and elastic fibres, which allow the aorta to adapt in response to pressure changes resultant from blood flow and accomplish its buffering function. Therefore, an abnormal aortic wall may lead to aneurismal growth and dissection of the aorta.

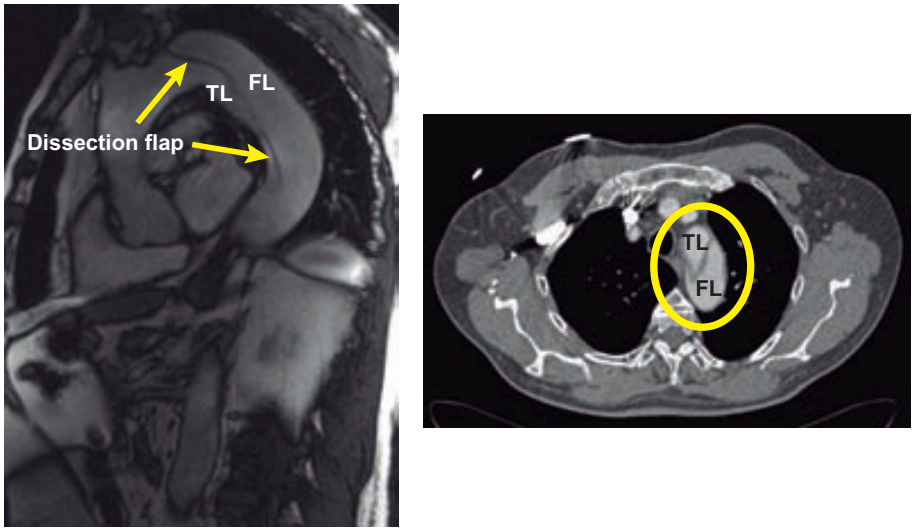

Figure 1.2: Clinical appearance of a descending aortic dissection. Longitudinal plane taken with magnetic resonance imaging (Left) and transversal plane imaged with computed tomography (Right). The images clearly show the dissection flap and the separation of the aorta into the true lumen (TL) and the false lumen (FL).

1.3 Aortic Dissection

An acute dissection (Fig. 1.2) is believed to start with the formation of an intimal tear allowing the pulsatile blood flow to penetrate along the aorta through the outer third of the media. Consequently, an aortic dissection is characterised by the rapid development of a dissection flap, which separates the main aortic lumen into the true lumen (TL; normal passage of blood flow) and the false lumen (FL; the new passage created). Approximately 90% of dissections are communicating, characterised by the presence of interluminal tears and flow in the FL (Nienaber 2006a).

In the anatomical Stanford system, aortic dissections are classified in type A and type B dissections. A type A dissection includes the ascending aorta while a type B dissection is only limited to the descending aorta. Descending aortic dissections often extend along the whole thoracic and abdominal aorta, including even the iliac arteries.

Moreover, aortic dissections can be temporally classified into acute or chronic dissections. A dissection is considered chronic when more than 2 weeks have elapsed since the acute event or if they are detected occasionally.

1.4 Treatment of Aortic Dissection

The treatment for aortic dissection will differ depending on its type.

An acute type A dissection should be handled as a surgical emergency (Erbel et al. 2001) since it carries an associated high risk of sudden death because of aortic rupture, aortic regurgitation, cardiac tamponade or myocardial infarction and thus, it requires effective diagnosis and open surgical management (Miller et al. 1979). Open surgery consists of the removal of the intimal tear and most of the dissected segment, with eradication of the FL and the reconstitution of the affected aorta, directly or through the implantation of a prosthetic tube, and repair of the aortic valve capacity, if necessary. In more than 60% of cases, a type B dissection persists after surgical repair of an acute type A dissection (Moore et al. 1996; Bernard et al. 2001). Although the main proximal tear is eliminated during treatment of the acute phase, there is usually persistence of residual interluminal tears after the most distal part of the prosthesis placed.

On the other hand, acute type B aortic dissection is less lethal than type A dissection (Glower et al. 1990; Masuda et al. 1991; Schor et al. 1996; Hagan et al. 2000) and so most of them (80%) are medically treated (Hagan et al. 2000). The medical treatment consists of blood pressure control using beta-blockers and vasodilators and regular anatomic and haemodynamic assessment by means of CT, TTE, TEE or MRI. Clinical experience has demonstrated that in the majority of the cases medical management of these patients is effective for stabilization and rupture prevention during the acute phase (Glower et al. 1990). An uncomplicated acute type B dissection is less often lethal (Akin et al. 2009) and shows higher rates of operative mortality and complications (Glower et al. 1990). Patients with type B dissection are usually older and surgery is more difficult, with risk of irreversible spinal injury and death ranging from 14% to 67% (Tsai et al. 2006). Therefore, in these patients surgery is only indicated to prevent or relief life-threatening complications that cannot be merely controlled with medical treatment, such as rupture, uncontrolled hypertension or progression of the dissection, organ or limb ischemia, persistent or recurrent intractable pain. However, medical therapy alone is associated to a mortality rate of 30% to 50% at 5 years and progressive aneurismal dilatation of the FL in 20% to 50% of cases at 4 years (Akin et al. 2009), since the rate of dilatation increases exponentially once the aorta is dissected (Coady et al. 1999) consequently increasing the risk of rupture.

Therefore, it is crucial to identify the potential variables that determine progressive aortic dilatation, in order to enable a more conscious and effective patient follow-up in the long-term.

1.5 Potential Factors Influencing Progressive Aortic Dilatation in Chronic Aortic Dissections

Aortic progressive dilatation is a consequence of the combined effect of an increase in haemodynamic stresses acting on the wall which lead to an alteration of biological mechanisms related to matrix metabolism and repair, that might reduce mechanical strength of the aortic wall and result in vessel enlargement (Fig. 1.3).

Haemodynamics thus play a significant role in wall remodelling and dilatation of the aorta.

An elevation in intraluminal pressures raises circumferential wall stress. In response to a chronic augmentation in tension, the aorta increases its diameter and becomes thicker to normalise wall tension. These changes will mostly increase aortic stiffness. Additionally, an acute increase in distending pressures will result in progressive diminished elasticity, even without changing wall properties, since that it is non-linearly elastic, where increased deformation leads to increased stiffness. The aorta is also exposed to longitudinal wall stresses, which are the combination of pressure, geometry and flow. An increase in longitudinal stress will cause elongation of the aorta and thus increases its tortuosity.

On the other hand, the pulsatile flow in combination with the geometry and structure of the wall, will determined the wall shear stress locally acting on the endothelial cells. Wall shear stress has effects on the integrity of the endothelium (Levesque et al. 1986; Shaaban et al. 2000). Very high flow rates and disturbed flow conditions, such as flow separation and turbulence, are determinants of areas of very high, low or oscillating shear stress, contributing to the remodelling, and potential impairment, of the endothelium through an up/down regulation of growth factors.

The influence of the haemodynamic stresses on the wall will depend on its properties. Aortic dissection is often associated with a degeneration and weakness of the aortic wall. In many cases, patients are elderly, with an aorta that has increased arterial stiffness over time because of degenerative changes in elastin in the wall, as a result of fatigue failure in response to cyclic stresses. In younger individuals, other underlying factors may be important, such as genetic disorders as Marfan syndrome, where the weakness of the aortic wall occurs because of separation and fragmentation of the elastic fibres and accumulation of collagen and mucoid material. In addition, the inflammatory response to an aortic injury as a consequence of, or in association with, risk factors, accelerates the degradation of elastin and collagen and cellular apoptosis, leading to vascular structural remodelling and degradation.

The changes in geometry and wall structure induced by alterations in wall and shear stresses will now have significant effects on flow dynamics. On one hand, the tortuosity will result in disturbed flows. On the other hand, changes in diameter and/or stiffness change wall stresses and can induce more impedance mismatch at the different parts of the vascular tree, thus resulting in wave reflection and associated augmentation of pressure.

Summarising, the interplay of all these factors over a period of time will initiate a persistent feedback, leading to progressive aortic dilatation and an increased risk of rupture.

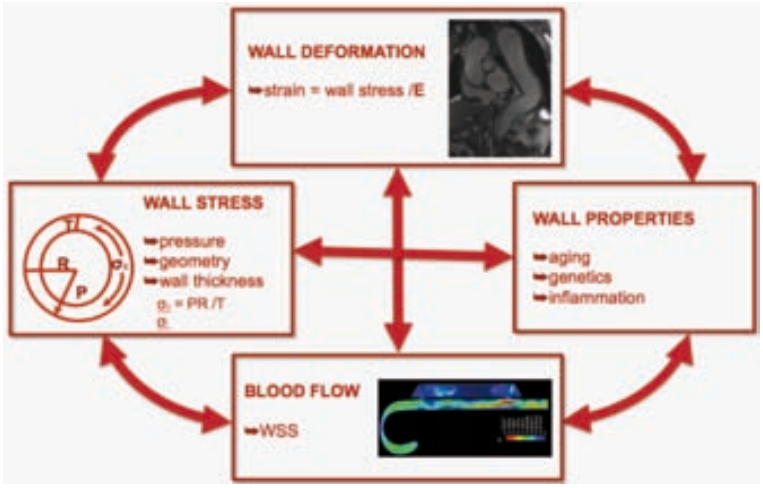

Figure 1.3: Potential factors participating in aortic aneurysmal growth in patients with chronic aortic dissections. Aortic dilatation is the result of the interplay of several biophysical, structural and biological aspects.

1.6 Reported Factors Influencing Aortic Enlargement and Dissection Outcome

Currently, the maximum total aortic diameter is mainly used to predict the outcome in chronic aortic dissections and decide on the best treatment approach, based on the comparison with clinical guidelines. However, the critical aortic diameter to treat the FL is still uncertain and to choose the adequate type of treatment thus not straightforward (Masuda et al. 1991; Kato et al. 1995; Marui et al. 1999; Iguchi et al. 1998; Neya et al. 1992). Additionally, aortic diameter is not always enlarged in aortic dissection and rupture (Neri et al. 2005; Nienaber et al. 2006b; Chang et al 2008) suggesting that the assessment of total aortic diameter alone cannot present the whole picture in aortic dissections and in addition to it, wall biomechanical properties and the haemodynamic state of the FL should be also taken into account.

As a consequence, several other clinical features have been suggested to aid in the prediction of aortic dilatation in chronic aortic dissections (Table 1.1).

The degree of thrombosis of the FL have been linked to progressive aortic dilatation. Some studies (Erbel et al. 1993; Sueyoshi et al. 2009; Miyahara et al. 2011) have suggested the thrombosis of the FL as a good prognosis sign. Patients with complete or

partial obliteration of the FL showed lower risk of late aortic events than those with a patent FL, as a consequence of lower wall stress resultant from low flows and pressures inside the FL. On the other hand, FL patency was a significant risk factor for late enlargement of the FL (Erbel et al. 1993; Bernard et al. 2001; Evangelista et al. 2012). Contradictorily, other studies have found that partial thrombosis of the FL is an independent predictor of higher aortic growth and post-discharged mortality, compared with complete FL patency or thrombosis (Tsai et al. 2007; Trimarchi et al. 2012). These studies speculate that while a patent FL may have a paired proximal inflow and distal outflow, the presence of a thrombus may occlude the distal discharge from the FL and lead to an increase in FL (mainly diastolic) pressures. The study performed by Clough et al. 2012 also did not find FL thrombosis to be protective from aortic enlargement.

With regards to the patency of the FL, tear size, number and location seem to be also major determinants of dissection healing and cause of death. In most of the patients, a dominant/primary tear is identified and its position seems to coincide with the area of greatest dilatation (Evangelista et al. 2012; Clough et al. 2012). Depending on the study, a large proximal tear (Roberts et al. 1990; Tsai et al. 2008; Evangelista et al. 2012) as well as a large distal tear (Clough et al. 2012) has been suggested as a risk predictor of dissection-related events and FL dilatation. Moreover, limited outflow from a patent FL might be the cause of long-term FL dilatation and rupture (Tsai et al. 2008).

The evaluation of intraluminal blood flow in aortic dissections could also give relevant information about the haemodynamic stresses and potential pathological flow patterns involved in the aneurismal growth of the FL. Patients with enlarged patent FL seem to be associated with a significant variation in flow velocities and slower helical flow patterns, whose location coincides with the areas where the FL wall is dilated whereas stable patients seem to present laminar or stagnant flows in the FL (Amano et al. 2011). It is in line with the study performed by Müller-Eschner et al. 2011 in a patient with chronic type B dissection, where the enlarged FL was associated with disturbed and complex flows. Clough et al. 2012 also detected that the amount of helical flow in the FL was significantly and directly related to the degree of FL dilatation.

Even when hypertension is identified as one of the most significant risk factors for type B aortic dissection development, the incidence of aortic dissections is low in hypertensive individuals and to our extent of knowledge, none of the existing clinical studies performed during the follow-up of these patients have identified hypertension as a predictor of mortality or dissection-related event, even when hypertension is prevalent in these patients (Roberts et al. 1990; Tsai et al. 2007; Sueyoshi et al. 2009; Miyahara et al. 2011; Evangelista et al. 2012). Hence, there certainly should be additional aspects that predispose a hypertensive subject to the development of a type B aortic dissection. In a study performed by Shirali et al. 2013 using multidetector computed tomography angiography, hypertensive individuals with development of a type B aortic dissection differed from the rest of hypertensive subjects. They presented enlargement of the ascending aorta and the aortic arch, increased length and tortuosity of the entire

aorta. These geometric changes in the setting of hypertension and dilatation may induce disturbed or turbulent blood flows and subsequent dissection/dilatation progression.

Wall compliance and mechanical strength are also factors that could be connected to the dilatation of the FL. A weakened aortic wall will be more sensitive to the action of haemodynamic forces and is thus exposed to a higher risk of aneurysm formation and aortic rupture (Nienaber et al. 2006b; Evangelista and González-Alujas 2006). In the setting of chronic type B aortic dissections, patients with progressive FL enlargement are older, hypertensive, affected by Marfan syndrome or with a higher incidence of atherosclerosis, thus showing a decrease in wall strength.

Eventually, the presence of abdominal arteries arising from the FL has also been directly associated to a higher amount of flow volume within the FL and enlargement of the dissected aorta (Inoue et al. 2000).

Table 1.1: Clinical features suggested to aid in the prediction of aortic dilatation in chronic aortic dissections

PROGRESSION	*PROTECTION*
Partial thrombosis of the FL (Tsai et al. 2007; Trimarchi et al. 2012; Clough et al. 2012)	Thrombosis of the FL (Erbel et al. 1993; Sueyoshi et al. 2009; Miyahara et al. 2011)
Patent FL with large open communication between the TL and the FL (Roberts et al. 1990; Erbel et al. 1993; Bernard et al. 2001; Clough et al. 2012; Evangelista et al. 2012)	Patent FL with good communication between TL and FL (Tsai et al. 2007; Tsai et al. 2008; Trimarchi et al. 2012)
Disturbed and complex flows in the FL (Amano et al. 2011; Müller-Eschner et al. 2011; Clough et al. 2012)	Laminar or stagnant flows in the FL (Amano et al. 2011)
Hypertension in conjunction with aortic geometric changes, such as enlargement, elongation and tortuosity (Shilari et al. 2013)	
Affected mechanical strenght of the aortic wall (mainly the media layer; Nienaber et al. 2006b, Evangelista and González-Alujas 2006)	
Presence of abdominal arteries arising from the FL (Inoue et al. 2000)	

TL, True lumen; *FL*, False lumen

1.7 Hypothesis and Objectives

In this thesis, we start from the hypothesis that progressive aortic dilatation in patients with chronic aortic dissections is determined by anatomic-geometrical configurations, such as interluminal communication and incidence of side branches in the FL; biomechanical factors, such as wall compliance; and mechanical stimuli, such as intraluminal pressures and flows.

The main goal of this thesis is to develop a systematic an integrated approach to the study of chronic aortic dissections, focussing on the complementary information and knowledge that can be obtained by combining in-vitro, in-silico and in-vivo data.

The different approaches are used to:

1) Gain insight into the relationship between the potential geometrical (tear size, number and location and incidence of side branches communicating with the FL) and biomechanical (wall compliance) parameters of severe aortic enlargement and the induced intraluminal flows and pressures.

2) Characterize intraluminal haemodynamic in aortic dissections.

3) Better understand the mechanisms underlying haemodynamic phenomena in aortic dissections.

CHAPTER 2

A Multi-method Approach towards Understanding the Pathophysiology of Aortic Dissections – The complementary Role of In-silico, In-vitro and In-vivo Information

Abstract - *Management and follow-up of chronic aortic dissections continue to be a clinical challenge due to progressive aortic dilatation. To predict dilatation, guidelines suggest follow-up of the aortic diameter. However, dilatation is triggered by haemodynamic parameters (pressure and wall shear stresses (WSS)), and geometry of false (FL) and true lumen (TL). We aimed at a better understanding of TL and FL haemodynamics by performing in-silico (CFD) and in-vitro studies on an idealized dissected aorta and compared this to a typical patient. We observed an increase in diastolic pressure and wall stress in the FL and the presence of diastolic retrograde flow. The inflow jet increased WSS at the proximal FL while a large variability in WSS was induced distally, all being risk factors for wall weakening. In-silico, in-vitro and in-vivo findings were very similar and complementary, showing that their combination can help in a more integrated and extensive assessment of aortic dissections, improving understanding of the haemodynamic conditions and related clinical evolution.*

Adapted from Paula A. Rudenick, Maurizio Bordone, Bart H. Bijnens, Eduardo Soudah, Eugenio Oñate, David García-Dorado and Arturo Evangelista. A multi-method approach towards understanding the pathophysiology of aortic dissections – The complementary role of in-silico, in-vitro and in-vivo information. In: Camara, O., Pop, M., Rhode, K., Sermesant, M., Smith, N., Young, A. (Eds). *Statistical Atlases and Computational Models of the Heart 2010. Lecture Notes in Computer Science*. 2010;6364:114-123.

2.1 Introduction

Aortic pathologies represent an important subgroup within cardiovascular diseases, and while their prevalence is limited, they are associated with a very high morbidity and mortality (>50% in the acute phase). Despite improved diagnostic and therapeutic techniques, the management and follow-up of aortic dissections continue being a challenge in clinical practice.

Classic aortic dissection is believed to begin with the formation of a tear in the aortic intima that exposes an underlying media layer to the pulsatile pressure of the intraluminal blood (Fig. 2.1) leading to a longitudinal cleaving of the media layer along the aortic wall, causing the dissection. The dissection process extends typically antegrade (driven by the forward force of the aortic blood flow) but sometimes retrograde from the site of the intimal tear. The lumen will be divided into two parts, the true (TL) and the false lumen (FL). In 90% of cases TL and FL are communicated through entry and exit sites in the dissection flap. The distension of FL during the pulsatile pressure inside the lumina can cause intimal flap movement, distorting the TL shape and narrowing its calibre, potentially leading to TL collapse obstructing side branches and inducing visceral ischemia.

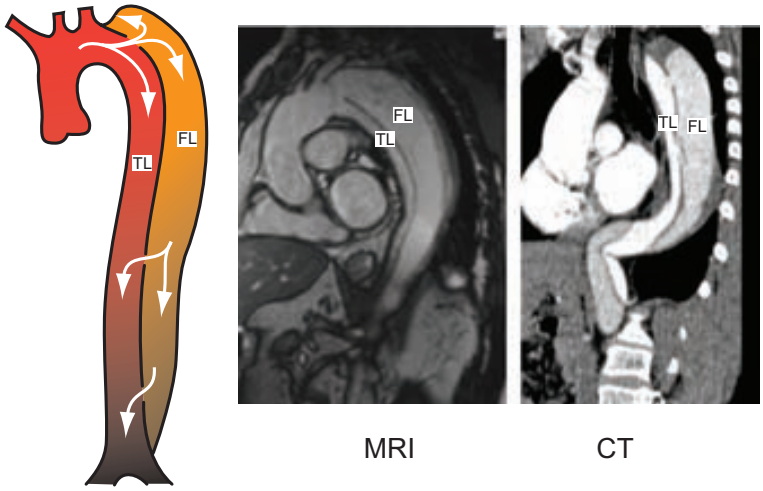

Figure 2.1: A classic dissection of the descending aorta (Left). The typical clinical appearance on magnetic resonance (Middle) and computed tomography (Right) images. *TL*: True lumen; *FL*: False lumen.

While acute ascending aortic dissections require immediate surgery, descending aortic dissections are often treated medically and persist in the chronic phase (Nienaber et al. 2006b). However, these patients still have high mid/long term mortality during the

chronic phase, mainly due to the progressive dilatation of the aorta and subsequent rupture.

In current clinical practice, prediction of outcome is mainly based on maximum total aortic diameter, which is compared with guidelines for deciding the best therapeutic approach. However, previous work has shown that maximum diameter is not a reliable determinant of rupture and progression (Bernard et al. 2001; Nollen et al. 2004; Neri et al. 2005; Nienaber et al. 2006b). In addition to it, haemodynamic parameters (intraluminal pressure and flow conditions/wall shear stresses), geometric factors (such as the shape and curvature of the aorta and the communications between FL and TL), and intrinsic wall properties, all play an important role in the progress of dilatation and risk of rupture.

Whereas an integrated clinical approach towards the biomechanics and haemodynamics of the dissected aorta is still lacking, based on clinical observations and patient registries, several markers have been suggested to assist in the prediction of dilatation. The patency of the descending aorta FL may be responsible for progressive aortic dilation (Nienaber et al. 2006b) and partial thrombosis of the FL has been found as a predictor of post-discharge mortality in patients with type B acute aortic dissection (Tsai et al. 2007).

It was also observed that prognosis of patients with open communication between TL and FL is poorer than in those without such communication, and free communication with high flow rates carries a higher risk for reoperation because of the high flow pressure and wall stress. Nevertheless, complete obliteration of the FL can occur despite open communication and is possibly related to the size of communication (Erbel et al. 1993). Poor inflow in the TL and lack of outflow in the FL may have impact in FL dilation and rupture during follow-up period (Tsai et al. 2008).

Therefore, from clinical observations, the importance of tear size and location is clear. However, the contradictory findings on which situations are leading to further dilatation of the FL show that there is still a lack of understanding of the interplay of all variables.

Another factor that could affect the dilation of the FL is the compliance or mechanical strength of the dissected aortic wall. Arteries respond to changes in blood pressure and flow conditions by remodelling. Wall shear stress (WSS) is the tangential force resulting from the friction that the flowing blood exerts on the luminal surface. It has been shown that WSS can change the morphology and orientation of the endothelial cell layer (Levesque et al. 1986). Prolonged high WSS is known to cause vessel dilation and internal elastic lamina fragmentation, and may be the responsible for dissection initiation (Shaaban et al. 2000). On the other hand, inflammatory and atherosclerotic pathways, triggered by low WSS, could also play an important role in dissection pathogenesis. Excessively low WSS could lead to atherosclerotic inflammatory infiltration and thereby cause deterioration of the aortic wall that could lead to mechanical weakening and rupture (Malek et al. 1999).

Therefore, it is expected that better aortic morphologic and hemodynamic analysis will be much more predictive for aortic dilatation and will improve the clinical stratification of the risk of these patients, facilitating a better therapeutic management.

The aim of this study is to assess whether an integrated approach towards TL and FL haemodynamics will allow us to define risk markers of severe aortic enlargement. For this, in-silico and in vitro studies were performed to investigate the impact of morphological characteristics on the haemodynamics of the TL and FL and the findings were compared to a typical patient from our hospital.

2.2 Methods

2.2.1 In-vivo

In our hospital, chronic aortic dissection patients undergo regular follow-up with trans-thoracic and trans-oesophageal echocardiography for the quantification of changes in aortic size. Additionally, an MRI study, including short-axis phase-contrast acquisition of blood flow in the distal FL and TL (Fig. 2.2) is performed and when clinically indicated, a CT study is additionally done.

Figure 2.2: Typical results from a clinical MRI phase-contrast study. Left: instantaneous volume flow in FL (blue) and TL (red); Middle: measurements in TL; Right: measurements in FL. *TL*: True lumen; *FL*: False lumen.

2.2.2 In-silico

Idealized Geometry. A Computational 3D model of typical type B aortic dissections was constructed with the CAD software GiD (CIMNE, Barcelona) (Fig. 2.3) (GiD website). The dimensions of the model, including the aortic arch and the ascending aorta, were selected based on anatomical measurements (Williams et al. 1997; Strotzer et al. 2000). These are: aortic diameter=20 mm; dissected segment diameter=40 mm; FL length=160 mm; TL thickness=3 mm; dissection flap thickness=2 mm; and FL thickness=1 mm. A proximal and distal tear was included with 10 mm diameter, corresponding to 25% of the dissected segment diameter.

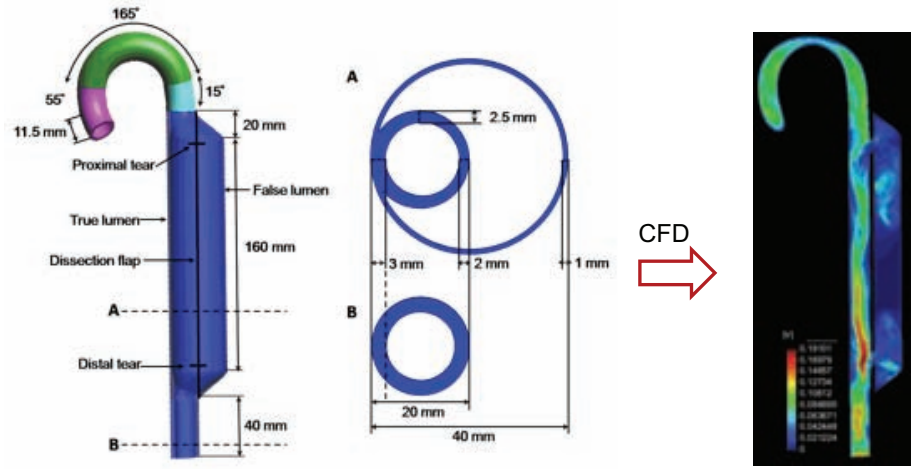

Figure 2.3: Left: Idealized geometry of an aortic dissection including the dissected section (A) and the non-dissected aortic section (B); Right: The result of the CFD simulations, showing the velocities at the longitudinal mid-plane of the dissection.

Computational Fluid Dynamics (CFD) Simulation. The computational mesh consisted of approximately 1.1 million tetrahedral elements with a size range of 0.5-1.0 mm and was created with GiD (CIMNE, Barcelona). The CFD simulation was performed using CFD-Tdyn (CompassIS, Barcelona), solving the Navier-Stokes equations. The no-slip wall of the dissection model was assumed to be rigid, assuming that in chronic dissection there is reduced flap motion, so that a rigid flap is a good first approximation. Additionally, several studies suggested that the difference in flow induced pressure variations and consequent wall stress between rigid and elastic aortic models is negligible (Leung et al. 2006; Borghi et al. 2008). Realistic time dependent velocity and pressure waveforms (adapted from Reymond et al. 2009) were applied at the inlet and outlet of the fluid domain respectively. We assessed intra-luminal pressure and instantaneous volume flow in the FL and TL at the distal and proximal descending aorta, respectively. The WSS distribution at the TL and FL surface was calculated and the velocity vectors at the mid-plane of the dissected geometries were analysed.

2.2.3 In-vitro

Phantom. A simplified physical phantom (without the aortic arch), similar to the 3D geometry used for the in-silico approach, was made from a compliant and flexible material to meet the tensile strength of the aorta. The model was constructed from two individual parts to simulate the dissection: the TL and the FL. These parts were joined

together to form the final model. The TL consisted of a silicone tube of 16 mm inner diameter and 2 mm wall thickness in which holes were made to create the tears.

The FL part was custom made by first creating the geometry using modelling clay and PVC tubes. Next, from this, a two-part silicone (RTV) mould is made, which can be used to create multiple wax casts of the FL. Both halves of the mould are held together for casting a replica from beeswax. After solidifying, any mould marks remaining on the wax were carefully polished away. The wax replica was used in a lost-wax technique to create a latex (Kryolan) phantom by dipping the replica in liquid latex many times at intervals of 1 hour. Once the coating was finished, the model was heated, to remove the wax.

Experimental Set Up. A dynamic flow circuit, mimicking the human circulatory system, was set up to evaluate flow and morphological characteristics under controlled conditions (Fig. 2.4). The circuit consisted of a pulsatile pump, a compliance chamber, the dissection model, and a collecting system, connected in series. The flow pump (Harvard Apparatus) was programmed to simulate pulsatile left ventricle output with a heart rate=70 bpm; stroke volume=70 ml; and systolic/diastolic phase ratio=30/70. Peripheral resistance and systemic pressure were adjusted with the use of resistors (adjustable valves) placed proximal and distal from the phantom.

Measurements / Imaging. TL and FL pressure waveforms were measured with a fluid filled catheter at the distal and proximal sections. Flow was measured using an ultrasonic flow meter (Transonic Systems Inc). Pressure and flow waveforms were digitized using a PowerLab 16/30 with LabChart Pro acquisition and analysis software (ADInstruments, Colorado Springs, CO, USA). Phantom geometry as well as fluid appearance and velocities within the phantom were assessed by two-dimensional and Doppler ultrasound using a high-end portable clinical ultrasound scanner (Vivid Q - GE Healthcare) (Fig. 2.4).

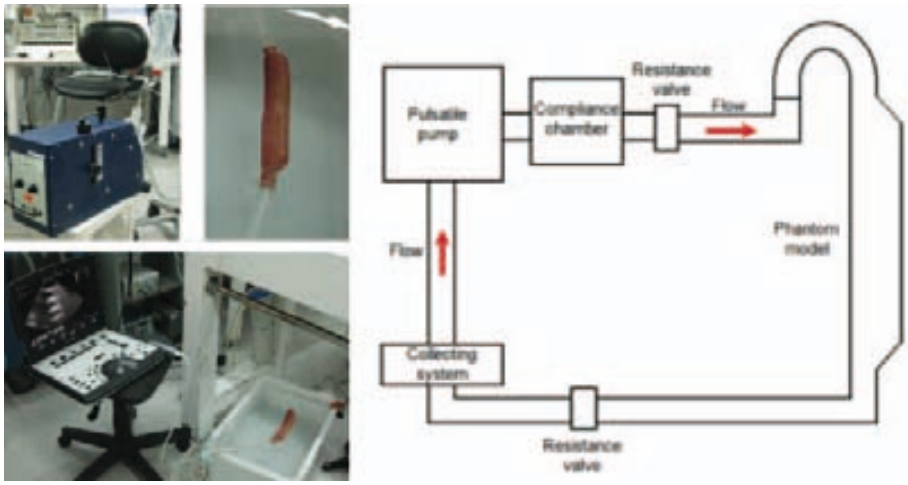

Figure 2.4: Experimental set up for the in-vitro measurements. Right: diagram of the circuit. Left: different components of the circuit (top left: pulsatile pump; top right: latex phantom; bottom: portable ultrasound machine and phantom in a water tank).

2.3 Results

2.3.1 CFD Simulations

At the distal tear, higher FL pressures were observed at the onset of the cycle, resulting in an antegrade jet through the tear, whereas the FL/TL pressure gradient inverted at the end of the cycle leading to deceleration and inversion of the velocities and resulting in retrograde flow through the distal tear.

Figure 2.5 shows the resulting absolute volumetric flows. FL flow variations are remarkably different from the TL, with a biphasic pattern and high early systolic flow. Figure 2.6 shows the normalized velocities during the cycle, obtained at different positions in the model. As can be observed, flow direction in the TL is dominantly antegrade (positive), except at the proximal section were its direction slightly reverses during early diastole. However, in the FL, fluid velocities begin to be retro grade from late systole, resulting in the reverse flow shown in the flow pattern plots (Fig. 2.7). Through the entry tear, we can observe a clear inflow during systole and outflow during diastole, while there is outflow during systole and inflow during diastole through the exit tear. The magnitudes of the velocities at both tears are similar. However, there is a shift in the time course indicating the propagation of the fluid wave.

From the assessment of the flow pattern in the dissected region (Fig. 2.7), we observe a bidirectional flow in the FL with a prominent retrograde during diastole. The most significant elevation in WSS is seen at the impact zone of the entry jet at end-systole, whereas during diastole there was a high variability of WSS in the distal zone.

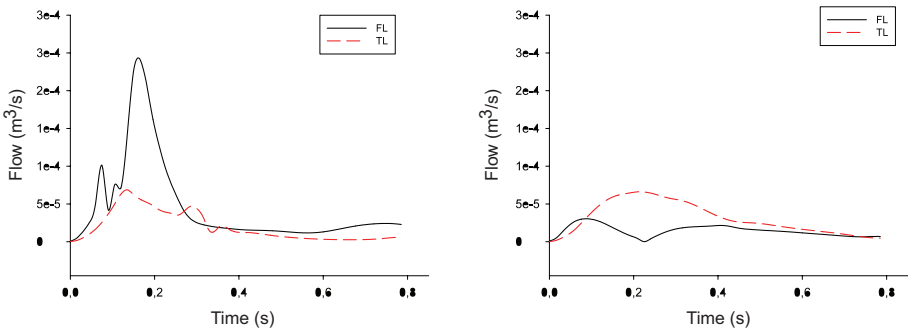

Figure 2.5: The instantaneous flow (modulus) in the true (TL) and false lumen (FL) at proximal (left) and distal (right) sections.

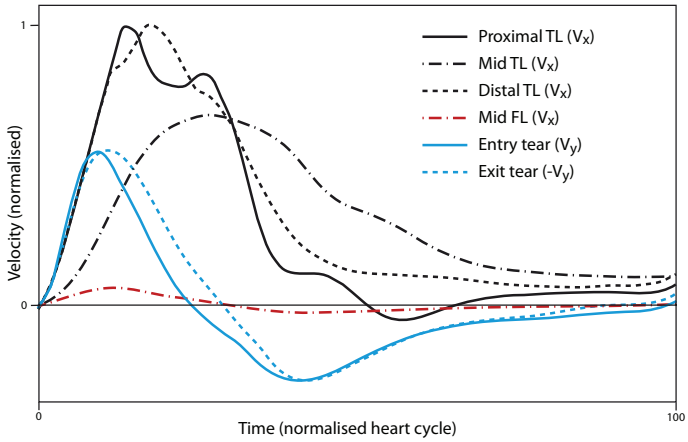

Figure 2.6: Normalized mean velocities changes of the true (TL) and false lumen (FL), at different positions of the phantom, and in the entry and exit tears.

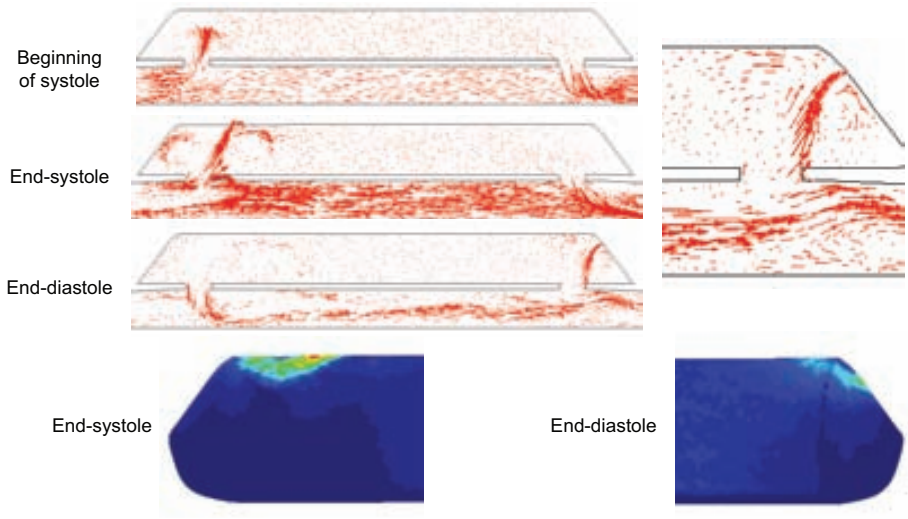

Figure 2.7: Top: flow patterns at beginning and end-systole and end-diastole. The zoomed area shows the presence of false lumen (FL) diastolic retrograde flow at the exit tear. Bottom: WSS distributions at the FL surface. Left: the entry tear at end-systole; right: the exit area at end-diastole.

2.3.2 In-vitro Measurements

Figure 2.8 shows the echocardiographic image and measured Doppler flows for the in-vitro setup. The morphology of TL, FL and exit-tear can be easily recognised and the Doppler traces show the systolic forward flow and diastolic retrograde flow.

Figure 2.9 shows the pressure measurements at distal and proximal section in TL and FL. Distal pressures were higher than proximal pressures, also coinciding with the high WSS area detected in the CFD simulations. Comparing pressures between lumina, diastolic pressures in the FL were higher than in the TL. A high pressure gradient between TL and FL is measured at the distal section, which explains the presence of a remarkable reverse flow at the distal tear of the phantom.

2.3.3 Comparison of In-silico and In-vivo Data

Figure 2.10 shows the comparison of the instantaneous flow profiles of the simulated geometry and from one of the patients in our clinic (obtained from MRI phase-contrast velocity measurements). This patient had a large entry tear (12 mm) and showed rapid dilatation of the FL over the course of the follow-up (10%/year over 10 years). As can be seen, the observed profiles are remarkably similar, illustrating the usefulness of the in-silico approach to study the haemodynamics of typical patients.

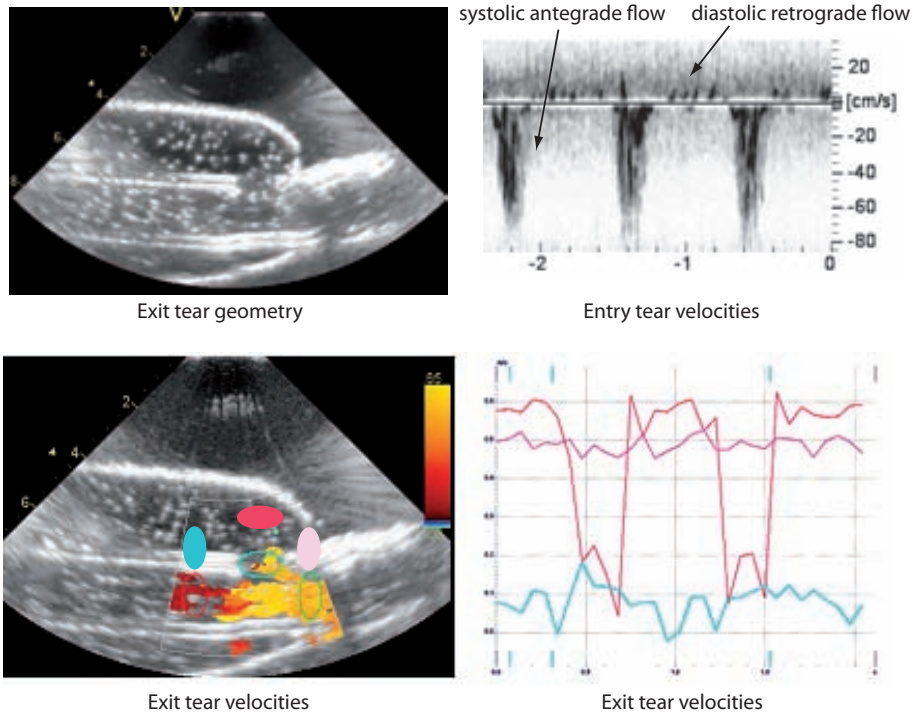

Figure 2.8: Echocardiography of the in-vitro setup. Left: longitudinal cut of the phantom at the distal part and colour flow Doppler. Top right: pulsed Doppler velocity waveform at the entry tear; bottom right: colour Doppler velocity waveforms at the exit tear: Red: velocity through the exit tear; Pink: TL velocity distal from the exit tear; Cyan: TL velocity proximal to the exit tear.

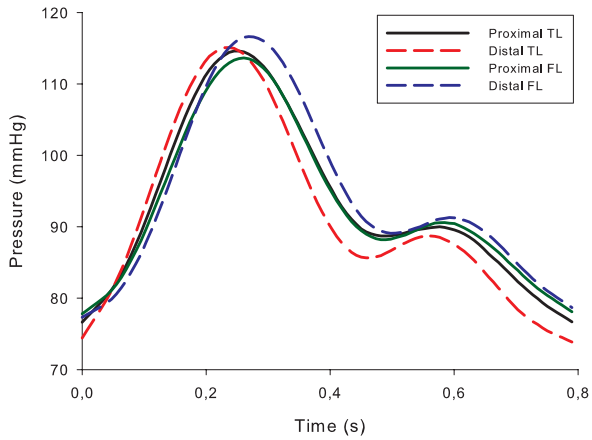

Figure 2.9: Measured pressure profiles at proximal and distal sections of the true (TL) and false lumen (FL).

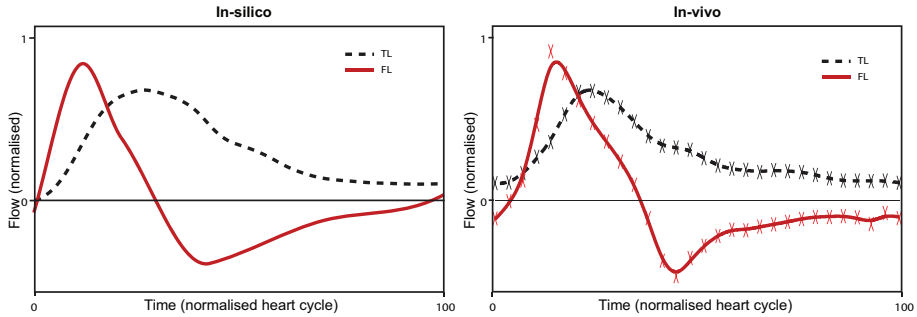

Figure 2.10: Comparison of the in-silico instantaneous flow with the measurements from a typical patient. *TL*: True lumen; *FL*: False lumen.

2.4 Discussion

The dilatation of the dissected aorta depends on multiple factors. The cyclic wall stress in the FL is determined by the blood pressure changes, in interaction with the wall properties. Wall properties themselves are related to genetics, chronic pressure levels and flow (in particular WSS).

In our findings, the diastolic pressure in the FL was higher than in the TL, exposing the already weak and thin FL wall to higher wall stress. Additionally, pressures are higher at the distal section than at the proximal section, explaining the distal propagation of dissections.

Complex flow patterns have been thought to increase inflammatory cell infiltration in artery wall, increasing risk rupture (Gimbrone et al. 2000; Davies et al. 2005). We show both in-silico and in-vitro that the entry-jet and flow reversals result in complex flow patterns in the FL. A concentrated, jet-like flow is noted, directly impinging on the FL wall at the proximal and distal site during peak systole and diastole, respectively. This fast proximal jet might explain the eccentric dilatation of the proximal FL observed in a subset of patients.

An important hemodynamic factor that influences vascular remodelling, aortic expansion and rupture is WSS. WSS influences the morphology and orientation of endothelial cells (Levesque et al. 1986). An acute increase in WSS leads to an increase of the aortic diameter and weakening of the aortic wall because of loss of elastic tissue, change of muscle cell orientation, and acceleration of cell deterioration. On the other hand, the exposure of the arterial wall to low or variable WSS may increase intercellular permeability and increase the vulnerability of these regions of the vessel to atherosclerosis and weakening that could ultimately lead to rupture.

The cumulative effect of increases in pressure (wall stress) and changes in elastic properties, initiated by altered WSS, results in increased risk of further dilatation and rupture.

2.4.1 Limitations

There are many limitations in both in-silico and in vitro studies of an aortic dissection. We used a flexible dissection phantom to mimic the aortic wall compliance. Despite being an idealized model, its dimensions are based on clinical measurements and this generic model is ideal for parametric studies.

Whereas the overall flow and pressure waveforms were very similar, we had some differences of values between the results obtained with the in-silico and in-vitro models. It was mainly because we compared a flexible physical phantom with a rigid computational model, and boundary conditions did not correspond exactly to the ones of the in-vitro model. Furthermore, the resistance and compliance of the experimental set up was not perfect, resulting in rather flat velocities when pressure waveforms were adjust to mimic human measurements.

Despite these mentioned differences, in-silico and in-vitro results follow a similar behaviour and are thus useful and complementary as a first validation of our results and in helping to explain clinical observations. Additionally, a wider range of dissection geometries, corresponding to the variety of patients' appearances in clinical practice, should be studied to obtain a full understanding of the haemodynamics in aortic dissection.

2.4.2 Clinical relevance

At present, follow-up and treatment of patients with aortic dissection seem to be non-ideal and it remains difficult to balance the high morbidity and mortality rates

registered during the chronic phase of the disease with the severe side effects and risks of surgical or endovascular interventions. In current clinical practice, prediction of outcome in aortic dissections is mainly based on maximum total aortic diameter, which is compared to clinical guidelines for deciding the best therapy. However, this has proven to show severe limitations in assessing the genesis and evolution of aortic dissection (Nollen et al. 2004; Neri et al. 2005). So, the need for better predictors of the evolution of aortic dissection is evident, especially to assess FL dilatation and to evaluate and titrate a better pharmacological management.

Our study provides a methodology to assess haemodynamic and WSS differences originating from different geometrical configuration. Understanding these differences and assessing them in clinical practice with imaging modalities such as MRI, Transesophageal Echocardiography (TEE) and CT, will play an important role in the diagnosis and follow-up of aortic dissections. Combining measurements from imaging together with computational flow analysis using patient-specific geometries and boundary conditions could additionally enable to obtain a much more detailed view on the haemodynamic and wall stress conditions in aortic dissections, thus helping to provide an integrated view on the patient and enable the prediction of local remodelling that could be induced.

2.5 Conclusion

We evaluated haemodynamic parameters in the TL and FL of a chronic aortic dissection. For this, we have constructed a model of a type B dissection which allows studying aortic geometries, including different tear locations and sizes, both using in-silico computer simulations and in-vitro phantom measurements and if which the results can be directly compared to clinical patients. From one of these experimental in-vitro and in-silico models we showed the flow dynamics in the FL, contributing to novel ways for a better understanding of the haemodynamic conditions and related clinical evolution in patients with a chronic aortic dissection.

CHAPTER 3

An In-vitro Phantom Study on the Influence of Tear Size and Configuration on the Haemodynamics of the Lumina in Chronic Type B Aortic Dissections

Abstract - *Management and follow-up of chronic aortic dissections continue being a clinical challenge due to progressive dilatation and subsequent rupture. To predict complications, guidelines suggest follow-up of aortic diameter. However, dilatation is triggered by haemodynamic parameters (pressures/wall shear stresses) and geometry of false (FL) and true lumen (TL), information not captured by diameter alone. Therefore, we aimed at better understanding the influence of dissection anatomy on TL and FL haemodynamics. In-vitro studies were performed using pulsatile flow in realistic dissected latex/silicone geometries varying tear number, size, and location. We assessed three different conformations: I) proximal tear only; II) distal tear only; III) both proximal and distal tears. All possible combinations (8) of small (10% of aortic diameter) and large (25% of aortic diameter) tears were considered. Pressure, velocity and flow patterns were analysed within the lumina (at proximal and distal sections) and at the tears. We also computed the FL mean pressure index (FPI_{mean}%) as a percentage of the TL mean pressure, to compare pressures among models. The presence of large tears equalized FL/TL pressures compared to models with only small tears (Proximal FPI_{mean}% 99.85 ± 0.45 vs 92.73 ± 3.63; Distal FPI_{mean}% 99.51 ± 0.80 vs 96.35 ± 1.96; P<.001). Thus, large tears resulted in slower velocities through the tears (systolic velocity < 180 cm/s) and complex flows within the FL whereas small tears resulted in lower FL pressures, higher tear velocities (systolic velocity >290 cm/s) and a well-defined flow. Additionally, both proximal and distal tears act as entry and exit. During systole, flow enters the FL through all tears simultaneously while during diastole, flow leaves through all communications. Flow through the FL, from proximal to distal tears or vice versa, is minimal. Our results suggest that FL haemodynamics heavily depends on cumulative tear size and thus it is an important parameter to take into account when clinically assessing chronic aortic dissections.*

Adapted from Paula A. Rudenick, Bart H. Bijnens, David García-Dorado and Arturo Evangelista. An In-vitro Phantom Study on the Influence of Tear Size and Configuration on the Hemodynamics of the Lumina in Chronic Type B Aortic Dissections. *Journal of Vascular Surgery*. 2013;57(2):464-474.

3.1 Introduction

Aortic dissections represent an important cardiovascular disease. While having low prevalence, they are associated with high morbidity and mortality (Anagnostopoulos et al. 1972; Mèszáros et al. 2000). Aortic dissections are believed to begin with the formation of an intimal tear that exposes the media to pulsatile pressure of the intraluminal blood. This leads to longitudinal media cleaving, dividing the lumen into two parts, the true (TL) and false lumen (FL).

While acute ascending aortic dissections require immediate surgery, descending dissections are often treated medically and persist chronically (Suzuki 2003; Nienaber et al. 2006b). Nevertheless, a significant number of patients experience posterior dissection-related adverse events and still have high mid/long term mortality, mainly caused by dissection progression or recurrence or increasing aortic dilatation, all of which may cause subsequent rupture (Tsai et al. 2006).

In current clinical practice, decision-making in chronic dissections is mainly based on maximum total diameter, even if it has been shown that this parameter alone is not a reliable determinant of rupture and progression (Nollen et al. 2004; Neri et al. 2005; Nienaber et al. 2006b; Pape et al. 2007). In addition, haemodynamic parameters (intraluminal pressure and flow conditions/wall shear stresses) (Bernard et al. 2001; Tsai et al. 2007) geometric factors (such as aortic morphology, FL-TL communications and relative FL/TL axial size) (Suzuki et al. 2003; Song et al. 2007; Tsai et al. 2008) and biomechanical properties of the wall (Nienaber et al. 2006b; Evangelista and González-Alujas 2006) are all related to chronic dilatation and rupture risk.

Particularly, low and high spatial and temporal variations of wall shear stress (WSS), and complex and disturbed flow patterns contribute to deterioration of the wall (Gimbrone et al. 2000; Davies et al. 2005). While tissue loses integrity, a feedback loop is initiated leading to further dissection progression and lumen expansion, which eventually can lead to rupture. High pressures are also responsible for wall expansion and its degradation due to increased circumferential tension, loss of muscle and elastic cells and collagen accumulation (Gusic et al. 2005; Evangelista and González-Alujas 2006).

Therefore, a better understanding and assessment of aortic morphology and haemodynamics is needed to predict dilatation and improve clinical stratification of risk of these patients, facilitating a better therapeutic management.

Some studies using in-vitro models to evaluate haemodynamics in chronic dissections have been published. Chung et al. 2000 studied the effects of anatomic and physiologic factors involved in TL collapse; Tsai et al. 2008 studied the impact of intimal tear size, number and location on FL pressure; and Iwai et al. 1991 analyzed flow phenomena. However, none have performed an integrated analysis of the influence of tear configuration on TL/FL flow, pressures and velocities across tears.

The aim of our study was to evaluate the influence of different morphologic configurations on TL/FL haemodynamics in descending aortic dissections. For this, we ac-

complished in-vitro studies, under physiological pressure/flow conditions, on idealized flexible models varying tear size, number and location.

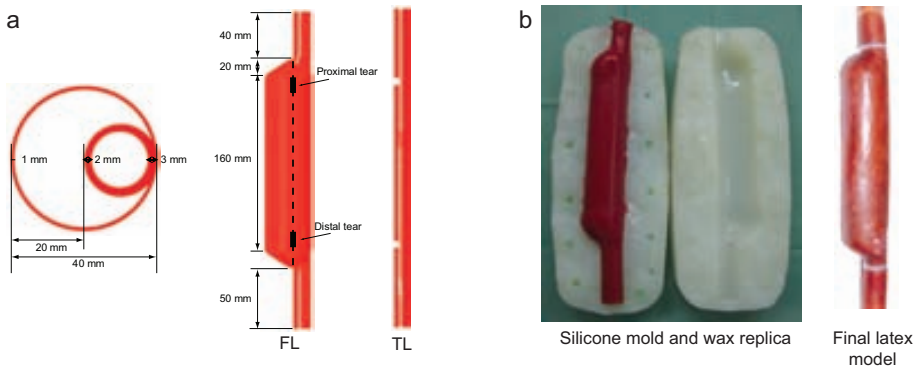

Figure 3.1: (a) Synthetic geometry of a type B aortic dissection. Schematic diagram of the dissected aortic section. (b) Consecutive processing steps developed to make latex phantoms of type B aortic dissections.

3.2 Methods

In order to study the effects of physiological flow in different geometries, we assessed flow patterns and haemodynamics in flexible models using a pulsatile circuit mimicking the cardiovascular system.

3.2.1 Phantom

Compliant phantoms of dissected aortas (Fig. 3.1) were made. The models (excluding the aortic arch) were constructed using anatomic measurements obtained from literature (Williams et al. 1997; Strotzer et al. 2000; Erbel et al. 2001; Wolak et al. 2008; Malayeri et al. 2008) to create a simplified version of a potential patient with a chronic type B dissection, similar to the models used by others (Iwai et al. 1991; Chung 2000; Tsai et al. 2008). Each model consisted of two parts to mimic a dissection. The TL wall was made of silicone and the FL outer wall of latex. The TL consisted of a silicone tube (16 mm inner diameter; 2 mm wall thickness) in which holes were made. The FL was made by first creating the desired geometry using clay and PVC tubes. Next, a silicone mould (Room-Temperature-Vulcanizing silicone elastomer; Jordi Sagristá; Spain) was generated, which formed the basis to create multiple wax casts. After solidifying, the wax models were polished and used in a lost-wax technique to create a phantom by dipping in liquid latex (Kryolan Spain, S.L.) many times at 1-hour intervals. To remove superfluous wax, the model was heated once the coating was finished.

To simulate proximal and distal tears, circular holes of 4 or 10 mm diameter were created, corresponding to 10% and 25% of the dissected segment diameter (40 mm)

respectively, and representing a clinically mild or severe dissection. The proximal tear was placed 20 mm from the onset of the dissected segment while the distal tear was located 20 mm before the end of it.

The models studied differed in tear size, number and placement. We assessed three different conformations: I) proximal tear only; II) distal tear only; III) both proximal and distal tears. All possible combinations were considered for each of these morphologic configurations (Fig. 3.2; notation: $C_{\text{proximal size, distal size}}$).

Anatomical configuration	Proximal tear diameter (mm)	Distal tear diameter (mm)
$C_{4,0}$	4	-
$C_{10,0}$	10	-
$C_{0,4}$	-	4
$C_{0,10}$	-	10
$C_{4,4}$	4	4
$C_{4,10}$	4	10
$C_{10,4}$	10	4
$C_{10,10}$	10	10

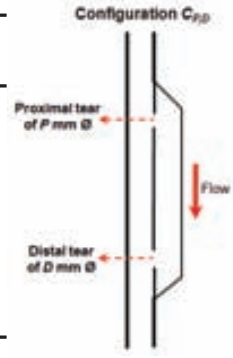

Figure 3.2: Geometric description of the different models of aortic dissections used in this study. Each configuration is referred to as $C_{P,D}$, where P indicates the diameter of the proximal tear and D the distal tear diameter. *C*, Case.

3.2.2 Setup

A dynamic flow circuit, mimicking the circulatory system, was set up to evaluate flow and haemodynamic characteristics under controlled conditions (Fig. 3.3a). Its components were: a pulsatile pump, a compliance chamber (1000 cm^3), the dissection model and a fluid collector, all connected by PVC tubes. The entrance length was sufficiently long to get a fully developed, non-turbulent flow at the model inlet. The circuit contained water at room temperature. Graphite powder (180 g in 7 L) was added as contrast agent for ultrasonic imaging. The pump (model 1423, Harvard Apparatus, MA, USA) was programmed to mimic normal left ventricular output (heart rate=65 bpm, stroke volume=70 mL and systolic/diastolic duration ratio=30/70). To adjust peripheral resistance and systemic pressure, valves were placed proximal and distal from the phantom. To simulate typical conditions in a normal aorta, the pressure waveform and pulse pressure at the inlet of each model were adjusted to obtain a systolic pressure of 120-125 mm Hg and diastolic pressure of 80-90 mm Hg. This resulted in a flow of about 5 L/min.

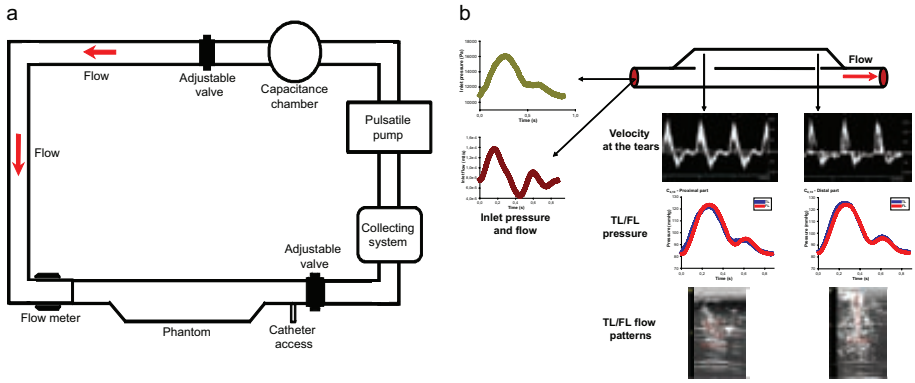

Figure 3.3: (a) Diagram of the pulsatile flow circuit. Valves are used to regulate the peripheral resistance and a compliance chamber damps the pump outflow. (b) Example of measurements performed in each model of dissection. *TL*, True lumen; *FL*, False lumen.

3.2.3 Measurements

Figure 3.3b illustrates the measurements in each phantom. Retrograde catheterization was performed from an access distal from the model. TL/FL pressures were recorded with a Mikro-tip catheter (SPC-350 5F, Millar Instruments, TX, USA) at the distal and proximal sections as well as at the inlet of each model, proximal to the dissection.

Flow was measured using an ultrasonic flowmeter (Transonic Systems Inc, NY, USA) at the inlet (15 cm proximal) of the models. Pressure and flow waveforms were acquired using a PowerLab 16/30 with LabChart Pro (ADInstruments, Colorado Springs, CO, USA). We performed echocardiographic imaging with a high-end clinical scanner (Vivid Q – i12L-RS transducer; GE Healthcare, Spain). Grayscale and B-flow imaging were used to visualize structures and flow patterns in the lumina, while velocities at the tears were acquired using pulsed wave Doppler.

3.2.4 Data Analysis

Pressures were temporally aligned based on inlet flow measurements (using minimal flow as reference) and averaged over at least 10 cycles. Pressures were baseline corrected by diastolic inlet pressure and normalized by inlet pulse pressure for model comparison. The systolic time period was defined from minimal inlet flow to the time where pressure decreased to half of its maximal excursion. Systolic and diastolic means were calculated accordingly.

As in Tsai et al. 2008 we computed the FL diastolic pressure index ($FPI_{diastolic}$%) as a percentage of TL diastolic pressure; FL systolic pressure index ($FPI_{systolic}$%) as a percentage of TL systolic pressure; and FL mean pressure index (FPI_{mean}%) as a percentage of TL mean pressure.

Differences in systolic (systolic%) and diastolic pressure (diastolic%) were assessed as a percentage of systolic and diastolic pressure at the inlet, respectively.

3.2.5 Statistical Analysis

All data are expressed as means ± SD. Least squares linear regression was performed to test correspondence between pressure and flow. Group means were analysed by the one-factor ANOVA test. The Mann Whitney U test was used to analyse difference of indexes ($FPI_{systolic}$%, $FPI_{diastolic}$% and FPI_{mean}%) between models with only small tears and at least a large tear. A P value <.05 was considered significant.

3.3 Results

3.3.1 Pressure

Table 3.1 and Table 3.2 show the pressure measurements. In the presence of only small tears (Fig. 3.4; $C_{4,0}$, $C_{0,4}$ and $C_{4,4}$), mean (normalized), systolic mean and diastolic mean FL pressures were lower compared to TL, increasing when there were both proximal and distal small tears. With only small tears, the difference between systolic mean and diastolic mean pressure was less, with damped FL pressure curves (Fig. 3.5a). The existence of at least one large tear increased systolic mean and diastolic mean pressures and led to larger FL pressure variation.
Models with only small tears resulted in bigger pressure gradients between TL and FL, with FL pressure significantly lower than TL compared to cases with at least one large tear (Table 3.3) (Proximal FPI_{mean}% 92.73 ± 3.63 vs 99.85 ± 0.45; Distal FPI_{mean}% 96.35 ± 1.96 vs 99.51 ± 0.80; P<.001), except for the diastolic FL/TL pressure gradient at the distal part, where these models showed a higher pressure difference than those with large tears (Distal $FPI_{diastolic}$% 101.19 ± 0.33 vs 100.07 ± 1.37; P<.001). FL pressure waves were displaced with respect to TL curves with a delayed systolic peak. On the other hand, models with at least a large tear had increased FL pressures equalizing the FL/TL pressure gradient and exhibiting more similar TL and FL pressure waveforms than in presence of only small tears (Fig. 3.5b).

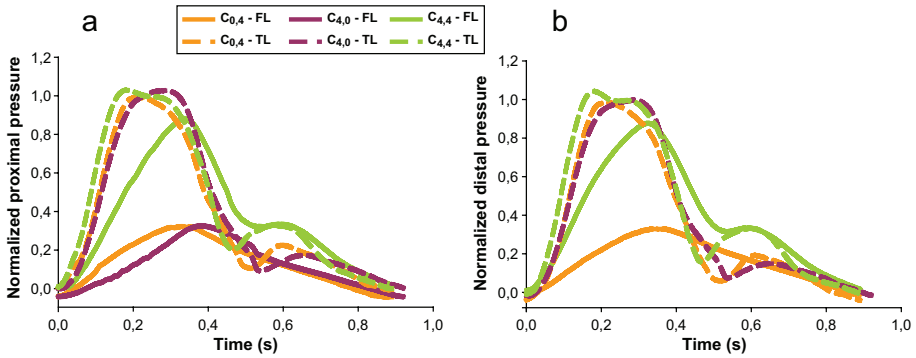

Figure 3.4: Profiles of (a) normalized proximal and (b) distal pressures in presence of only small tears.

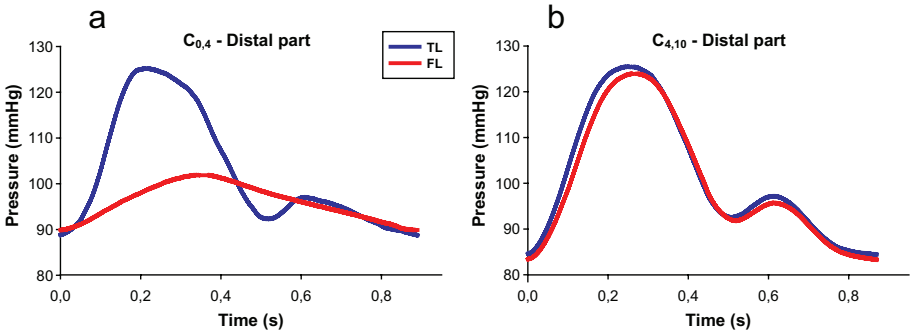

Figure 3.5: Pressure profiles in the true lumen (TL) and false lumen (FL) (a) in the presence of only small tears and (b) in the presence of at least a big tear.

Table 3.1: Pressure (normalized) in all phantoms at different locations

Location	*Model*			
	$C_{4,0}$ $n = 10$	$C_{10,0}$ $n = 11$	$C_{0,4}$ $n = 10$	$C_{0,10}$ $n = 10$
TL Proximal				
Systolic%	101.02 ± 0.25	100.37 ± 0.21[a]	99.90 ± 0.26[a,b]	101.95 ± 0.15[a,b,c]
Diastolic%	99.79 ± 0.23	99.98 ± 0.30	99.48 ± 0.21[b]	101.21 ± 0.14[a,b,c]
Norm mean	0.51 ± 0.01	0.51 ± 0.01[a]	0.49 ± 0.01[a,b]	0.54 ± 0.00[a,b,c]
Systolic mean	0.67 ± 0.02	0.66 ± 0.01	0.65 ± 0.01	0.70 ± 0.01[a,b,c]
Diastolic mean	0.15 ± 0.01	0.20 ± 0.01[a]	0.16 ± 0.00[b]	0.19 ± 0.01[a,b,c]
	$n = 10$	$n = 11$	$n = 10$	$n = 10$
FL Proximal				
Systolic%	77.17 ± 0.09	100.25 ± 0.21[a]	80.87 ± 0.18[a,b]	103.66 ± 0.18[a,b,c]
Diastolic%	97.68 ± 0.17	100.04 ± 0.33[a]	98.20 ± 0.31[a,b]	101.03 ± 0.22[a,b,c]
Norm mean	0.14 ± 0.00	0.50 ± 0.01[a]	0.14 ± 0.01[b]	0.57 ± 0.01[a,b,c]
Systolic mean	0.16 ± 0.01	0.62 ± 0.01[a]	0.19 ± 0.01[a,b]	0.66 ± 0.01[a,b,c]
Diastolic mean	0.05 ± 0.01	0.20 ± 0.01[a]	0.04 ± 0.0[b]	0.22 ± 0.00[a,b,c]
Comparison of proximal pressures				
$FPI_{systolic}$%	76.39 ± 0.17	99.83 ± 0.27[a]	80.99 ± 0.27[a,b]	101.69 ± 0.22[a,b,c]
$FPI_{diastolic}$%	97.89 ± 0.16	100.03 ± 0.36[a]	98.69 ± 0.41[a,b]	99.83 ± 0.29[a,c]
FPI_{mean}%	88.84 ± 0.12	99.54 ± 0.26[a]	91.91 ± 0.29[a,b]	99.69 ± 0.24[a,c]
	$n = 10$	$n = 10$	$n = 11$	$n = 10$
TL Distal				
Systolic%	100.08 ± 0.22	101.12 ± 0.15[a]	99.74 ± 0.16[a,b]	104.65 ± 0.05[a,b,c]
Diastolic%	98.66 ± 0.20	98.65 ± 0.30	98.22 ± 0.18[a,b]	100.37 ± 0.12[a,b,c]
Norm mean	0.49 ± 0.00	0.50 ± 0.01[a]	0.47 ± 0.00[a,b]	0.58 ± 0.00[a,b,c]
Systolic mean	0.64 ± 0.02	0.66 ± 0.01	0.62 ± 0.02[b]	0.73 ± 0.00[a,b,c]
Diastolic mean	0.13 ± 0.00	0.14 ± 0.01[a]	0.12 ± 0.00[a,b]	0.19 ± 0.00[a,b,c]
			$n = 11$	$n = 10$
FL Distal				
Systolic%			81.11 ± 0.15	104.65 ± 0.29[c]
Diastolic%			99.57 ± 0.29	101.99 ± 0.56[c]
Norm mean			0.16 ± 0.01	0.59 ± 0.01[c]
Systolic mean			0.21 ± 0.01	0.69 ± 0.02[c]
Diastolic mean			0.07 ± 0.01	0.23 ± 0.01[c]
Comparison of distal pressures				
$FPI_{systolic}$%			81.29 ± 0.20	100.00 ± 0.28[c]
$FPI_{diastolic}$%			101.39 ± 0.32	101.61 ± 0.59
FPI_{mean}%			94.45 ± 0.17	100.25 ± 0.46[c]

FL, False lumen; *TL*, True lumen; $FPI_{systolic}$%, FL systolic pressure index; $FPI_{diastolic}$%, FL diastolic pressure index; FPI_{mean}%, FL mean pressure index. [a, b, c, d, e, f, g] denote significant differences with respect to $C_{4,0}$, $C_{10,0}$, $C_{0,4}$, $C_{0,10}$, $C_{4,4}$, $C_{4,10}$ and $C_{10,4}$, respectively.

Table 3.1: Continued

Model			
$C_{4,4}$ $n = 10$	$C_{4,10}$ $n = 12$	$C_{10,4}$ $n = 10$	$C_{10,10}$ $n = 10$
$101.03 \pm 0.42^{b,c,d}$	$101.62 \pm 0.18^{a,b,c,d,e}$	$100.38 \pm 0.08^{a,c,d,e,f}$	$100.76 \pm 0.13^{b,c,d,e,f}$
99.93 ± 0.43^{d}	$101.50 \pm 0.22^{a,b,c,d,e}$	$98.00 \pm 0.20^{a,b,c,d,e,f}$	$100.53 \pm 0.19^{a,b,c,d,e,f,g}$
$0.52 \pm 0.01^{c,d}$	$0.54 \pm 0.00^{a,b,c,e}$	$0.49 \pm 0.00^{a,b,c,d,e,f}$	$0.52 \pm 0.00^{a,b,c,d,f,g}$
$0.72 \pm 0.02^{a,b,c,d}$	$0.70 \pm 0.01^{a,b,c,d,e}$	$0.64 \pm 0.01^{a,b,d,e,f}$	$0.66 \pm 0.01^{d,e,f,g}$
$0.20 \pm 0.01^{a,c}$	$0.23 \pm 0.00^{a,b,c,d,e}$	$0.15 \pm 0.01^{b,c,d,e,f}$	$0.21 \pm 0.01^{a,c,d,f,g}$
$n = 10$	$n = 12$	$n = 10$	$n = 10$
$96.17 \pm 0.12^{a,b,c,d}$	$102.80 \pm 0.20^{a,b,c,d,e}$	$101.41 \pm 0.11^{a,b,c,d,e,f}$	$100.84 \pm 0.16^{a,b,c,d,e,f,g}$
$100.28 \pm 0.20^{a,c,d}$	$101.33 \pm 0.26^{a,b,c,e}$	$99.90 \pm 0.14^{a,c,d,e,f}$	$100.40 \pm 0.32^{a,b,c,d,f,g}$
$0.44 \pm 0.00^{a,b,c,d}$	$0.56 \pm 0.01^{a,b,c,d,e}$	$0.52 \pm 0.00^{a,b,c,d,e,f}$	$0.52 \pm 0.01^{a,b,c,d,e,f}$
$0.51 \pm 0.01^{a,b,c,d}$	$0.69 \pm 0.01^{a,b,c,d,e}$	$0.64 \pm 0.01^{a,b,c,d,e,f}$	$0.65 \pm 0.01^{a,b,c,d,e,f}$
$0.22 \pm 0.00^{a,b,c,d}$	$0.23 \pm 0.01^{a,b,c,d,e}$	$0.18 \pm 0.00^{a,b,c,d,e,f}$	$0.20 \pm 0.01^{a,c,e,f,g}$
$95.17 \pm 0.35^{a,b,c,d}$	$101.03 \pm 0.24^{a,b,c,d,e}$	$101.02 \pm 0.17^{a,b,c,d,e}$	$100.09 \pm 0.22^{a,c,d,e,f,g}$
$100.35 \pm 0.40^{a,c,d}$	$99.67 \pm 0.23^{a,c,e}$	$101.94 \pm 0.32^{a,b,c,d,e,f}$	$99.87 \pm 0.32^{a,c,e,g}$
$97.45 \pm 0.34^{a,b,c,d}$	$99.68 \pm 0.14^{a,c,e}$	$100.61 \pm 0.21^{a,b,c,d,e,f}$	$99.70 \pm 0.22^{a,c,e,g}$
$n = 11$	$n = 11$	$n = 10$	$n = 10$
$101.44 \pm 0.30^{a,c,d}$	$104.42 \pm 0.17^{a,b,c,d,e}$	$100.61 \pm 0.10^{a,b,c,d,e,f}$	$101.42 \pm 0.33^{a,c,d,f,g}$
$99.52 \pm 0.22^{a,b,c,d}$	$104.30 \pm 0.23^{a,b,c,d,e}$	$96.89 \pm 0.13^{a,b,c,d,e,f}$	$100.86 \pm 0.37^{a,b,c,d,e,f,g}$
$0.52 \pm 0.01^{a,b,c,d}$	$0.61 \pm 0.00^{a,b,c,d,e}$	$0.48 \pm 0.00^{a,b,d,e,f}$	$0.53 \pm 0.01^{a,b,c,d,e,f,g}$
$0.72 \pm 0.01^{a,b,c}$	$0.77 \pm 0.01^{a,b,c,d,e}$	$0.64 \pm 0.01^{d,e,f}$	$0.67 \pm 0.00^{b,c,d,e,f,g}$
$0.19 \pm 0.01^{a,b,c}$	$0.29 \pm 0.01^{a,b,c,d,e}$	$0.13 \pm 0.01^{b,d,e,f,g}$	$0.21 \pm 0.01^{a,b,c,d,e,f,g}$
$n = 11$	$n = 11$	$n = 10$	$n = 10$
$95.98 \pm 0.13^{c,d}$	$103.16 \pm 0.13^{c,d,e}$	$100.66 \pm 0.18^{c,d,e,f}$	$100.17 \pm 0.27^{c,d,e,f,g}$
$100.52 \pm 0.18^{c,d}$	$102.91 \pm 0.25^{c,d,e}$	$97.92 \pm 0.24^{c,d,e,f}$	$99.82 \pm 0.26^{d,e,f,g}$
$0.44 \pm 0.00^{c,d}$	$0.58 \pm 0.00^{c,d,e}$	$0.49 \pm 0.01^{c,d,e,f}$	$0.50 \pm 0.01^{c,d,e,f,g}$
$0.54 \pm 0.01^{c,d}$	$0.71 \pm 0.01^{c,d,e}$	$0.62 \pm 0.01^{c,d,e,f}$	$0.64 \pm 0.01^{c,d,e,f,g}$
0.22 ± 0.00^{c}	$0.26 \pm 0.01^{c,d,e}$	$0.15 \pm 0.01^{c,d,e,f}$	$0.19 \pm 0.00^{c,d,e,f,g}$
$94.59 \pm 0.37^{c,d}$	$98.79 \pm 0.26^{c,d,e}$	$100.06 \pm 0.22^{c,e,f}$	$98.87 \pm 0.36^{c,d,e,g}$
100.99 ± 0.21^{c}	$98.63 \pm 0.43^{c,d,e}$	101.11 ± 0.30^{f}	$99.09 \pm 0.42^{c,d,e,g}$
$98.26 \pm 0.22^{c,d}$	$98.59 \pm 0.33^{c,d}$	$100.19 \pm 0.19^{e,e,f}$	$99.10 \pm 0.38^{c,d,e,g}$

Table 3.2: Pressure measurements in all phantoms at different locations

Location	*Model*			
	$C_{4,0}$ $n = 10$	$C_{10,0}$ $n = 12$	$C_{0,4}$ $n = 12$	$C_{0,10}$ $n = 10$
Inlet				
Systolic (mm Hg)	118.85 ± 0.18	120.68 ± 0.18	125.73 ± 0.27	118.04 ± 0.11
Diastolic (mm Hg)	78.46 ± 0.13	80.82 ± 0.18	90.20 ± 0.25	80.20 ± 0.20
	$n = 10$	$n = 11$	$n = 10$	$n = 10$
TL Proximal				
Systolic (mm Hg)	120.07 ± 0.29	121.16 ± 0.25	125.61 ± 0.32	120.34 ± 0.18
Diastolic (mm Hg)	78.29 ± 0.18	80.80 ± 0.25	89.73 ± 0.19	81.17 ± 0.11
Mean (mm Hg)	93.77 ± 0.17	97.82 ± 0.21	103.46 ± 0.09	97.56 ± 0.10
	$n = 10$	$n = 11$	$n = 10$	$n = 10$
FL Proximal				
Systolic (mm Hg)	91.72 ± 0.10	120.98 ± 0.26	101.68 ± 0.23	122.37 ± 0.21
Diastolic (mm Hg)	76.64 ± 0.13	80.85 ± 0.26	88.57 ± 0.28	81.03 ± 0.18
Mean (mm Hg)	83.30 ± 0.08	97.37 ± 0.26	95.08 ± 0.25	97.26 ± 0.18
	$n = 10$	$n = 10$	$n = 11$	$n = 10$
TL Distal				
Systolic (mm Hg)	118.95 ± 0.26	124.31 ± 0.19	125.40 ± 0.20	123.53 ± 0.06
Diastolic (mm Hg)	77.40 ± 0.15	82.54 ± 0.25	88.59 ± 0.16	80.50 ± 0.09
Mean (mm Hg)	92.85 ± 0.11	99.49 ± 0.19	102.46 ± 0.13	97.77 ± 0.06
			$n = 11$	$n = 10$
FL Distal				
Systolic (mm Hg)			101.98 ± 0.18	123.53 ± 0.34
Diastolic (mm Hg)			89.81 ± 0.26	81.79 ± 0.45
Mean (mm Hg)			96.01 ± 0.19	98.01 ± 0.46

FL, False lumen; *TL*, True lumen.

Table 3.2: Continued.

Model			
$C_{4,4}$ $n = 12$	$C_{4,10}$ $n = 13$	$C_{10,4}$ $n = 10$	$C_{10,10}$ $n = 11$
121.08 ± 0.37 81.71 ± 0.28	120.16 ± 0.16 80.94 ± 0.25	118.22 ± 0.13 79.77 ± 0.15	120.34 ± 0.15 80.79 ± 0.19
$n = 10$	$n = 12$	$n = 10$	$n = 10$
122.33 ± 0.51 81.66 ± 0.35 98.84 ± 0.38	122.11 ± 0.22 82.15 ± 0.17 99.16 ± 0.19	118.67 ± 0.10 78.18 ± 0.16 95.08 ± 0.10	121.25 ± 0.15 81.22 ± 0.15 97.83 ± 0.16
$n = 10$	$n = 12$	$n = 10$	$n = 10$
116.43 ± 0.14 81.95 ± 0.16 96.33 ± 0.12	123.52 ± 0.24 82.02 ± 0.21 98.99 ± 0.19	119.89 ± 0.13 79.69 ± 0.11 95.66 ± 0.11	121.35 ± 0.20 81.11 ± 0.26 97.52 ± 0.22
$n = 11$	$n = 11$	$n = 10$	$n = 10$
122.82 ± 0.36 81.32 ± 0.18 98.60 ± 0.21	125.47 ± 0.20 84.42 ± 0.19 101.42 ± 0.19	118.94 ± 0.12 77.29 ± 0.11 94.57 ± 0.09	122.05 ± 0.40 81.49 ± 0.30 98.07 ± 0.36
$n = 11$	$n = 11$	$n = 10$	$n = 10$
116.21 ± 0.16 82.14 ± 0.14 96.87 ± 0.13	123.96 ± 0.15 83.30 ± 0.21 100.03 ± 0.17	118.97 ± 0.21 78.11 ± 0.20 94.71 ± 0.16	120.55 ± 0.33 80.65 ± 0.21 97.09 ± 0.23

Table 3.3: Indexes in anatomic configurations with only small tears and at least a large tear

Location	*Anatomic configuration*	
	Only small tears $n = 30$	*At least a large tear* $n = 50$
Proximal part		
$FPI_{systolic}$%	84.18 ± 8.13	100.74 ± 0.72
$FPI_{diastolic}$%	98.98 ± 1.09	100.28 ± 0.91
FPI_{mean}%	92.73 ± 3.63	99.85 ± 0.45
	$n = 20$	$n = 40$
Distal part		
$FPI_{systolic}$%	87.94 ± 6.83	99.41 ± 0.67
$FPI_{diastolic}$%	101.19 ± 0.33	100.07 ± 1.37
FPI_{mean}%	96.35 ± 1.96	99.51 ± 0.80

$FPI_{systolic}$%, FL systolic pressure index; $FPI_{diastolic}$%, FL diastolic pressure index; FPI_{mean}%, FL mean pressure index.
$P < .001$ for all comparisons.

3.3.2 Tear Velocity

Velocities across the communications (Fig. 3.6 and Table 3.4) are determined by the pressure gradient and therefore were different for the different tear sizes and configurations.

Flow was bidirectional, with flow from TL to FL during systole and in the opposite direction during diastole. Thus, during systole, there was inflow into the FL from both the proximal and distal tear while in diastole there was discharge from both tears simultaneously suggesting that most of the volume entered end left the FL from the same tear instead of going from a proximal entry towards a distal exit.

The presence of only small tears exhibited clearly elevated maximum systolic and diastolic velocities across the same tear (systolic velocity > 290 cm/s and diastolic velocity > 160 cm/s). The presence of two small tears slightly reduced velocities compared to cases with only one small tear. On the other hand, in the presence of at least one large tear, peak systolic and diastolic velocities, even at small tears, were decreased by more than half in some cases. Flow was always bidirectional, but, in these cases, with an important discharge during early diastole and almost no discharge at late diastole.

In addition, $C_{4,10}$ showed a bidirectional flow across the small proximal tear with a tricyclic structure during diastole, directed from FL to TL at early diastole and then going in and going out again.

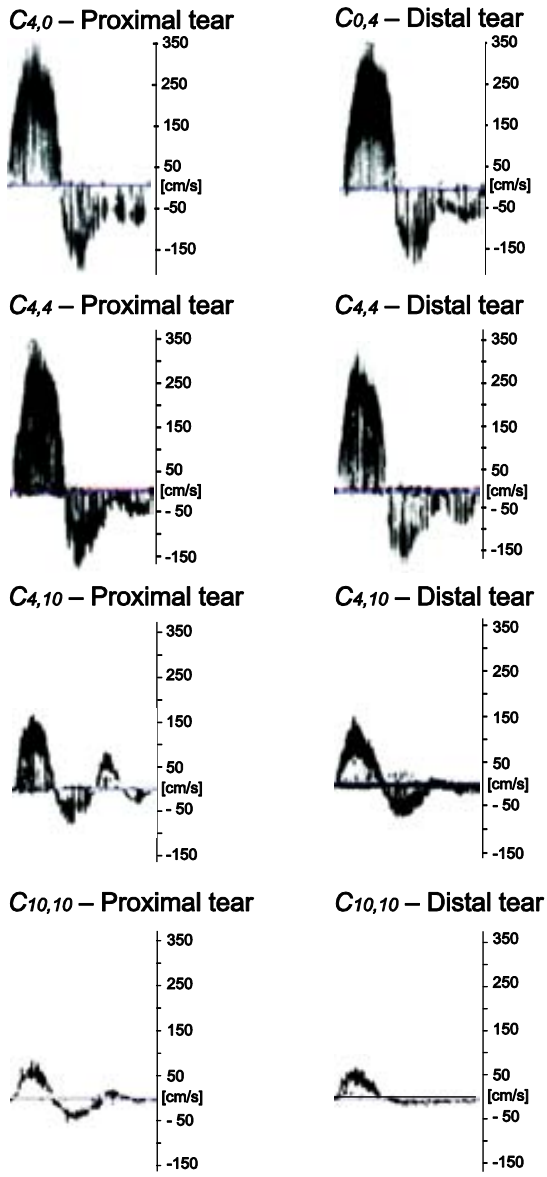

Figure 3.6: Velocities through the tears in different morphologic configurations: with only one small tear; two small tears; one small tear and one large tear; and two large tears. The highest systolic and diastolic velocities corresponded to models with only small tears. Inward/systolic velocities are positive and outwards/diastolic velocities are negative. *C*, Case.

Table 3.4: Peak systolic and diastolic velocities across proximal and distal tears in all phantoms

	Model			
Location	$C_{4,0}$ $n = 10$	$C_{10,0}$ $n = 10$	$C_{0,4}$ $n = 10$	$C_{0,10}$ $n = 10$
Proximal tear				
Peak systolic velocity (cm/s)	319.400 ± 9.800	149.310 ± 1.493		
Peak diastolic velocity (cm/s)	186.300 ± 5.460	78.600 ±1.647		
Distal tear				
Peak systolic velocity (cm/s)			324.900 ± 3.071	172.200 ± 6.233
Peak diastolic velocity (cm/s)			185.400 ± 6.433	86.100 ± 3.446

3.3.3 Correspondence between Pressures and Velocities

Since we measured tear velocities and pressure gradients non-simultaneously and with different technologies, we checked correspondence between maximal velocities calculated (using the simplified Bernoulli equation) from the gradients of measured pressures and maximal Doppler velocities. Figure 3.7 shows the statistically significant linear regression.

3.3.4 Volume Exchange

The volume passing through a tear was derived using pulsed-wave Doppler by integrating velocities over one cycle and multiplying by the area.

Figure 3.8 shows the total volume going in and out of the tears in the different models during one cycle. The total incoming (V_{in}) and outgoing (V_{out}) volume for each model was the same (conservation of volume). Cases $C_{10,0}$ and $C_{0,10}$ (only one big tear) showed the highest V_{in}, even more than case $C_{10,10}$ which has two big tears. Case $C_{0,4}$ also showed a bigger total V_{in} than case $C_{10,10}$. Therefore, total incoming volume was not necessarily directly related to number and size of tears but rather to the combination of tears.

Figure 3.9 shows FL V_{in} and V_{out} for each model. $C_{4,0}$ and $C_{0,4}$ on one hand, and $C_{10,0}$ and $C_{0,10}$ on the other hand, had similar Vin, resulting from the same tear number and size despite different location.

All cases presented a balanced V_{in}/V_{out} rate at each tear.

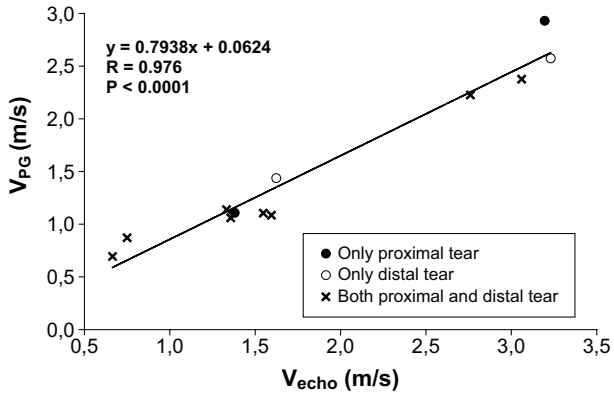

Figure 3.7: Relationship between the maximum velocity registered by ultrasound (V_{echo}) and the maximum velocity computed from the TL/FL pressure gradient using the simplified Bernoulli equation (V_{PG}). *TL*, True lumen; *FL*, False lumen.

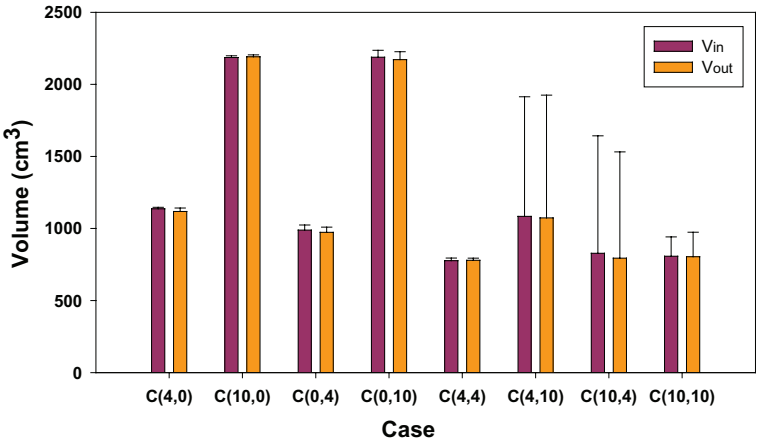

Figure 3.8: Total incoming (V_{in}) and outgoing (V_{out}) volume registered in the false lumen for each model during a pump cycle. *Error bars* represent SD.

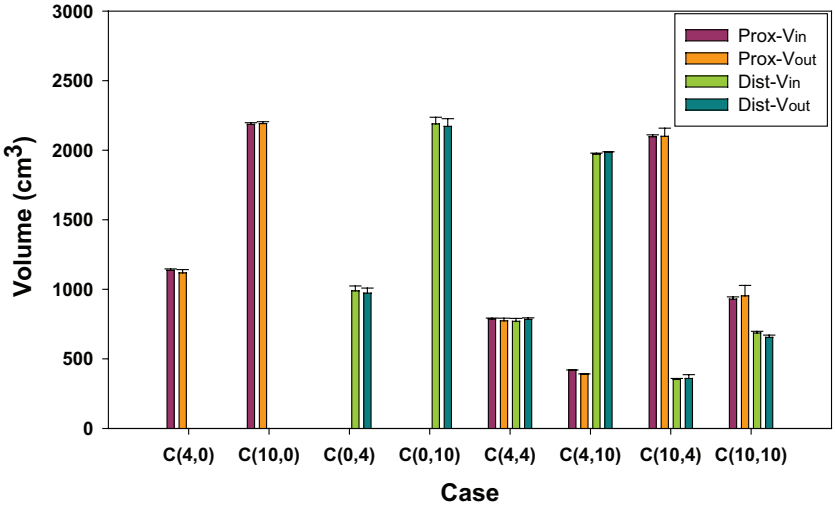

Figure 3.9: Volume going in (V_{in}) and going out (V_{out}) the false lumen across the proximal and distal tears for each model during a cardiac cycle. Error bars represent SD.

3.3.5 Flow Patterns

The way in which flow entered the FL depended on tear size (Fig. 3.10). A small tear resulted in a concentrated jet-like inflow directly hitting the FL wall, while a large tear resulted in a wider, less focused jet colliding with the wall in an oblique way and affecting a more extensive area. This pattern only depended on tear size, because no differences were detected between jets at proximal and distal tears when size was similar. Once flow entered the FL and mostly during diastole, the areas near large tears showed important flow separation, formation of vortices and development of turbulence. In particular, $C_{10,10}$ and $C_{0,10}$ showed large areas of turbulence at the distal site.

We observed bidirectional flow across tears in all models. Thus, all were acting as entry and exit during some periods of the cycle.

Although phantoms with open communication showed bidirectional FL flow, flow velocities in the middle section seemed to be significantly reduced with presence of only sporadic collisions of flows coming from different directions (Fig. 3.11a). Moreover, we observed low FL latent flow at the blind side in phantoms with only one tear. Here, flow propagated to the blind end and reflected back towards the open tear, resulting in flow collisions between entering and reflected flow. However, only in cases with a single small tear, there was a significant recirculation at the blind end and an important flow activity at the middle (Fig. 3.11b and Fig. 3.11c).

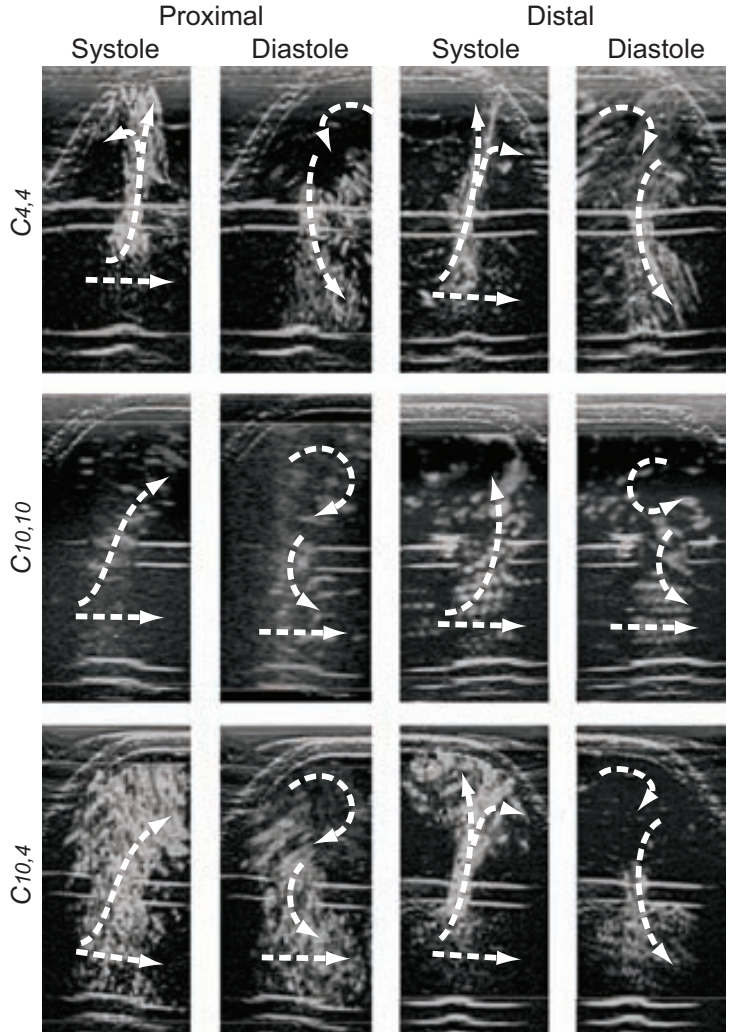

Figure 3.10: Flow patterns within the dissected models at peak systole and peak diastole. A concentrated jet-like inflow hitting the false lumen (FL) wall during peak systole is observed at small proximal and distal tears. On the other hand, inflow in the FL is a diffuse and oblique one in the FL at large proximal and distal tears. Vortex and turbulence formation in the FL at large tears are exhibited during peak diastole.

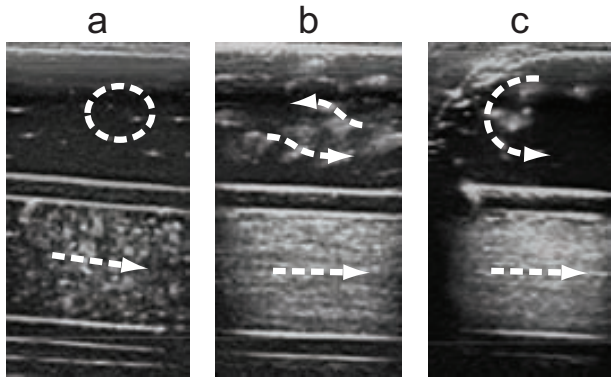

Figure 3.11: (a) Latent flow with sporadic collisions registered at the false lumen (FL) middle section of case $C_{10,4}$. (b) Significant bidirectional FL flow registered at the middle section of case $C_{0,4}$. (c) Reflection and recirculation at the blind end of case $C_{0,4}$. *C*, Case.

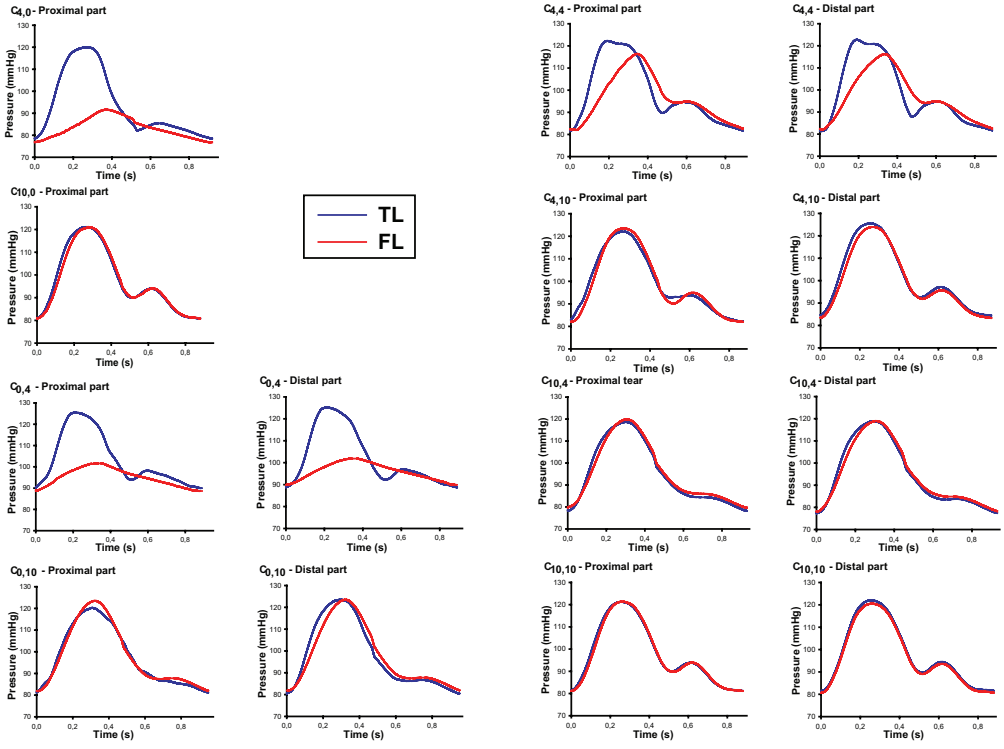

Figure 3.12: True lumen (TL) and false lumen (FL) pressure waveforms during a pump cycle at the proximal and distal part of the dissected segment.

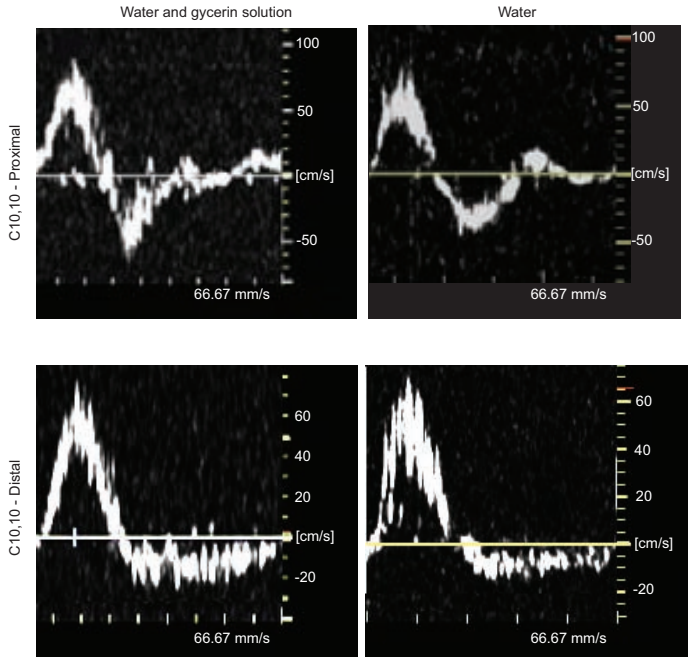

Figure 3.13: Velocities registered across the tears at the proximal and distal part of case $C_{10,10}$ for different perfusion fluids (water at room temperature vs. glycerin and water solution at 37ºC).

3.4 Discussion

Our main findings are that pressures, and therefore tear velocities, mainly depend on the accumulated size of all tears. With large tears present, irrespective of location, FL and TL pressures equalize and FL velocities are low with complex flow, whereas with only small tears, FL pressures never reach TL levels and high velocity jets, impinging the wall, are present. Additionally, both proximal and distal tears act as entry and exit into the FL. During systole, flow enters the FL through all tears simultaneously while during diastole, flow leaves through all communications. Flow within the FL, from proximal to distal tears or vice versa, is minimal. Therefore, the FL acts as a side-chamber of the TL, and FL pressure waveforms are a damped version of the TL's, with damping inversely proportional to the cumulative size of connecting orifices.

While some clinical (Strotzer et al. 2000; Inoue et al. 2000) and in-vitro (Iwai et al. 1991; Chung et al. 2000; Tsai et al. 2008) studies evaluated haemodynamics in aortic dissections, none performed an integrated analysis of influence of tear configuration on TL/FL flow, pressures and velocities across tears. The present in-vitro study provides insight in how TL and FL hydrodynamics are highly influenced by morphological configuration of aortic dissections, especially by tear presence/location and size. We assessed TL and FL pressures at the proximal and distal sites of the lumina, velocities across the tears and flow patterns within the whole FL, and showed how cumulative

tear size influences them, which has not been done before. This provides novel insight since flow is a relevant factor for remodelling and its behaviour is complex along the lumen. When managing patients with chronic type B dissections based on imaging, flow patterns and velocities can be easily assessed non-invasively, thus providing information on luminal pressures.

Our setup captured clinically observed phenomena, such as bidirectional tear flow (Mohr-Kahaly et al. 1989), multiphasic velocities during diastole (Massabuau et al. 2006), retrograde FL flow (Mohr-Kahaly et al. 1989; Strotzer et al. 2000, Inoue et al. 2000) and high FL pressures in the presence of large communications (Erbel et al. 1993).

Aortic dilatation is multi-factorial, depending mostly on wall-stresses induced by cyclic FL pressure. High pressure increases circumferential stress and distention. Chronically, this changes FL elasticity, due to loss of muscle-cells and collagen accumulation (Evangelista and González-Alujas 2006). In our findings, TL/FL pressure gradients, as well as FL pressures, were determined by tear size (Table 3.3, Fig. 3.12). Cases with at least one large tear showed pressure equalization and exposed FL to higher pressures, similar to Tsai et al. 2008 and Chung et al. 2000. Due to the damping effect of orifices, inhibiting fast pressure changes, FL pressures were lower during early systole, approaching TL pressures later during systole (if tears are sufficiently large). In diastole, FL pressure drops slower, resulting in slightly increased diastolic pressures, depending on presence/size of (mainly distal) tears. When diastolic pressure waveforms are realistic and long enough (as in our setup compared to Tsai et al. 2008), and orifices large, TL and FL diastolic pressures rapidly equalize. These findings, of dampened pressure waveforms, are supported by Tsai et al. 2008, where the difference between TL and FL pressures, especially for smaller tears, becomes bigger with increasing heart rate. Therefore, both cumulative orifice sizes, as well as duration of individual phases of the cycle, play a role in the resulting FL pressure trace.

These findings might explain clinical studies of dilatation after surgery with proximal tear closure, because of presence of residual distal communications with considerable cumulative size (Erbel et al. 2001; Schoder et al. 2007).

Flow patterns and haemodynamic forces play an important role in the pathogenesis of vascular diseases (Asakura et al. 1990; Raghavan et al. 2000). In-vivo observations indicate that flow complexity and WSS alterations play critical roles in remodelling (Kamiya et al. 1980; Cheng et al. 2006). Fast laminar flow and oriented high WSS encourage endothelial and smooth muscle development (Hoshina et al. 2003), enhancing tissue integrity while complex flow patterns with low/reciprocating WSS lead to increased inflammation, mechanical weakening, dilatation and rupture (Malek et al. 1999).

Our study exposes how presence of only small tears led to high tear velocities and more defined FL flows that may protect tissue integrity. On the contrary, the presence of at least a big tear reduced velocities significantly and resulted in higher vorticity close to big tears, and almost no volume displacement, suggesting that the tissue may be more susceptible to dilatation.

In all configurations, flow across tears was bidirectional, meaning that they acted as entry as well as exit during some periods of the cycle (in line with Stroetzer et al. 2000, Inoue et al. 2000 and Mohr-Kahaly et al. 1989). Volume exchange and tear velocities reflected this, where flow was directed from TL into FL during systole and in opposite direction during diastole, with balanced V_{in}/V_{out} ratios.

While evaluation of dissection haemodynamics, in particular flows and WSS, are difficult and complex in-vivo, an in-vitro approach offers means to study the integrative behaviour of dissections and show that tear size and placement clearly determine pressures, flow patterns and velocities.

3.4.1 Limitations

We used silicone/latex with potentially different compliance than the aorta. Coming closer to aortic compliance might result in a different distribution of volume going in/out at the tears, but is not expected to majorly change the conclusions and captured phenomena.

We studied idealized models with maximal two tears, while patients regularly present with more tears (Quint et al. 2003) or with the dissection beginning exactly at a tear. Our tears are normal to the flow while in patients these are often more in-line. However, while dynamic pressure, influenced by local flow, might vary, the major determinants of pressure drop over and velocity within tears are static pressures, which are mainly determined by tear size.

The phantoms lacked arterial branches while in reality several are present. This could result in more FL inflow and unidirectional flow instead of bidirectional flow as observed.

The idealized anatomy might influence results, as geometrical changes haemodynamics. Our model represents a linear dissection while in-vivo dissections can be more complex with presence of tortuosities and spiral flaps that may make the characteristics of the lumina more complex. Nevertheless, dimensions were based on clinical measurements and generic models seem to be ideal for parametric studies and to give first insight into the influence of dissection configurations on haemodynamics. As modelled in Tsai et al. 2008 phantoms had reduced flap motion. This is common in patients with chronic dissections that show a more rigid or calcified flap (LePage et al. 2001; Rubin et al. 2006). Tears were circular, which is a reasonable approximation to what is observed in humans in the chronic phase (Williams et al. 1993) and when focussing on pressures and maximal tear velocities.

We used water at room temperature as in Chung et al. 2000, which is less viscous than blood. However, we did not detect important differences in velocity values and patterns when using a glycerin/water solution at 37ºC, with viscosity and density similar to blood (Fig. 3.13).

Doppler was used to measure velocities. While being the technique of choice for clinical follow-up (Evangelista et al. 2010), it is angle-dependent. However, we ensured that the angle was small by imaging perpendicular to the wall.

We performed retrograde catheterization to measure pressures in order to maintain wall integrity, and to use a standard clinical approach for pressure assessment. This potentially caused partial tear obstruction by the transducer when in the FL. This also prevented measuring distal FL pressures in models with only a proximal tear, because of lack of catheter flexibility to make a 180o turn to access to the distal site.

3.4.2 Practical Application

At present, follow-up and treatment of patients with aortic dissection seem to be non-ideal and it remains difficult to balance high morbidity and mortality rates registered during the chronic phase of the disease, with side effects and risks of surgical or endovascular interventions. In current clinical practice, prediction of outcome is mainly based on maximum total aortic diameter, which is compared to clinical guidelines for deciding on the best therapy. However, this has proven to show severe limitations in assessing genesis and evolution of dissections (Nollen et al. 2004; Neri et al. 2005). Therefore, the need for better predictors of evolution of aortic dissection is evident, especially to predict FL dilatation and to evaluate and titrate a better pharmacological management.

The study by Evangelista et al. 2012 in patients with chronic dissections identified the presence of a large entry tear as predictor of complications and mortality. In line with this, our study demonstrates how cumulative tear size might negatively influence FL flow patterns and pressures, and velocities across tears. Therefore, this study provides information that could be of importance during follow-up of patients using imaging techniques, such as Magnetic Resonance Imaging, Transesophageal Echocardiography and Computed Tomography.

CHAPTER 4

Validation of Numerical Flow Simulations against In Vitro Phantom Measurements in Different Type-B Aortic Dissection Scenarios

Abstract - *An aortic dissection (AD) is a serious condition defined by the splitting of the arterial wall, thus generating a secondary lumen (the false lumen - FL). Its management, treatment and follow-up are clinical challenges due to the progressive aortic dilatation and potentially severe complications during follow-up. It is well known that the direction and rate of dilatation of the artery wall depend on haemodynamic parameters like the local velocity profiles, intraluminal pressures and resultant wall stresses. These factors act on the FL and true lumen (TL), triggering remodelling and clinical worsening. In this study, we aimed to validate a Computational Fluid Dynamic (CFD) tool for the haemodynamic characterization of chronic (type B) ADs. We validated the numerical results, for several dissection geometries, with experimental data obtained from a previous in-vitro study performed on idealized dissected physical models. We found a good correlation between CFD simulations and experimental measurements as long as the tear size was large enough so that the effect of the wall compliance was negligible.*

Adapted from Eduardo Soudah, Paula Rudenick, Maurizio Bordone, Bart Bijnens, David García-Dorado, Arturo Evangelista and Eugenio Oñate. Validation of Numerical Flow Simulations Against in Vitro Phantom Measurements in Different Type B Aortic Dissection Scenarios. *Computer Methods in Biomechanics and Biomedical Engineering*. 2013. In press.

4.1 Introduction

Aortic dissections (ADs) represent an important subgroup within the aortic diseases and are associated with a high morbidity and mortality (more than 50% in the acute phase) (Hagan et al. 2000). In particular, during the chronic phase, descending ADs (type B) dissections result in a high long-term morbidity and mortality because of dissection recurrence, progressive lumen dilatation (particularly of the false lumen (FL)) and aortic rupture (Fattori et al. 2011).

The haemodynamics within the lumina is one of the underlying factors associated with the progression of chronic ADs (Gimbrone et al. 2000; Davies et al. 2005). The intraluminal pressure has a direct effect on the aortic wall, determining local tissue mechanical stress. High pressures are therefore important risk factors for worse prognosis. Clinical observations show that the presence of large proximal tears (Evangelista et al. 2012) and a patent FL (Erbel et al. 1993) show a worse prognosis, maybe due to the high resultant FL pressures (Rudenick et al. 2013a) and associated wall stress. However, in clinical practice, intra-luminal pressures cannot be measured non-invasively.

Currently, the use of numerical tools to simulate and characterize blood dynamics in the cardiovascular system is becoming more easily available. Especially, the application of Computational Fluid Dynamics (CFD) simulations is emerging in the biomedical field and is presented as a reliable methodology to study cardiovascular diseases based on simulated haemodynamic parameters, like pressures and wall shear stress (WSS). However, validation of these numerical results is of particular interest and although there are some CFD studies oriented to the assessment of haemodynamics in type B ADs (Karmonik et al 2011, 2012), in none of them, a quantitative validation of the computational solutions has been performed.

Therefore, this study was aimed at applying a CFD methodology to the characterization of haemodynamics in chronic ADs (through the assessment of pressures in the lumina) for four different (idealized) dissection geometries and validating it with the in-vitro results from a previous study (Rudenick et al. 2013a).

Figure 4.1: Reproduction of the FEM geometry.

Table 4.1: Scenarios validated in the study

Case	*Proximal tear diameter (mm)*	*Distal tear diameter (mm)*
A	4	-
B	-	4
C	10	4
D	10	10

4.2 Methodology

The idealized geometric characteristics of the computational models, rheological data of the test fluid and the inflow and outflow boundary conditions for the numerical finite element method (FEM) simulations were based on the results from a previous in-vitro study (Rudenick et al. 2013a). We used the experimentally measured in-vitro pressures, at different sites of the dissected segment, to validate the values predicted by the numerical model.

4.2.1 Computational Models

Based on the geometry and dimensions of the physical phantoms, used in the in-vitro study (Rudenick et al. 2013a), the computational three-dimensional (3D) finite element models and fluid meshes were constructed with GiD (CIMNE, Barcelona, Spain) (Fig. 4.1) (CIMNE 2006; Bordone et al. 2010). The generic geometry consisted of 2 channels, the true lumen (TL) and the FL (surrounding the TL), connected by circular holes, representing the proximal and distal tears (Fig.2). The dimensions of the computational model were: TL diameter=14 mm; dissected segment diameter=40 mm; FL length=160 mm; dissection flap thickness=2 mm; TL length: 390mm. The centres of the proximal and distal tears were located at 175.5 and 320.5 mm, respectively, from the inlet of the model.

Four typical dissection geometries (Table 4.1), found in clinical practice, were numerically validated. These geometries represent different anatomic con-figurations, varying tear size (with a diameter of 4mm = a ‘clinically’ small tear or 10mm = a ‘clinically’ large tear), location (distal/proximal) and number (1/2).

The computational meshes consisted of approximately 1.5-2 million tetrahedral elements with a size range of 0.5-1.0 mm. A mesh sensitivity analysis was performed to ensure a smooth element with a tetrahedral element aspect ratio above 0.9 (ideal ratio=1 for an equilateral triangle).

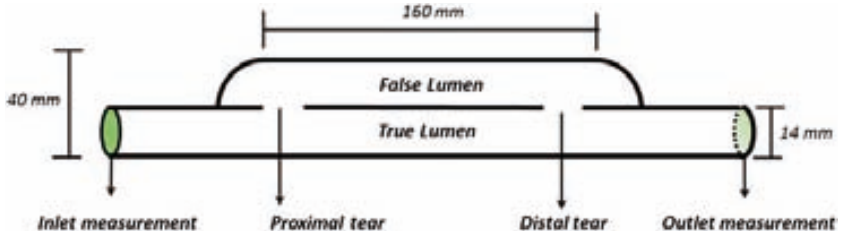

Figure 4.2: Generic geometry of an aortic dissection of type B.

4.2.2 Numerical Simulations

CFD simulations were performed using the CFD code Tdyn (CompassIS, Barcelona, Spain (Compass website)). This code solves the Navier-Stokes equations for an incompressible and homogeneous Newtonian fluid using a stabilized FEM.

We used water at 25 degrees Celsius as perfusion fluid, with a density of 996 kg/m^3 and a viscosity of 0.86 e^{-3} kg/(m s). We assumed it to be incompressible, homogeneous and Newtonian, with no external forces applied on it.

The no-slip wall of the dissection model was assumed to be rigid (Eq. 4.1). Since in chronic dissections there is reduced flap motion, a rigid flap is a good first approximation. In addition, Leung et al. 2006 suggested that the difference in flow induced pressure variations and consequent wall stress between rigid and elastic aortic models is negligible.

Time-dependent flow and pressure waveforms, obtained from the in-vitro experiments, were applied at the inlet and outlet of the fluid domain, respectively. A fully developed parabolic velocity profile was applied at the inlet (Eq. 4.2), and a time dependent normal traction, according to the luminal pressure profile, is imposed at the outlet (Eq. 4.3). Mathematically, these boundary conditions can be expressed as follows:

$$\quad (4.1)$$

$$\quad (4.2)$$

$$\quad (4.3)$$

where d_r is the inner radius of the TL, u_r is the Cartesian components of the velocity vector in the Z-direction, and $u(t)$ and $p(t)$ are the time-dependent velocity and pressure waveforms taken from the in-vitro experiments. Pressure boundary conditions are given by (Eq. 4.3), where t_n is the normal traction at the outlet, I is the standard identity matrix and n represents the normal vector of the respective boundary.

Due to the high *Re* number within the tear areas, a turbulence model is included. The turbulence model chosen was the Spalart-Allmaras model (Spalart et al. 2000). The aim of this model is to improve the predictions obtained with algebraic mixing-length models to develop a local model for complex flows, and to provide a simpler alternative to two-equations turbulence models. The model uses the distance to the nearest wall in its formulation, and provides smooth laminar-turbulent transition capabilities. It does not require a grid resolution in wall-bounded flows as fine as the two-equation turbulence models, and it shows good convergence for simpler flows. The empirical results used in the development of the model were mixing layers, wakes and flat-plate boundary layer flows. The model gives very accurate predictions of complex turbulent flows. It also shows improvements in the prediction of flows with adverse pressure gradients compared to k-e and k-v models.

The CFD simulations were performed over a time of 1.8s (representing two cardiac cycles). The time integration method chosen was a backward Euler, using a biconjugate gradient non-symmetric solver (Barrett et al. 1994) in order to accelerate the calculation time performance. We used a pressure stabilization of fourth order and automatic velocity advection stabilization. The total CPU time for a single CFD analysis in a standard PC with Microsoft Windows XP, 32-bit 4 GB RAM and dual-core 2.83 GHz CPU was about 10 h depending of the case.

For each simulation analysis, we assessed the intraluminal pressures in the FL and TL at the distal and proximal sites of the dissected model, where appropriate (Fig. 4.2).

4.2.3 In-vitro Data

For validation of the numerical simulations, we used the setup and experimental data from a previous in-vitro study (Rudenick et al. 2013a).

The in-vitro setup consisted of a dynamic flow circuit mimicking the cardio-vascular system, where a pulsatile pump, a compliance chamber, a dissection phantom and a collecting system were connected in series (Fig. 4.3).

The phantom was a compliant model made of latex and silicone to recreate a simplified typical AD, where FL and TL are connected by circular holes resembling the tears in the dissection flap.

Pressures were measured, using retrograde catheterization, within the FL and TL of the model at a proximal and distal site, using a pressure transducer (SPC-350 5F, Millar Instruments, Texas, USA). Only for Case A, FL distal pressure could not be measured using this approach since the catheter could not be bended 180 degrees. Flow traces were measured at the inlet of the model, 15 cm before the dissected segment, with an ultrasonic flow meter (Transonic Systems, Inc., Ithaca, NY, USA). Pressure and flow measurements were registered/digitized using a PowerLab 16/30 with LabChat Pro acquisition and analysis software (ADInstruments, Colorado Springs, CO, USA). A more detailed description of the in-vitro setup can be found in (Rudenick et al. 2013a).

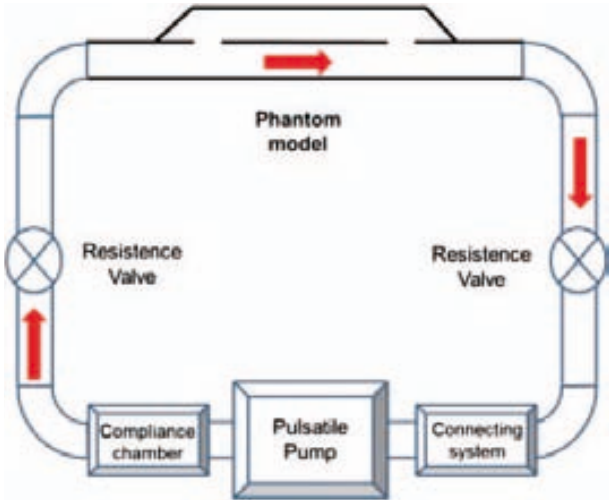

Figure 4.3: Schema of the dynamic flow circuit used for the in-vitro experiments.

4.2.4 In-silico Configurations and Imposed Boundary Conditions

Figure 4.4 shows the four configurations of ADs modelled together with the sites where in-vitro pressures were available and in-silico ones were validated.

Figure 4.5 (Top) shows the in-vitro pressure profiles measured at the outlet in the hydraulic model for the four dissection configurations. Note that the pressure waveform was realistic, representing normal haemodynamic conditions in this area of the human aorta, with a peak pressure occurring at the interval 0.27-0.3 s and a biphasic diastolic period. Figure 4.5 (Bottom) shows the velocity profiles computed from the flows measured at the inlet for the four configurations in the hydraulic model. The cycle period has a duration included between 0.88 and 0.95 s, with a peak flow occurring at 0.18-0.2 s.

4.3 Results

In this section, we compare the in-vitro pressure waveforms with the numerical predictions. It is important to stress that none of the parameters involved in the simulation have been tuned, except for phase matching of the onset of the experimental and numerical systolic ejections during data post-processing.

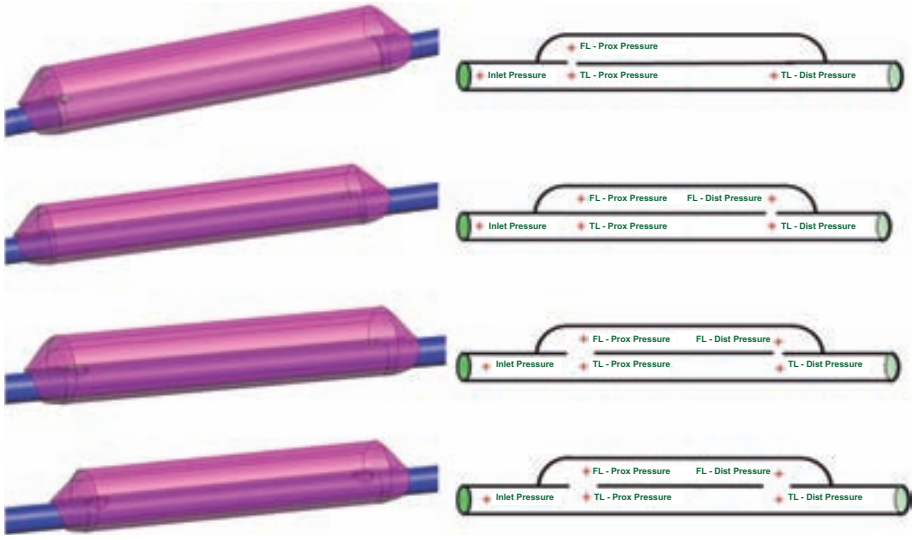

Figure 4.4: In-silico FEM geometries (Right) and schematic representation (Left) for the four in-vitro type B AD scenarios. From top to bottom: Case A, Case B, Case C and Case D.

4.3.1 Comparison between Experimental and Numerical Results

Figures 4.6-9 show the comparison between the experimental and numerical pressure waveforms at four representative points for each of the dissected models. For each, the inlet pressures, together with relevant points in the TL and FL are presented. Table 4.2 provides the numerical values for the difference between measured and simulated cases.

In all cases, the inlet and TL pressures are very similar for the measured and simulated traces. Since the outlet pressure was used as a boundary condition, the further away from it, towards the inlet, the more different the pressure curve, but differences are within acceptable levels. This can be caused by differences between the numerical and experimental models (rigid/elastic wall) and some uncertainties in the experimental setup (e.g. the exact location and position of the catheter inside the aorta), which makes it more difficult to exactly compare the in-vitro and in-silico measurements.

For cases with at least one large hole (Cases C and D), the FL pressures are also very comparable between measurements and simulations.

Only for cases with only one small hole (Cases A and B), the FL measured pressures are clearly different from the simulated ones, while the shapes and values of the profiles at the TL positions are quite similar. Since the measured values are much lower and seem to have been low-pass filtered, the difference can be explained to a large extent by the difficulty to reproduce the experimental measurements in an elastic model with the numerical, rigid wall model.

In addition, all the pressure measurements were done using retrograde catheterization (Evangelista et al. 2012), which may have caused partial obstruction of the tears, thus reducing their effective size and altering the pressure measurements at the proximal and distal FL (especially for small holes as in Cases A and B).

Quantitatively, there are modest relative errors between the numerical and experimental waveforms (Table 4.2) for most of the measurements. Except for the FL with only small holes, these errors, depending of the point studied, are < 10% for the pressure profile. In Case A, the TL error at the proximal section is < 9% and at the distal section it is 0.3%, showing a good approximation for the TL in this configuration of AD. In Case B, pressure profiles at the TL are even closer to the experimental measurements and the mean error is around 2% at the proximal TL and 0.2% at the distal TL. In Case C, the inlet error is 7.3%, in the distal FL and proximal TL points the errors are around 5% and in the proximal TL the error is 4.64%. For the TL, the mean error in Case D is 3.64% with a maximum value of < 9.4 %.

Therefore, we can conclude that the CFD simulation are able to capture the main features of pressure traces observed in-vitro, such as the diastolic decay and peaking and steepening of pulse pressure for the different points measured in the TL and FL. Only in case of the presence of only small tears, the FL pressures are not reliable using this approach.

Table 4.2: Error values in percentage for the different positions of measurement

	Distal FL			*Distal*			*Proximal FL*		
Case	Min.	Max	Mean	Min.	Max.	Mean	Min.	Max.	Mean
A	-	-	-	-4.4	3.17	0.24	-4.62	2.24	-14.1
B	-28.1	8.55	-5.4	-6.07	4.58	0.20	-27.3	2.73	-8.37
C	-19.2	8.81	5.27	-8.47	5.1	2.60	-18.17	8.75	-0.85
D	-9.68	0.23	-3.64	-6.27	0.98	-1.81	-8.1	-2.2	-4.4

Table 4.2: Continued

	Proximal TL			*Inlet*		
Case	Min.	Max.	Mean	Min.	Max.	Mean
A	-8.96	4	-1.23	-26	9.4	-5.25
B	-9.5	2.84	-2.05	-12.4	1.1	-4.71
C	16.47	9.01	4.64	25.2	13.63	7.3
D	-23.8	-0.02	-10.15	-8.78	0.48	-3.4

TL, True lumen; *FL*, False lumen

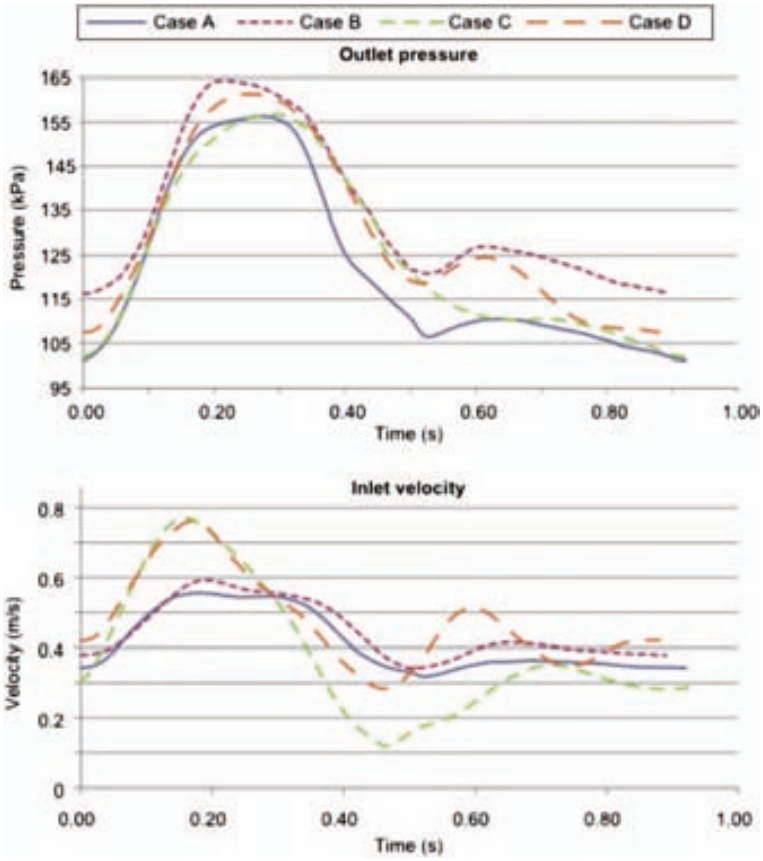

Figure 4.5: Pressure profiles measured at the outlet (Top) and velocity profiles computed from the flows measured at the inlet (Bottom) of the in-vitro models for the four dissection scenarios.

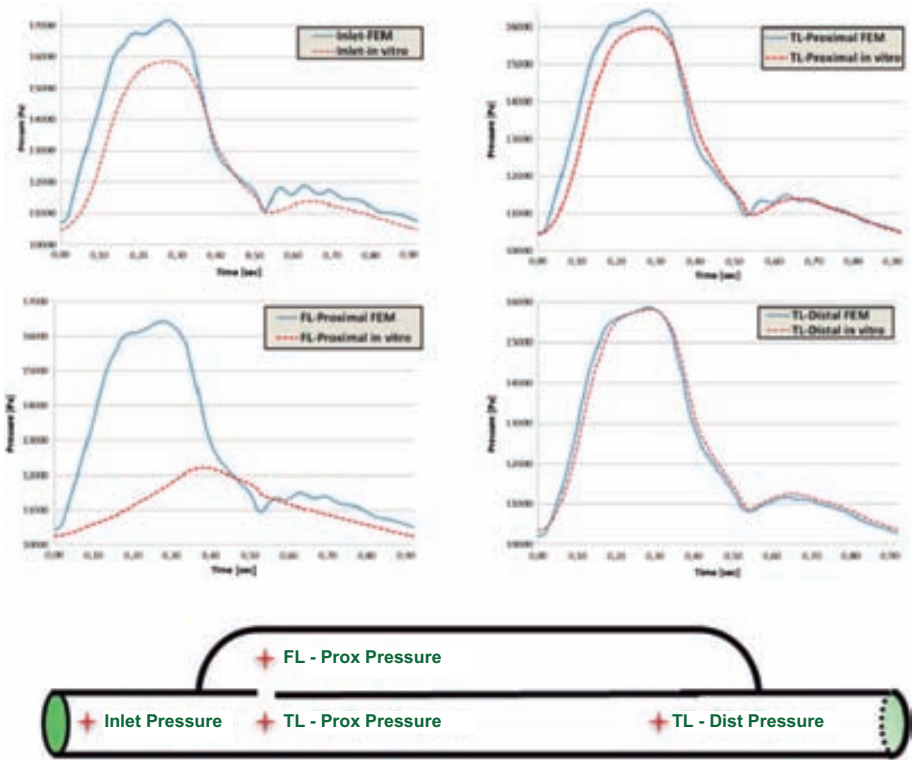

Figure 4.6: Case A: Pressure comparison between in-vitro (red dotted line) and FEM results (blue line) in the inlet, proximal and distal TL sites and proximal FL sites.

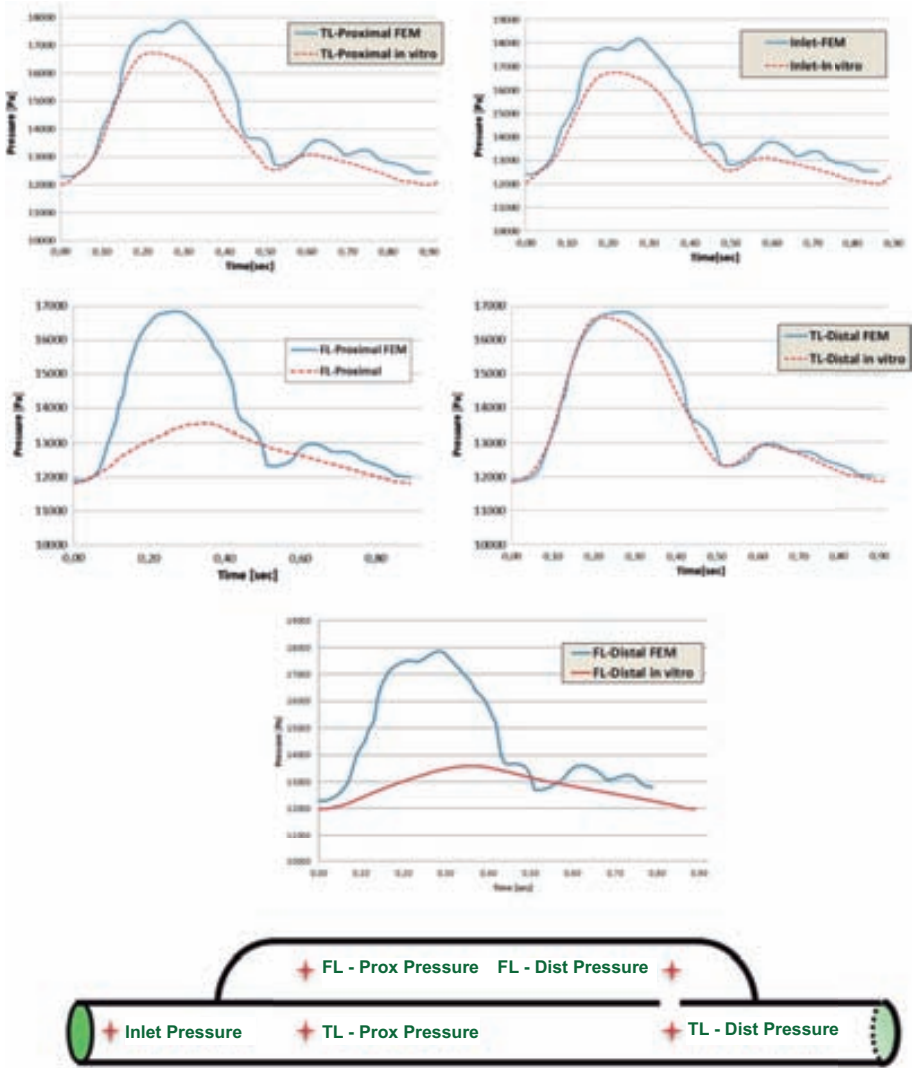

Figure 4.7: Case B: Pressure comparison between in-vitro (red dotted line) and FEM results (blue line) in the inlet and proximal and distal TL and FL sites.

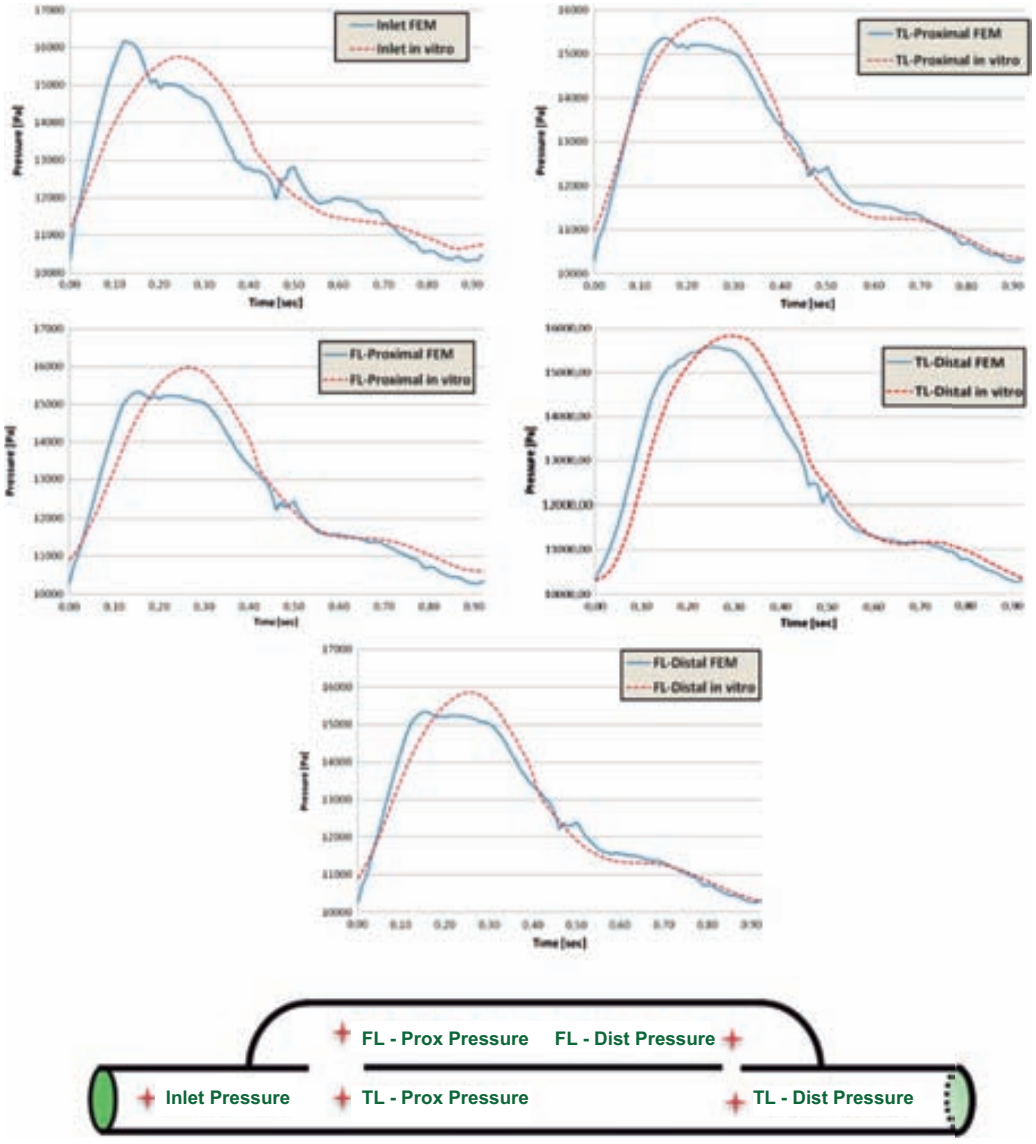

Figure 4.8: Case C: Pressure comparison between in-vitro (red dotted line) and FEM results (blue line) in the inlet and proximal and distal TL and FL sites.

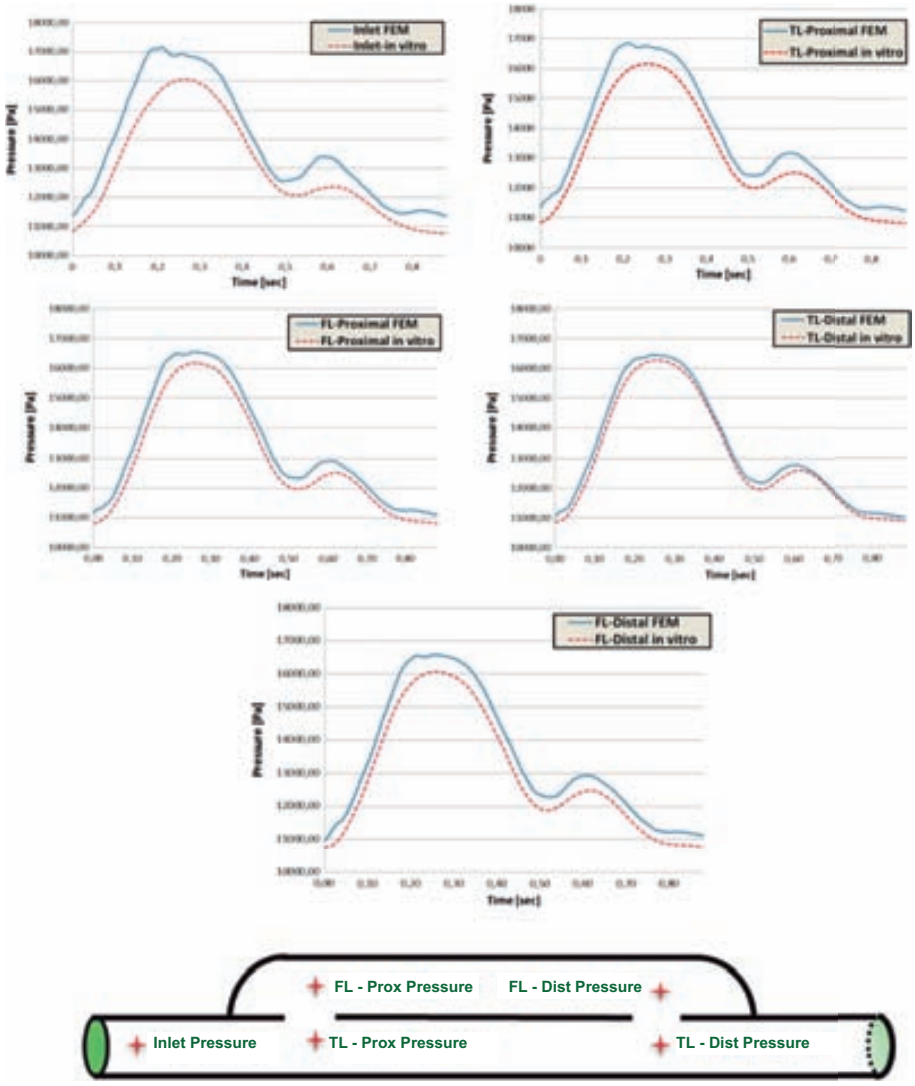

Figure 4.9: Case D: Pressure comparison between in-vitro (red dotted line) and FEM results (blue line) in the inlet and proximal and distal TL and FL sites.

4.4 Discussion

We have evaluated the use of a CFD methodology against in-vitro measurements in four idealized configurations of chronic ADs. Following our previous findings (Rudenick et al. 2010), on the complementarity of in-vitro and in-silico approaches to assess haemodynamics in ADs of type B, this is the first attempt, to our knowledge, to quantitatively test the accuracy of a CFD model in the prediction of intra-luminal pressures in different clinical scenarios for this pathology.

Our results show the ability of the CFD model to capture the main features of the experimental pressure waveforms in the TL and also the FL, as long as the connection between TL and FL is trough large holes. The average relative errors of the numerical predictions are < 10% for the pressure profile at all locations studied. In general, relative errors are smaller at locations close to the outlet boundary condition, where the pressure matches its experimental counterpart. Discrepancies between experimental and numerical results may arise from a combination of the material properties of the in-vitro and in-silico models, from the way that in-vitro pressures are measured and from the assumptions and simplifications of the CFD model. We are comparing a flexible physical phantom with a rigid computational model. Consequently, the elasticity of the latex wall of the FL has an important effect on damping the cyclic pressures and flows when entering the FL trough a small connection, thus resulting in lower peak systolic pressures.

The pressures change along the geometry and it is difficult to determine the exact position of the transducer inside the phantoms and thus to exactly correlate the in-vitro measurements with the in-silico predictions.

Despite the detected differences, in-silico and in-vitro results show a similar behaviour making them useful and complementary to study the properties of ADs (which in a lot of patients do have large communications). This encourages the use of our CFD methodology to characterize intra-luminal pressures in chronic ADs of type B.

While our approach is not an in-vivo validation, it has the fundamental ad-vantage of reducing the uncertainty of the parameters involved in the numerical simulation. While the phantom geometries are idealized models, their dimensions are based on clinical and experimental measurements, resulting in a generic model for parametric studies. Indeed, although the experimental set-up is only an approximation of a human AD of type B, it is able to reproduce pressure and velocity waveforms clearly representing those that can be expected physiologically (Evangelista et al. 2012).

AD is often associated with degeneration and diminished compliance of the aortic wall. Independent on the type of dissection (type A or B), most patients are elderly (Mehta et al. 2004; Tsai et al. 2006), with an aortic wall that has increased stiffness as a result of natural fatigue failure in response to permanent cyclic stresses. There are also other underlying factors in the clinical history of these patients that may lead to vascular remodelling and degradation of the aortic wall and thus reduce its elasticity, such as hypertension, genetics disorders as Marfan's syndrome, or atherosclerosis. Under these considerations, a rigid-wall numerical model was supposed to be appropriate for mod-

elling aortic dissections. Nevertheless, it is not a good approximation when communication between the lumina is not large enough, in which case the effects of wall compliance seem to play a key role in intraluminal haemodynamics. The inclusion of wall compliance in the numerical simulations of these cases and a detailed analysis of how it affects intraluminal haemodynamics are topics for further studies.

4.5 Conclusion

We have validated, in four different configurations of an idealized chronic AD, the ability of our CFD methodology to characterize intra-luminal pressures. The numerical simulations were able to capture the main pressure wave propagation observed in most phantom models, showing a good correlation with the experimental TL intra-luminal pressures as well with FL pressures in case of large communications. From a clinical point view, intraluminal pressure is one of the reported factors influencing aortic dissection long-term evolution. Intraluminal pressure has a direct impact on the aortic wall, determining local tissue mechanical stress, and that is why one of the preferred treatments for patients with type B aortic dissections is an aggressive blood pressure control. On the other hand, it has been shown that the presence of large tears and patent false lumen is associated with long-term complications and mortality (Evangelista et al. 2012). However, currently, intraluminal pressures are impossible to be measured in a non-invasive way and therefore, it is still not well understood how they are affected by the communication between the lumina. Hence, the CFD methodology presented could provide an additional way for a better understanding of the haemodynamic conditions and related clinical evolution in patients with chronic ADs. Moreover, joining traditional measurements, from imaging analysis, together with CFD analysis, creating and using patient-specific or disease-specific geometries with accurate boundary conditions, might enable to obtain much more detailed information of hemodynamic behaviour of the aorta. The fusion of these approaches could offer improved information about wall stress conditions in aortic diseases, in particular in ADs, for predicting local remodelling induced by the same physiological conditions as in a patient studied.

CHAPTER 5

Assessment of Wall Elasticity Variations on Intraluminal Haemodynamics in Type B Aortic Dissections

Abstract - *Type B aortic dissection (TBAD) is associated with high morbidity and mortality rates. Aortic wall elasticity is a variable often altered in TBAD patients and potentially involved in long-term outcome. However, its relevance is still mostly neglected. To gain more detailed knowledge of how wall elasticity might influence intraluminal haemodynamics in TBAD, a lumped-parameter model was developed based on experimental data from a pulsatile hydraulic circuit and validated for 8 clinical scenarios. Next, the variations of intraluminal pressures and flows were assessed as a function of wall elasticity. In comparison with the most rigid-wall case, an increase in elasticity to physiological values was associated with a decrease in systolic and increase in diastolic pressures of up to 33% and 63% respectively, with a subsequent decrease in the pressure wave amplitude of up to 86%. Moreover, it was related to an increase in multidirectional intraluminal flows and transition of behaviour as 2 parallel vessels towards a vessel with a side-chamber. The model supports the extremely important role of wall elasticity as determinant of intraluminal pressures and flow patterns for TBAD, and thus, the relevance of considering it during clinical assessment and computational modelling of the disease.*

Adapted from Paula A. Rudenick, Bart H. Bijnens, Patrick Segers, David García-Dorado and Arturo Evangelista. Assessment of Wall Elasticity Variations on Intraluminal Haemodynamics in Type B Aortic Dissections. 2014. Submitted.

5.1 Introduction

Aortic dissection is a cardiovascular disease caused by the formation of intimal tears in the aortic wall. The constant action of pulsatile pressure may separate the wall layers within the media as a consequence. Subsequently, the lumen is divided into two lumina separated by the intimal flap: the true (TL) and false lumen (FL), which communicate through tears. The TL is the normal passageway of blood while the FL is the passage enclosed by the dissected layers (Fig. 5.1a).

Despite success of acute treatment of type B aortic dissections (TBADs) (confined to the descending aorta) and advances in this field, patient follow-up continues showing a high number of late complications and mortality after surgery or medical treatment (Tsai et al. 2006; Evangelista et al. 2012), mostly because of FL aneurismal dilatation, eventually leading to rupture (Khan and Nair 2002).

Aortic wall elasticity is, besides haemodynamics, a variable often altered in TBAD and potentially involved in long-term outcome. Moreover, as far as we are concerned, current in-silico studies are only based on rigid-wall simulations (Tse et al. 2011; Cheng et al. 2013; Karmonik et al. 2013) originating from studies in mono-luminal aortas and under the assumption that elasticity may have limited effect on the haemodynamic parameters analysed (Cheng et al. 2010). This is done in order to simplify the computational and modelling approach, since a fluid structure interaction (FSI) simulation in aortic dissections is far more difficult to implement than in the single luminal case. However, comparing our previous findings on rigid and compliant models (Rudenick et al. 2013b; Soudah et al. 2013), flow direction across tears and along the cardiac cycle, as well as intraluminal pressures, do seem to be significantly influenced by wall elasticity. Furthermore, in our clinical observations, flow at both the proximal and distal tear is directed towards the FL in systole (even in the absence of significant side branches), which is impossible with a fully rigid wall. Therefore, the rigid-wall assumptions made when simulating mono-luminal aortas and aortic aneurisms are not valid anymore when a parallel lumen is present due to a dissection.

The aim of this study is to contribute to the understanding of haemodynamic and biomechanical phenomena relevant for the long-term of TBAD by means of a lumped-parameter model. Lumped-parameter models help to recreate and understand several flow aspects of a system (including the effects of wall elasticity), minimizing the need for complex in-silico, in-vivo or in-vitro experiments. Compared to these approaches, lumped-parameter models are able to quantitatively and qualitatively describe extensive pressure and flow waveforms without providing detailed solution on, mainly, local phenomena. They do provide a reasonable initial means to assess the overall system behaviour, and have a great potential to perform fast, easy and scalable studies on the influence of individual parameters.

In this study we have improved the first simplified version of our lumped-parameter model with regards to its mathematical formulation, calibration and validation. The proposed model was calibrated and validated using experimental data. Next, it was

used to study in more detail the effects of elsticity on intraluminal pressures and flow patterns across the tears.

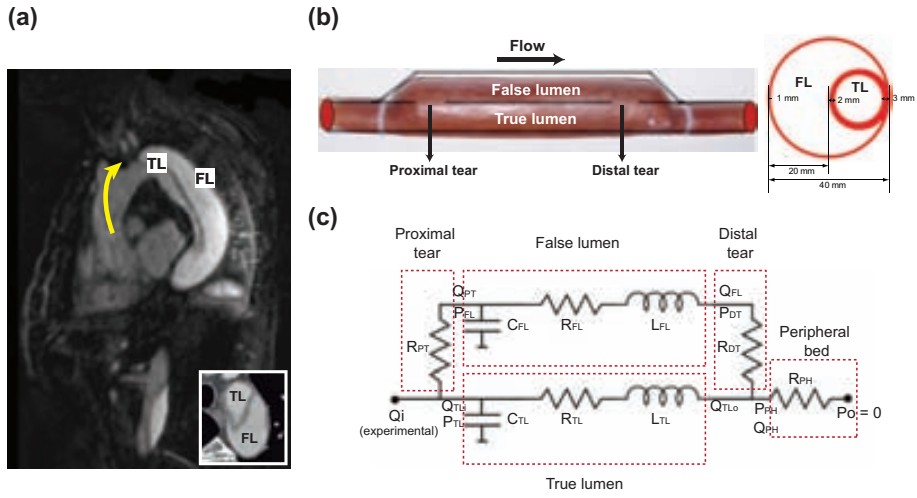

Figure 5.1: (a) Clinical appearance of a descending aortic dissection in the longitudinal plane. Transversal plane showing the distinction between TL and FL (Bottom right) (b) Proposed anatomic representation of a descending aortic dissection. Longitudinal diagram of the experimental model (Left) and cross-sectional plane of the dissected segment (Right). (c) Schema of the lumped-parameter model. The dissected region was modelled as two parallel compartments communicated by resistances (rigid tears). Dashed lines enclose the different compartments of the model: Proximal tear (PT), false lumen (FL), true lumen (TL), distal tear (DT) and peripheral (PH) bed.

5.2 Materials and Methods

5.2.1 Anatomic Scenarios

A TBAD was modelled as two parallel channels: TL (0.008 m inner radius; 0.002 m wall thickness; 0.16 m length) and FL (0.01615 m inner radius; 0.001 m wall thickness; 0.16 m length) communicated by holes to represent tears (Fig. 5.1b). We modelled 8 anatomic scenarios based on the possible permutations of varying tear size (4/10 mm diameter), number (1/2) and location (proximal/distal of the dissected region), which provides a good spectrum to validate our model. The notation $C_{\text{PROXIMAL SIZE,DISTAL SIZE}}$ is used for designing each scenario where the subscript 0 denotes absence of a tear.

5.2.2 In-vitro Experimental Model

Data from our previous in-vitro study (Rudenick et al. 2013a) were used for building and validating the model.

Briefly, TBAD was modelled as a physical phantom of compliant material where FL and TL were communicating via 4 mm/10 mm-diameter holes, mimicking clinically considered small and large tears, respectively, which was connected to a dynamic fluid circuit.

TL and FL pressures were measured at the proximal and distal sites of the phantom using retrograde catheterization with a pressure transducer (SPC-350 5F, Millar Instruments, TX, USA.) Velocities across tears were monitored using pulsed-wave Doppler echocardiography. Inlet flow waveforms were measured 15 cm proximal to the dissected segment using a flow probe (Transonic Systems Inc, NY, USA). Pressure and flow waveforms were recorded using a PowerLab 16/30 together with LabChart Pro software (ADInstruments, Colorado Springs, CO, USA). The perfusion fluid was water at 25^{o}C.

A detailed description of the phantom and the circuit can be found in (Rudenick et al. 2013a).

5.2.3 Mathematical Formulation of the Lumped-parameter Model

A lumped-parameter model of a TBAD was developed to recreate intraluminal haemodynamics (Fig. 5.1c). Only the dissected region was represented where TL and FL were modelled as parallel compartments connected by resistances to mimic rigid tears.

The formulation of the model was mainly based on a lumped-parameter description of the blood flow in a compliant cylindrical vessel (Formaggia and Veneziani 2003; Milisic et al. 2004; Shi et al. 2011). The mathematical description is given by the simplification and averaging of the Navier-Stokes equations for an incompressible fluid and the introduction of the electrical-network analogy of these equations.

Following this analogy, each lumen of the dissected segment was modelled as an individual compartment using an L-type network where the components were the local resistance to flow (R_{LUMEN}), compliance of the lumen wall (C_{LUMEN}) and intraluminal inertial properties of flow (L_{LUMEN}).

The peripheral connection was represented by a pure resistance (R_{PH}) to describe the systemic vascular bed which was computed by dividing the experimental mean outlet pressure by the corresponding mean outflow.

Proximal and distal tears were modelled as rigid entities by resistances R_{PT} and R_{DT}, respectively.

The electrical components of each lumen were computed following Equations 5.1-3, where l and r are lumen length and radius; μ and ρ represent the fluid dynamic viscosity (8.9E-4 Pa s) and density (997.0479 kg m^{-3}); E the wall Young's modulus; and h the wall thickness.

$$R_{lumen} = \frac{8\mu l}{\pi r^4} \tag{5.1}$$

$$L_{lumen} = \frac{\rho l}{\pi r^2} \tag{5.2}$$

$$C_{lumen} = \frac{3\pi r^3 l}{2Eh} \tag{5.3}$$

In the TL, since the upstream flow (Q_{TLi}) is known and assuming that the downstream pressure (P_{PH}) is given, the upstream pressure is governed by:

$$\frac{dP_{TL}}{dt} = \frac{Q_{TLi} - Q_{TLo}}{C_{TL}} \tag{5.4}$$

and the downstream flow rate is:

$$\frac{dQ_{TLo}}{dt} = \frac{P_{TL} - P_{PH} - R_{TL}Q_{TLo}}{L_{TL}} \tag{5.5}$$

A similar reasoning is followed for modelling the FL (assuming known upstream flow (Q_{PT}) and downstream pressure (P_{DT})) where Eq. 5.6 and Eq. 5.7 define the upstream pressure and the downstream flow, respectively:

$$\frac{dP_{FL}}{dt} = \frac{Q_{PT} - Q_{FL}}{C_{FL}} \tag{5.6}$$

$$\frac{dQ_{FL}}{dt} = \frac{P_{FL} - P_{DT} - R_{FL}Q_{FL}}{L_{FL}} \tag{5.7}$$

Since tears and peripheral connection are modelled as pure resistances, following Ohm's law, the flow at the proximal tear is given by:

$$Q_{PT} = \frac{P_{TL} - P_{FL}}{R_{PT}} \tag{5.8}$$

upstream pressure at the distal tear is :

$$P_{DT} = R_{DT}Q_{FL} + P_{PH} \tag{5.9}$$

and upstream pressure at the peripheral connection is:

$$P_{PH} = R_{PH}Q_{PH} + P_O \tag{5.10}$$

Finally, based on Kirchhoff's junction rule, flows at the TL inlet and at the end junction of both lumina are:

$$Q_{TLi} = Q_i - Q_{PT} \tag{5.11}$$

$$Q_{PH} = Q_{FL} + Q_{TLo} \tag{5.12}$$

The resultant system of differential algebraic equations was numerically solved with Matlab (MathWorks, Natick, MA) using the function ODE15s (time step: 0.01s). The solver was iterated until a steady state.

Table 5.1: Estimated parameters' values of the lumped-parameter model

Parameter	Value
R_{PT},R_{DT} (MPa (m^3 s^{-1})$^{-1}$)	
Small tear	295.97
Large tear	19.12
E_{TLwall} (MPa) / C_{TL} (m^3 MPa^{-1})	1.07 / 0.012E-3
E_{FLwall} (MPa) / C_{FL} (m^3 MPa^{-1})	
$C_{4,0}$	3.82 / 0.833E-3
$C_{10,0}$	2.41 / 1.320E-3
$C_{0,4}$	2.97 / 1.070E-3
$C_{0,10}$	1.55 / 2.051E-3
$C_{4,4}$	4.19 / 0.758E-3
$C_{4,10}$	2.86 / 1.110E-3
$C_{10,4}$	1.51 / 2.110E-3
$C_{10,10}$	2.49 / 1.275E-3

PT: proximal tear; *DT:* distal tear; *TL:* true lumen; *FL:* false lumen; *PH*: peripheral

5.2.4 Estimation of the Model Parameters for the Experimental Scenarios

The values of most of the components of the model were computed from geometric and haemodynamic data using Eq. 5.1-3. However, since the Young's moduli of the phantom lumina were unknown and the velocity profiles at the tears were not parabolic, values of C_{TL}, C_{FL}, R_{PT} and R_{DT} were estimated via fitting the model to the experimental data using the Matlab implementation of the Nelder-Mead simplex direct search algorithm (convergence criteria of 1E-6) (Table 5.1). The fitting algorithm optimised the sum of the root mean square errors between the predicted and the experimental TL and FL pressures waveforms, at the distal and proximal tears. A preliminary parameter study was firstly conducted to determine the valid range of values for each parameter to estimate their initial values.

Some assumptions were made for the parameter estimation. Since a different phantom was used for each scenario and the FL latex piece was custom made, the compliance of these pieces could differ from one model to another due to thickness variations resulting from their making process. Therefore, we estimated the Young's modulus of the FL wall for each model in order to estimate its compliance. On the other hand, since the TL was made out of a standard silicone tube, the TL wall elasticity was estimated and fixed for all cases. A similar approach was used for the resistance value of a small and a large tear. Under the previous assumptions, at first, a simultaneous fitting

was performed for cases $C_{0,4}$ and $C_{0,10}$ with the same model variables, except for the resistances at the tears and FL wall elasticity. This first step provided a common value for TL wall compliance, the reference resistance values for a small and a large tear, and the FL wall compliance for each model. Afterwards, only the FL wall elasticity was fitted for the rest of the cases while fixing TL wall elasticity and tear resistances with the previously predicted values. Thus, we got a common dataset of parameters for all experimental scenarios, except for FL wall elasticity that was assumed to differ from one scenario to another.

5.2.5 Model Validation

Firstly, the mathematical model was used to simulate 8 different experimental scenarios where numerical predictions could be compared against experimental results. The corresponding experimental inflow waveform was imposed at the inlet and a zero-pressure was imposed at the outlet in all cases.

We quantified the goodness of fit by computing the relative root mean square error (rRMSE) between predicted and experimental pressure waveforms close to the tears. A qualitative comparison was performed between predicted velocities profiles across the tears and the counterpart pulsed-wave Doppler measurements. For each scenario, we also compared predicted and experimental input impedances (Zins). Zin was computed as the complex ratio of corresponding pressure and flow harmonics. Magnitude and phase angle were computed for the first 10 harmonics.

5.2.6 Simulation of Elasticity Variations

Finally, the model was used to assess the effects of changes in wall elasticity on pressures and flow patterns through the analysis of several haemodynamic variables: a) proximal and distal TL and FL systolic pressure (SP); b) proximal and distal TL and FL diastolic pressure (DP); c) proximal and distal TL and FL pulse pressure (PP) (PP= SP – DP); d) pressure gradient across tears through the false lumen systolic/diastolic pressure index ($FPI_{systolic/diastolic}$%) as a percentage of TL systolic/diastolic pressure (Rudenick et al. 2013a); f) time shifting of proximal and distal FL pressure waveform with respect to the corresponding TL pressure waveform (TSF = time of SP_{FL} – time of SP_{TL}); g) quantification of change in direction between flows at the proximal and distal tears through the index of direction (ID = $\sum(|Q_{PT} + Q_{DT}|/(|Q_{PT}| + |Q_{DT}|))$; PT = proximal tear; DT = distal tear). Values range between 0 and 1, where a value 1 corresponds to proximal and distal flows moving in the same direction along the lumina.

The analysis was conducted on scenarios $C_{4,4}$ and $C_{10,10}$, which were taken as reference cases, most often present in clinical practice. For both scenarios, the Young's moduli of the lumina's walls were simultaneously changed by a factor of 0.35 to 1E7, so that the elasticity ranged from the one corresponding to a 20/30-year-old healthy individual (approx. 0.4 MPa) (Nichols et al. 2011; Roccabianca et al. 2013) to a rigid wall (approx. 1E7 MPa).

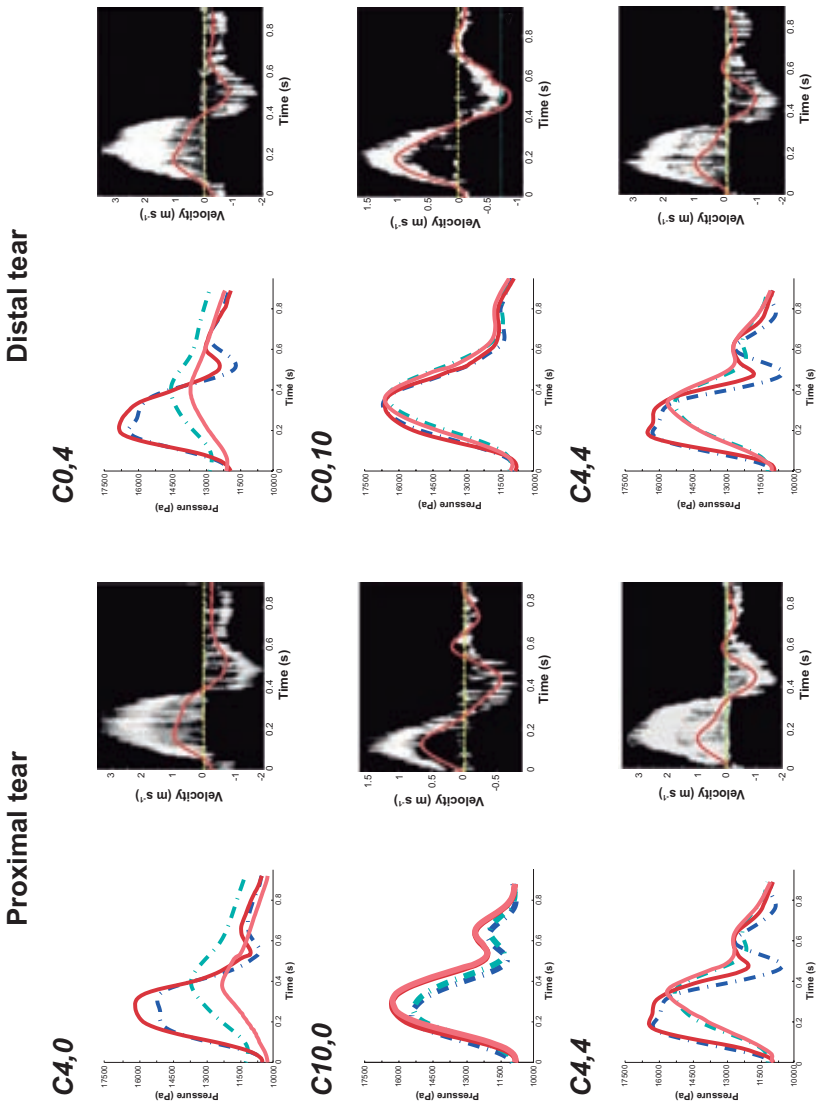

Figure 5.2: Comparison between experimental and predicted intraluminal pressures and velocities across the tears, at the proximal and distal sites of the model, for the eight experimental scenarios assessed. Doppler positive velocities are directed from the TL to the FL and negative velocities the other way around.

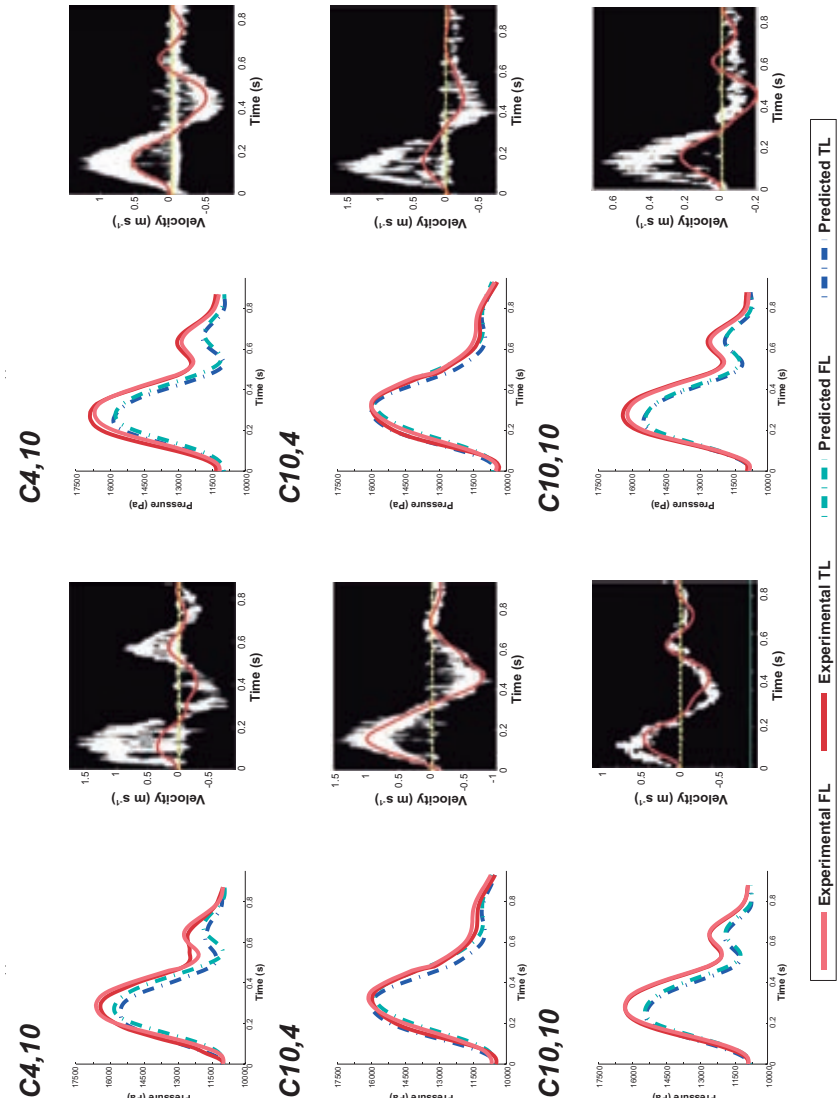

Figure 5.2: Continued.

5.3 Results

5.3.1 Mathematical versus Experimental Model

We found an overall good agreement in both profile and values, between predicted and experimental TL/FL pressures, for all experimental scenarios at both proximal and distal tears. As shown in Fig. 5.2 and Table 5.2, the overall predicted waveforms were close to the measured ones and rRMSEs for pressure were below 10%.

When qualitatively comparing predicted (= mean flow in the tear) with Doppler flow velocities (= spectrum of all velocities present in the tears) across the tears (Fig. 5.2), there was an overall satisfactory agreement with the largest discrepancies observed at the small tears. The mathematical predictions reproduced the overall behaviour of experimental waveforms and generally there was a good quantitative agreement.

The pattern of Zin was similar between the numerical simulations and the experimental cases (Fig. 5.3), where the model Zin gives a reasonable overall estimate of the experimentally measured Zin, for both moduli and phase angles. While there was overall good agreement, the model does not fully represent the oscillations seen on the experimental impedance modulus and phase, because the numerical model does not exactly describe high frequency details such as inflection point and elevation in pressures (Murgo et al. 1980). However, the inlet pressure corresponding to each scenario has a power spectrum concentrated at the low frequencies (Fig. 5.3) where most of the signal information is found.

From this, we can conclude that the predictive capability of our model is satisfactory.

Table 5.2: Relative root square mean error (rRMSE) between predicted and measured pressures at the proximal and distal tears, for each scenario.

	Scenario							
rRMSE (%)	$C_{4,0}$	$C_{10,0}$	$C_{0,4}$	$C_{0,10}$	$C_{4,4}$	$C_{4,10}$	$C_{10,4}$	$C_{10,10}$
Proximal tear								
TL pressure	3.70	7.00			5.46	6.27	3.17	6.28
FL pressure	9.09	5.75			2.02	5.74	2.27	5.52
Distal tear								
TL pressure			2.65	1.29	4.95	8.09	2.19	6.27
FL pressure			5.02	1.83	1.73	6.61	1.52	5.02

TL, True lumen; *FL*, False lumen

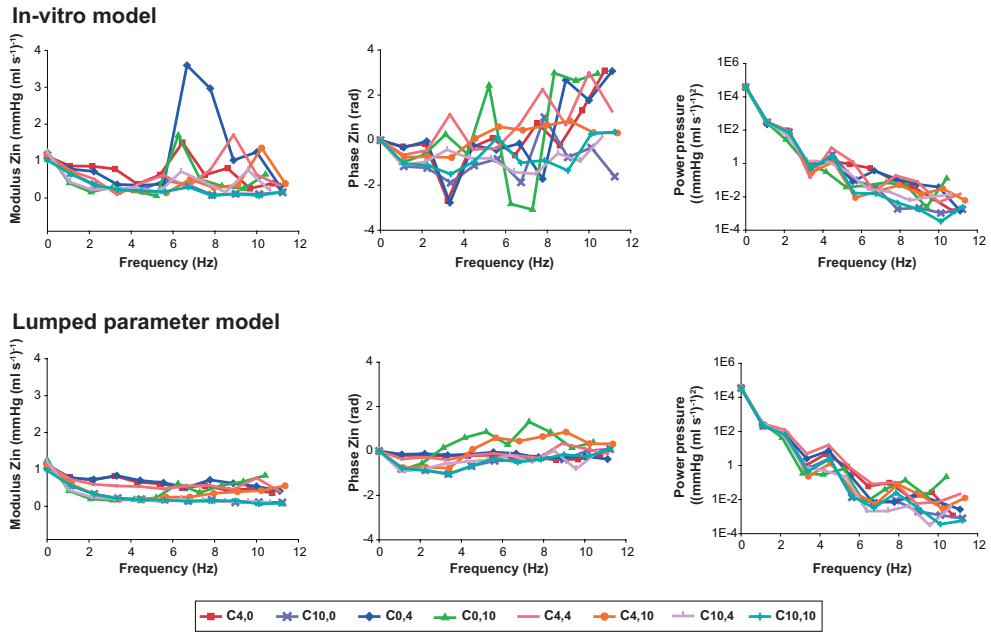

Figure 5.3: Experimental and predicted input impedance (Zin) modulus (left) and phase (centre), and power spectrum of the inlet pressure (right) computed for the eight anatomic scenarios studied.

5.3.2 Changes in Wall Elasticity

Pressures. Independent on location (distal/proximal), a higher elasticity was associated with more damped TL and FL pressure curves (Fig. 5.4), with lower SPs, higher DPs, and thus lower PPs (Fig. 5.5). As the wall became stiffer, TL/FL pressure gradients across the tears decreased, so that FL SPs increased and FL DPs decreased approaching corresponding TL pressures, with resultant values of $FPI_{systolic}$% and $FPI_{diastolic}$% close to 100% (Fig. 5.6). This effect was more pronounced for scenario $C_{4,4}$ where TL/FL pressure gradients at the reference configuration were larger than in scenario $C_{10,10}$ (Proximal $FPI_{systolic}$%: 94.2% vs. 100.2%; Proximal $FPI_{diastolic}$%:105.8% vs. 99.8%). In the presence of a high elasticity, FL pressure waveforms arrived later at both proximal and distal locations compared to TL pressure curves (Fig. 5.7) while when elasticity was decreased, time delay of FL pressure waveforms decreased until zero for the most rigid scenarios, where TL and FL curves overlapped.

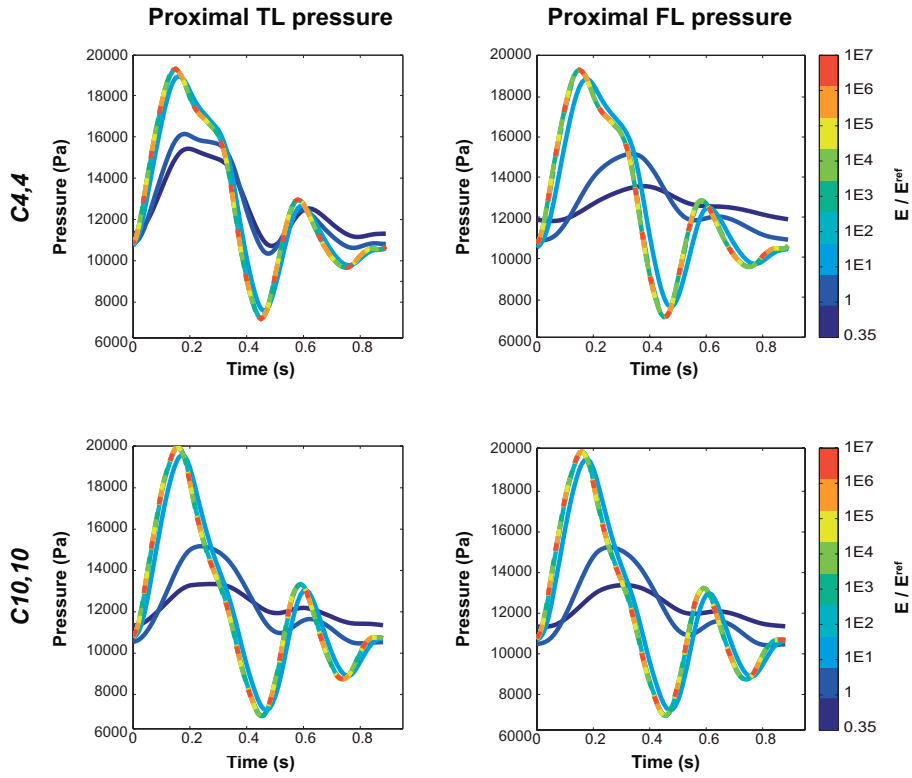

Figure 5.4: Variations in predicted intraluminal true (TL) and false lumen (FL) pressures, close to the proximal tear, with changes in wall elasticity, for cases $C_{4,4}$ and $C_{10,10}$. E represents the wall elasticity of the lumina and E^{ref} its corresponding reference value.

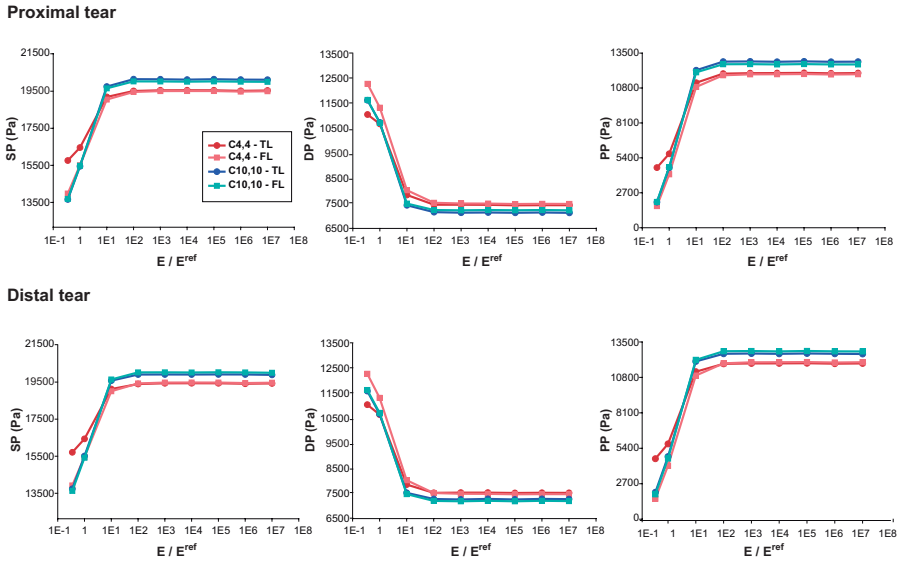

Figure 5.5: Values of predicted true (TL) and false lumen (FL) systolic pressure (SP), diastolic pressure (DP) and pulse pressure (PP), computed at different levels of wall elasticity for scenarios $C_{4,4}$ and $C_{10,10}$. E represents the wall elasticity of the lumina and E^{ref} its corresponding reference value.

Flows. Figure 5.8 displays the effect of wall elasticity on flow waveforms across the tears. In the presence of high wall elasticity, the FL behaved as a side chamber of the TL, so that during the cardiac cycle flow went into or out of the FL simultaneously at proximal and distal tears. On the other hand, as wall elasticity decreased, TL and FL acted as parallel compartments, so that flow entering the FL at the proximal tear at the same time went out the FL from the distal tear and vice versa. This phenomenon can be better appreciated through the assessment of the ID (Fig. 5.9), which decreased with increasing stiffness until becoming zero. The effect was also more evident for case $C_{10,10}$, where intraluminal communications are larger than in case $C_{4,4}$ and thus, more flow is passing through the tears.

Additionally, increased wall elasticity was associated with flow waveforms across the tears with higher amplitude, time-delayed peak flow and increase of flow reversal at both lumina (Fig. 5.8).

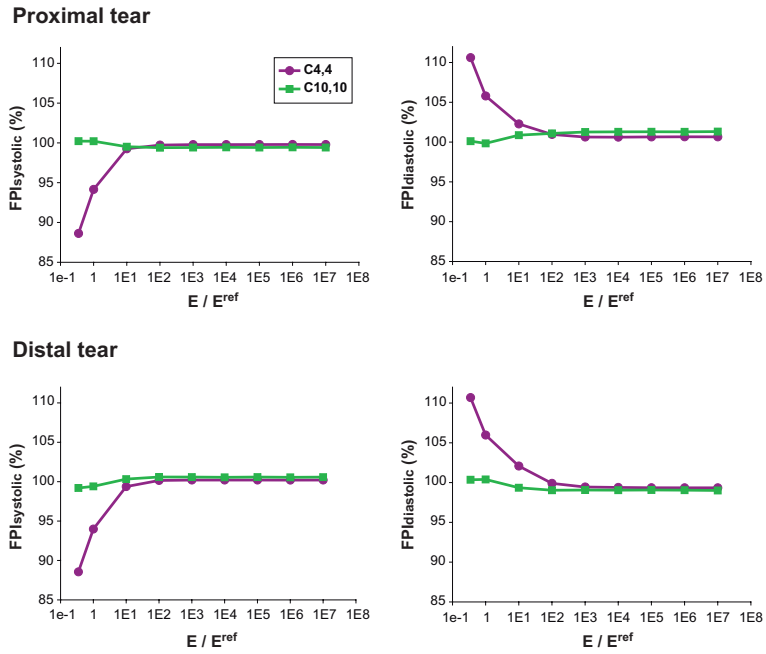

Figure 5.6: Variations in predicted false lumen systolic ($FPI_{systolic}$%) and diastolic pressure ($FPI_{diastolic}$%) indexes with changes in wall elasticity, at the proximal and distal tears for scenarios $C_{4,4}$ and $C_{10,10}$. E represents the wall elasticity and E^{ref} its corresponding reference value.

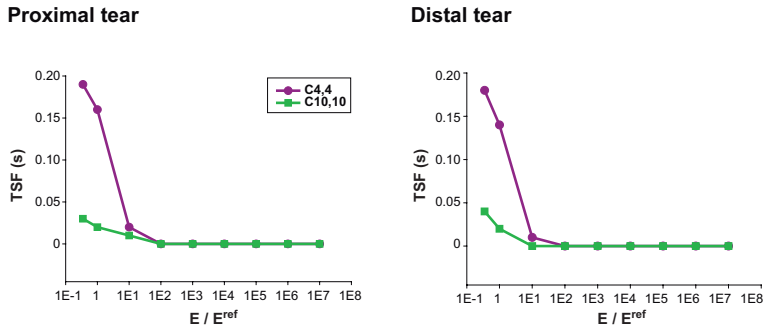

Figure 5.7: Time shifting experienced by the predicted false lumen pressure waveform in comparison with the true lumen pressure waveform (TSF) for the different levels of wall elasticity, at the distal and proximal sites of the dissected model. E represents the wall elasticity and E^{ref} its corresponding reference value.

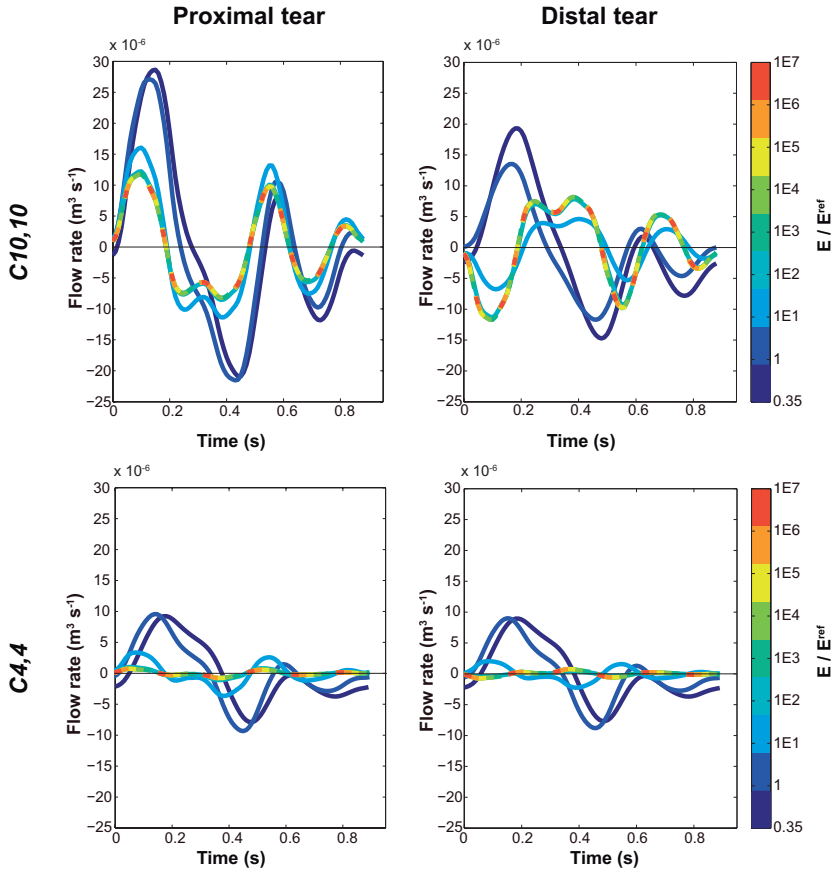

Figure 5.8: Variations in predicted flow waveforms across the proximal and distal tears with changes in wall elasticity, for cases $C_{4,4}$ and $C_{10,10}$. Positive flow rate corresponds to flow from the true lumen towards the false lumen. E represents the wall elasticity and E^{ref} its corresponding reference value.

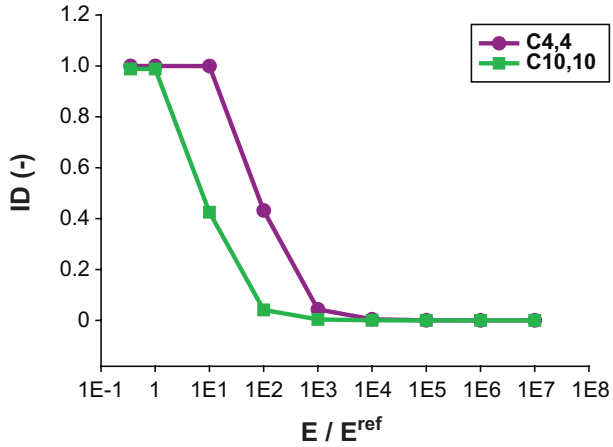

Figure 5.9: Index of direction (ID) computed at different levels of wall elasticity for scenarios $C_{4,4}$ and $C_{10,10}$. The ID quantifies the change of direction between the flows across the proximal and distal tears, so that high ID values mean proximal and distal flows simultaneously moving from the true lumen to the false lumen or vice versa. E represents the wall elasticity and E^{ref} its corresponding reference value.

5.4 Discussion and Conclusions

A detailed knowledge of the flow phenomena in TBADs is of importance in diagnosis and better understanding of their chronic development and clinical outcome. The main scope of this study was the development/validation of a lumped-parameter model of a TBAD as a first simple approach for the characterization of intraluminal pressures and flows and study the influence of e.g. wall elasticity on flow directions and pressure elevations without a need for capturing detailed local flow phenomena. This has the advantage that it allows assessment of individual factors affecting global pressures and flows in a more feasible and scalable way than could be performed by complementary complex in-vivo, in-vitro and in-silico approaches. The model was validated with previous experimental in-vitro scenarios and was in turn used to assess the effects of wall elasticity variations on intraluminal pressures and flows.

Overall, a good agreement was found between the model-based predictions and experimental measurements. The proposed model recreated experimental pressure and velocity measurements for the different scenarios. Instantaneous values and profiles of predicted intraluminal pressures were consistent with the in-vitro approach, showing an rRMSE less than 10% for all cases.

Overall, qualitative features of velocity waveforms through tears were also in good agreement, keeping in mind that spectral Doppler measures the whole range of velocities within the sample volume at each instant of time (with the envelope corresponding to the maximal velocity in the centre of the flow profile) whereas only the instantaneous mean velocity is provided by the simulations. Large tears have a flat profile

(Womersley's parameter approx.: 12.5-13) and so a spectral Doppler with a narrow range of velocities while small tears develop a more parabolic velocity profile (Womersley's parameter approx.: 5) and thus a much broader Doppler range of velocities. Taking into account these considerations, the predicted velocity profiles across tears were comparable with pulsed-wave Doppler measurements at all tears.

The similarities between the experimental and predicted Zin gave also strong evidence of the robustness of the model to recreate experimental results and its validity to be used as a complementary approach.

The model allowed studying the effects of properties that have not been studied before in TBAD. Arterial elasticity is a biomechanical property with an important influence on arterial haemodynamics and thus clinical evolution, since it has clear effects on pressures and WSS (Evangelista and González-Alujas 2006; Nienaber et al. 2006b).

Our model shows that wall elasticity had major effects on flow patterns through tears. When wall elasticity was low enough, TL and FL behaved as parallel chambers, so that flow was one-way, simultaneously displacing fluid in both lumina from the proximal to the distal site and vice versa during the cardiac cycle. However, when wall elasticity was increased, tear flow dynamics completely changed and both proximal and distal tears simultaneously behaved as entry and exit sites. This additionally introduced significant flow reversal in the different compartments of the dissections, a phenomenon often seen in clinical practice (François et al. 2013). The scenario where both tears act as entry and exit sites simultaneously during a cardiac cycle could be a potential cause of simultaneous jets getting into the FL from several locations and the consequent presence of disturbed flows and WSS variability. This flow behaviour was previously observed when comparing our computational rigid-wall simulations (Rudenick et al. 2010) and in-vitro experiments (Rudenick et al. 2013a) and was one of the stimuli for the present study. The results are also in agreement with Tan et al. 2009, where turbulence intensity was significantly higher in a compliant model in comparison with a rigid model of a thoracic aortic aneurysm.

Wall elasticity also had clear effects on intraluminal pressures. Diminished elasticity resulted in FL pressure waves of higher amplitude with higher SP, lower DP and resultant higher PP, so that FL pressure profiles approached TL's, affecting TL/FL gradients. In the context of TBADs, this might be associated with FL expansion and TL narrowing (Williams et al. 1997; Chung et al. 2000), both potential complications during the long-term follow-up (Erbel et al. 2001).

The majority of 3D in-silico flow studies in the field of aortic diseases are based on rigid-wall assumption, under the assumption that the effect of wall elasticity on the quantitative results is rather limited for the haemodynamic parameters studied (Cheng et al. 2010). However, our findings showed that elasticity appears to be extremely relevant in the pressure and flow prediction of TBAD, where 2 parallel lumina are present, which is in line with the study performed on the aorta by Reymond et al. 2013. Wall elasticity seemed to affect pressures or flows depending on the size of communications between the lumina. When communications were large enough, wall elasticity seemed to be important in flow pattern determination while when communications were small

enough, wall elasticity played an important role in pressure prediction, as it is also shown in Soudah et al. 2013. Therefore, wall elasticity should be taken into account when assessing and studying aortic dissections' outcome.

These initial results seem promising to improve our understanding of haemodynamics in aortic dissections and can be further extended to study the effects of changes in morphologic configurations on lumen pressures and flows. Additionally, it suggests that wall elasticity, flow direction and its changes during the cardiac cycle, might be clinically relevant parameters to study in more detail in these patients.

In conclusion, the proposed model seems to be a good first approximation to assess flow and pressure waveforms in TBAD. The model in turn was useful to support the hypothesis that elasticity is a key biomechanical property to be considered in the haemodynamic assessment of aortic dissections and rises a red flag for further investigation.

5.4.1 Limitations

The model used is a lumped-parameter model representation, considering the TL and FL as two interacting compartments. Although the model provides pressure and flows at the inlets and outlets of these chambers incorporating time-shifts and waveform changes due to inertial and elasticity effects, it does not explicitly account for wave travel and reflections, not is it able to capture local flow phenomena induced by jets and turbulence. However, this simplification still allows for capturing overall pressure changes, tear velocities and flow directions.

Predicted velocities across the tears were computed under the assumption that tear areas were reduced a 25% by catheter obstruction when performing retrograde catheterization in the in-vitro experiments. Pressures in the in-vitro model were measured at the level of the tears, close to the place where a high speed jet was registered. However, the transducer tip was carefully placed far enough from the jet to avoid as much as possible the depression of the registered static FL pressures. Moreover, the model was calibrated to fit experimental TL and FL pressures at the same time, which was not 100% realistic, since during the experiments tears were in turn obstructed by the catheter (a unique catheter was used) when measuring FL pressures by retrograde catheterization and velocities across tears were measured before performing catheterization. FL diameter and lumina's thickness were also an approximation, since the physical model does not have a perfect circumferential FL cross-section and uniform lumina's thickness (Fig. 5.1b). Therefore, these assumptions might be inducing some error in the predicted pressures and velocities.

CHAPTER 6

False Lumen Flow Patterns as a Resultant of Morphological and Biomechanical Characteristics of Chronic Aortic Dissections. Implications for MRI Evaluation

Abstract - *A persistent false lumen (FL) is present in 70-80% of patients discharged after an acute aortic dissection and most of these patients have high risk of mid/long-term complications. FL flow starts to be assessable with MRI, but little is known on its determinants and predictive value. We investigated the origin of cyclic variations in the intraluminal flow patterns in chronic aortic dissections using a computational lumped-parameter model. For this, we assessed the changes in flow profiles induced by several key properties of dissected aortas, potentially involved in FL enlargement, such as wall stiffness, tear size and location and the presence of abdominal side branches arising from the FL. The time course of the directions of the flow within the FL is highly dependent on the position of assessment along the aorta. From the parametric study, we found that FL flow patterns (especially at the level of the diaphragm) showed their characteristic patterns due to variations in the cumulative size and spatial distribution of the communicating tears and the incidence of visceral side branches originating from the FL. Interestingly, changes in wall stiffness did not change the time course of flows whereas it significantly determined intraluminal pressures. FL flow patterns vary depending on the place of assessment along the dissection and are mostly influenced by the size and spatial distribution of tears and abdominal side branches. This data should be taken into consideration in the imaging protocol to define the predictive value of FL flows.*

Adapted from Paula A. Rudenick, Patrick Segers, Victor Pineda, David García-Dorado, Arturo Evangelista and Bart H. Bijnens. False Lumen Flow Patterns as a Resultant of Morphological and Biomechanical Characteristics of Chronic Aortic Dissections. Implications for MRI Evaluation. 2014. Submitted.

6.1 Introduction

Aortic dissection is a life-threatening condition. Whereas medical treatment might be a better choice than surgical intervention in a substantial amount of patients with acute type B aortic dissections without serious complications, up to 50% of these patients show progressive false lumen (FL) enlargement and spontaneous rupture during the chronic stage of the disease (Akin et al. 2009).

The dilatation of the aorta in aortic dissections has been linked to multiple haemodynamic factors, such as intraluminal blood pressures and flows, mostly within the FL (Erbel et al. 1993; Juvonen et al. 1999; Inoue et al. 2000; Amano et al. 2011). Open communication between true (TL) and FL (especially large tears) and patency of the FL seem to be the main sources of late complications in chronic aortic dissections (Inoue et al. 2000; Bernard et al. 2001; Evangelista et al. 2012).

Clinical magnetic resonance imaging (MRI) studies provide quantitative and qualitative intraluminal flow information in aortic dissection. Several studies (Strotzer et al. 2000; Clough et al. 2012; François et al. 2012) as well as our own clinical observations (Fig. 6.1), revealed significant flow pattern differences among individual patients (mostly in the FL), where complex flow patterns and the amount of volume in the FL have been associated to aortic expansion (Inoue et al. 2000; Amano et al. 2011; Clough et al. 2012). Therefore, intraluminal flow might have a predictive role in the long-term evolution of the patient. However, many of the current studies in literature are merely descriptive, technically limited, and not prospective, and do not directly allow linking flow patterns with clinical outcome. Therefore, little remains known on the determinants and relevance of these flow pattern differences in chronic aortic dissections as well as how these can/should be studied with imaging.

In this study, we hypothesized that the typical flow variations observed in most patients depend on only a few biophysical parameters that are known to be key for assessing aneurysmal dilatation in aortic dissections: wall elasticity (Nollen et al. 2004; Evangelista et al. 2006), occurrence of abdominal side branches originating from the FL (Inoue et al. 2000), tear size and tear location (Evangelista et al. 2012).

To test this hypothesis, we simulated the effects of changes in these parameters on intraluminal flow patterns using a computational lumped-parameter model. This allows determining the individual contribution of each of these parameters in the absence of measurement variability and other sources of noise.

The main goal was to identify the occurrence of characteristic flow patterns associated with each one of the key factors and to assess whether the model can explain the observations from MRI phase contrast imaging in typical patients. This might provide suggestions for the optimal assessment and interpretation of flow patterns in clinical practice and a new means to relate alterations observed to their determining factors and association with clinical outcome.

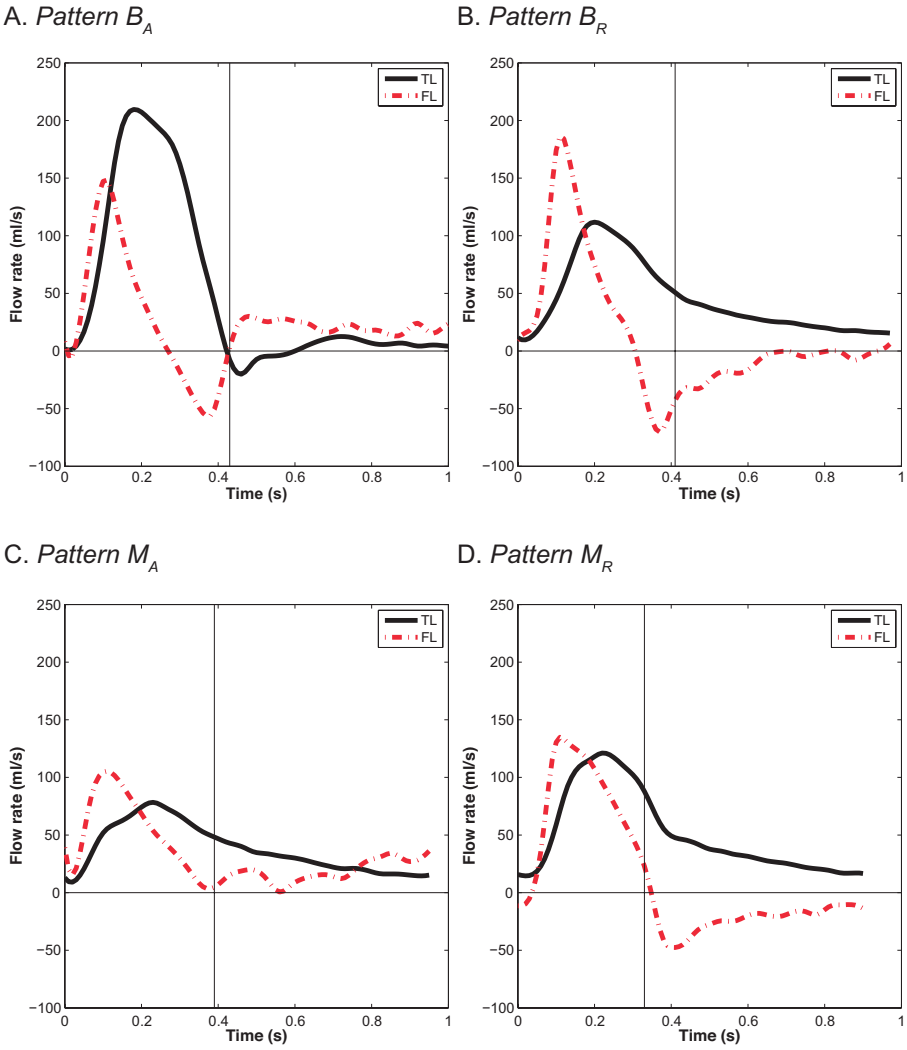

Figure 6.1: Four most typical FL flow patterns (assessed at the level of the diaphragm) observed in our population of patients in follow-up. They can be classified based on the direction of flow in systole and diastole: B_A: systolic biphasic flow and primarily diastolic antegrade flow; B_R: systolic biphasic flow and primarily diastolic retrograde flow; M_A: systolic monophasic flow and primarily diastolic antegrade flow; M_R: systolic monophasic flow and primarily diastolic retrograde flow. Antegrade flows are positive and retrograde flows are negative. *TL*, True lumen; *FL*, False lumen.

Table 6.1: Characteristics of the 4 patients selected.

	Patient – Flow pattern			
	1 - B_A	2 - B_R	3 - M_A	4 - M_R
Age	41	27	70	37
Gender	Male	Male	Male	Female
Stanford diagnosis	Type A	Type A	Type A	Type A
Extent	From proximal thoracic aorta to the left iliac artery	From proximal thoracic aorta to the right iliac artery	From the proximal thoracic aorta to the whole abdominal aorta	From the proximal thoracic aorta to the whole abdominal aorta
Time between acute event and MRI (days)	107	253	223	164
Procedure	Open repair with prosthetic tube	Open repair with prosthetic tube	Open repair with prosthetic tube	Open repair with prosthetic tube
Marfan syndrome	No	Yes	No	Yes
FL Thrombosis	None	None	None	Partial

TL, True lumen; *FL*, False lumen; *MRI*, Magnetic Resonance Imaging

6.2 Methods

6.2.1 Patients

To ensure relevance for a majority of patients with chronic aortic dissections and to identify the typical features present in representative flow patterns, we selected four typical patients, from our population in follow up, in whom we assessed the flows at the level of the diaphragm. Since TL flow patterns in our routine clinical experience do not show large variation during the cardiac cycle amongst patients, but FL flow on the other hand, typically can be very complex, we selected these cases to show the 4 most common FL flow patterns covering the vast majority of our clinical routine. Table 6.1 shows the clinical data from these patients. They underwent a regular follow-up (3-12 months interval between the acute phase and the imaging) with MRI in our hospital. The MRI studies were performed on a 3T scanner (Trio, Siemens Medical Solutions) equipped with fast gradient system characterized by a peak gradient amplitude of 45 mT/m and a maximal slew rate of 200 T/m/s.

For flow quantification, a breathhold segmented phase-contrast gradient-recalled echo through-plane sequence, with a temporal resolution of 25-35 ms and retrospective gating, was performed (TR = 57.6 ms; TE = 1.9 ms; flip angle = 30 degrees; parallel imaging with an acceleration factor of 2; matrix size = 192 mm2; field of view = 330 mm2; voxel size = 1.7x1.7x5 mm3; slice thickness = 5 mm; bandwidth = 550 Hz/pixel; 24–30 frames per cardiac cycle depending on heart rate; velocity encoding = 130 to 200 cm/s). Flow velocity-encoded MR imaging was performed in an oblique transverse

plane perpendicular to the course of the descending aorta at the level of the diaphragm. This location was chosen because minimal flow disturbance due to proximal tear flow or major branches in the vicinity was expected. Flow velocity-encoded MR imaging data were analysed (Argus flow software, Siemens). Regions of interest (ROI) in both the TL and the FL were manually segmented. Since the mean pixel value in both regions was proportional to the flow velocity, the instantaneous flow rate for each frame was computed as the product of the cross-sectional area and the average velocity. We consequently obtained a flow rate–time curve from the summation of the instantaneous flow rates for all the frames through the entire cardiac cycle.

6.2.2 Representative Aortic Geometry

For our further study, we choose the geometry from a typical aortic dissection as a reference case. It was described as two parallel channels (Fig. 6.2B): the TL (8.8 mm inner radius; 1.6 mm wall thickness) and the FL (15.5 mm inner radius; 0.8 mm wall thickness) communicated by circular large proximal and distal tears. The thoracic aorta (ThAo; 106 mm length) extended from just below the left subclavian artery to the diaphragm and the abdominal aorta (AbAo; 239 mm length) from the diaphragm to just above the beginning of the iliac arteries. These assumptions were based on the fact that most of our patients show dissections extending along both the ThAo and the AbAo.

The values of the radii of the lumina corresponded to the average values observed in our population of patients (Evangelista et al. 2012). Wall thicknesses and lengths were taken from literature (Reymond et al. 2009, Rudenick et al. 2013a, Mensel et al. 2013).

6.2.3 Computational Model

For the current study, we used an extension of the lumped-parameter model of an aortic dissection (Fig. 6.2A) previously reported in Rudenick et al. 2013b. The model has been quantitatively and qualitatively validated with in-vitro measurements performed on experimental models (Rudenick et al 2013a), giving evidence that it can provide accurate predictions of intraluminal pressures and flows in aortic dissections.

Briefly, the model is based on the description of the blood flow in a compliant cylindrical vessel and its mathematical description is given by the simplification and averaging of the Navier-Stokes equations for an incompressible fluid and the introduction of the electrical network analogy of these equations. The TL and FL were modeled as parallel compartments connected by resistances to mimic a proximal (R_{PT}) and distal tear (R_{DT}). Each compartment was represented by an individual L-type filter where local resistance to flow (R_{LUMEN}), wall compliance (C_{LUMEN}) and inertance to flow (L_{LUMEN}) were considered (Formaggia and Veneziani 2003).

For this study, some modifications were added to our original model. Firstly, the dissected segment was divided into the ThAo and the AbAo with their corresponding lumina: TL_{ThAo}, FL_{ThAo}, TL_{AbAo} and FL_{AbAo}. This enabled to evaluate the flows and

pressures at the proximal, diaphragm and distal levels of the model. Moreover, to account for the presence of visceral side branches originating from each of the lumina, resistances R_{TLsb} and R_{FLsb} were added at the AbAo segment to govern the amount of blood going to the abdominal arteries connected to the TL and FL, respectively.

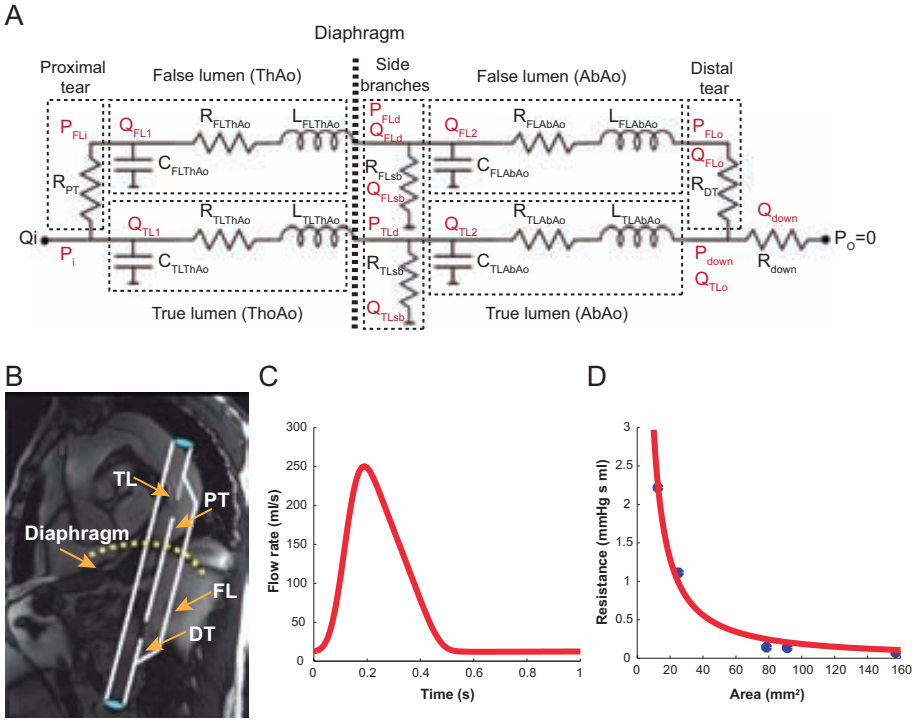

Figure 6.2: (A) Diagram of the lumped-parameter model of an aortic dissection including the presence of abdominal side branches (sb) and the modeling of the thoracic (ThAo) and abdominal (AbAo) aorta; (B) Clinical appearance of an aortic dissection with magnetic resonance imaging and the equivalent dissection geometry proposed; (C) Imposed inflow curve; (D) Value of interluminal resistance plotted as a function of the cumulative tear area, resulting from the calibration of the lumped-parameter model (Rudenick et al. 2013b) to the experimental one (Rudenick et a. 2013a). *FL*, False lumen; *TL*, True lumen; *PT*, Proximal tear; *DT*, Distal tear.

To establish the values of resistances at the tears as a function of the cumulative area of communication between the lumina, we used the values resulting from the calibration of the numerical model (see Chapter 5) to the experimental models (Rudenick et al. 2013a) (Fig. 6.2D). Since there is a clear trend of an inverse relation between the cumulative area of communication (in mm^2) and the resistance value (in mmHg ml s), an inverse power curve was fitted:

$$Resistance = K\ Area^{b} \quad (6.1)$$

The coefficients obtained for the best fit were K=47.42 and b = -1.20 ($R^2 = 0.99$).

See Chapter 5 for full details of the mathematical formulation of the lumped-parameter model.

For the simulations, a fluid density of 1050 kg/m^3 and viscosity of 0.004 Pa s was used. For the inflow at the inlet, we constructed a slightly simplified version of the flow that is observed in a typical patient (Fig. 6.2C). The inflow in the ThAo (at the level of the bifurcation of the pulmonary artery) was assumed to have a mean flow rate of approximately 68 mL/s and a peak systolic flow rate of 250 mL/s. The curve was created from values/profiles observed in literature (Reymond et al. 2009) and our patients. All the simulations were performed imposing the same inflow waveform and assuming a venous zero-pressure at the termini of the side branches and AbAo.

The total peripheral vascular resistance was estimated by dividing an assumed mean pressure of 100 mmHg by the mean inflow. The total peripheral resistance consisted of the resistances at the side branches of the lumina (R_{TLsb}, R_{FLsb}) plus the one corresponding to the vascular bed below the abdominal aorta (R_{down}).

For this study, we defined a reference case with circular large proximal and distal tears (approximately 10 mm diameter each), since this is most prevalent in clinical practice. Visceral side branches were only originating from the TL. The lumped-parameter model was calibrated for this case, so that the elasticity of the segments (E = 1.4 MPa) and peripheral resistance were adjusted to obtain a systolic pressure of 120 mmHg and diastolic pressure of 80 mmHg at the inlet. The resistance at the TL visceral side branches was adjusted to have 65% of the flow going into them (Nichols et al. 2011) (R_{TLsb} = 2.3 mmHg ml s) with the remainder 35% going towards the iliac arteries.

6.2.4 Simulations

First, in order to show the variability and evolution of the patterns when imaging the flows at any place from the proximal origin of the dissection towards the distal end, we determined TL and FL flow profiles at several positions along the course of the aorta. For this (in the absence of visceral side branches), we varied the length of the ThAo/AbAo in the lumped-parameter model, thus changing the point where flows were measured. Then, for our reference case (which includes TL visceral side branches), we determined the flow and pressure profiles at the proximal, diaphragm and distal levels in the TL and the FL.

Next, starting from the reference case, the computational model was used to predict the effects of the variation of potential key parameters (related to clinical outcome of chronic aortic dissections) on intraluminal flows. The parameters considered include: wall elasticity; abdominal arteries originating in the FL; cumulative tear size and tear location. The effects of the parameters were assessed at the proximal, diaphragm and distal levels of the dissected segment through the analysis of: a) flow patterns; b) the

proportion of the total flow that goes into the FL, irrespective of its direction (%TVF = $|TVF_{FL}|$ / ($|TVF_{TL}|$ + $|TVF_{FL}|$), with $|TVF_{TL}|$ and $|TVF_{FL}|$ the cumulative sum of the absolute value of the instantaneous volume flow in the FL and the TL, respectively); c) the percentage of systolic ($\%RSF_{FL}$); and d) diastolic retrograde flow ($\%RDF_{FL}$) in the FL.

6.3 Results

6.3.1 Spatial Variability of Flow Patterns

Figure 6.3 (A-B) show the variability of the flow patterns along both lumina for the reference case (in the absence of any visceral side branches originating from them). As can be observed, TL flows (Fig. 6.3A) are very similar and antegrade along the whole segment whereas FL flows (Fig. 6.3B,D) show important changes, with even inversion of the flow profile, along the dissected segment. At the ThAo, flows are predominantly antegrade in systole and retrograde in diastole, while they invert when approaching the distal tear, where they are mainly retrograde in systole and antegrade in diastole.

Figure 6.4 (A-D) show the flow and pressure profiles for the reference case (including TL visceral side branches). Here, the inversion of FL flow profiles at the proximal and distal level can de depicted and, at the diaphragm, an intermediate profile is present. The TL flow has an unchanged profile, with just lower values when distal from the visceral side branches. The pressure profiles do not vary importantly over the length of the aorta, with only a delay and slight increase in peak pressure in the TL while propagating over the length.

6.3.2 Changes in Wall Stiffness

As shown in Figure 6.5 (Left), an increase in wall stiffness (or a decrease in compliance) up to 50 % (Learoyd and Taylor 1996) of the whole dissected segment did not have significant impact on flows at the different levels. Nevertheless, increased wall stiffness led to a significant increase in pulse pressure in both TL and FL, and as a result, to an augmentation of systolic pressure and decrease in diastolic pressure (Fig. 6.5, Right).

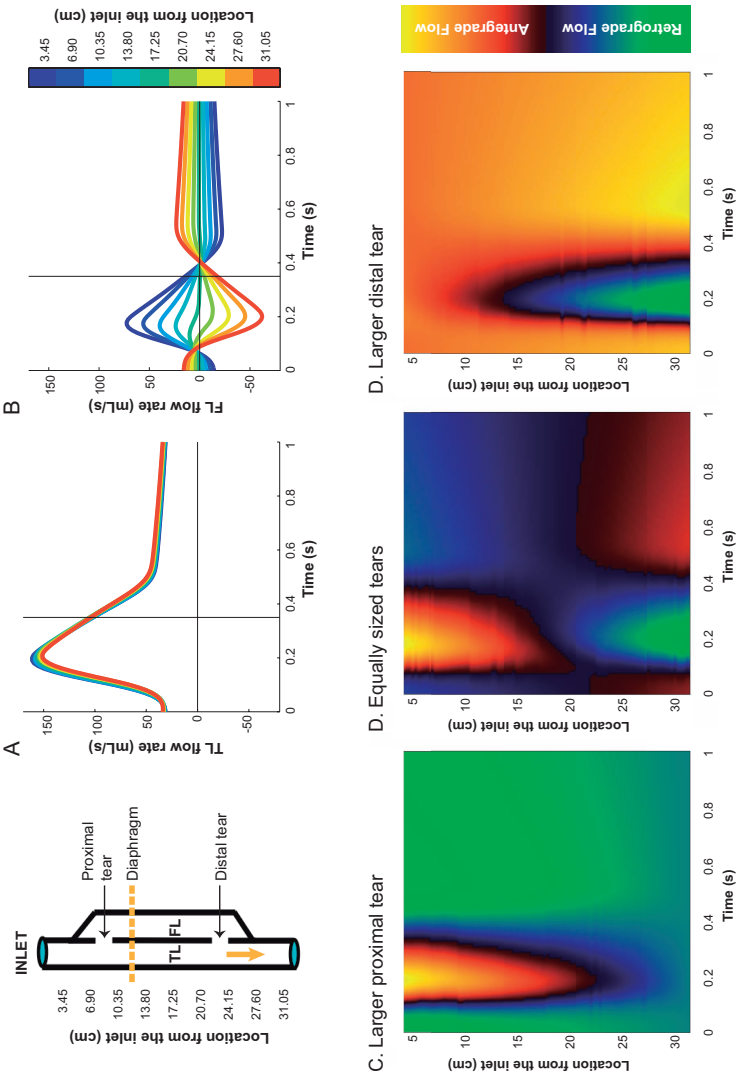

Figure 6.3: Spatial variability of flow patterns in the true lumen (TL; A) and the false lumen (FL; B,D) for the reference case and in the absence of any side branches originating from them. The spatial variability of FL flow patterns for the scenarios with a larger proximal (C) and a larger distal (D) tear is also illustrated. Antegrade flows are positive and retrograde flows are negative.

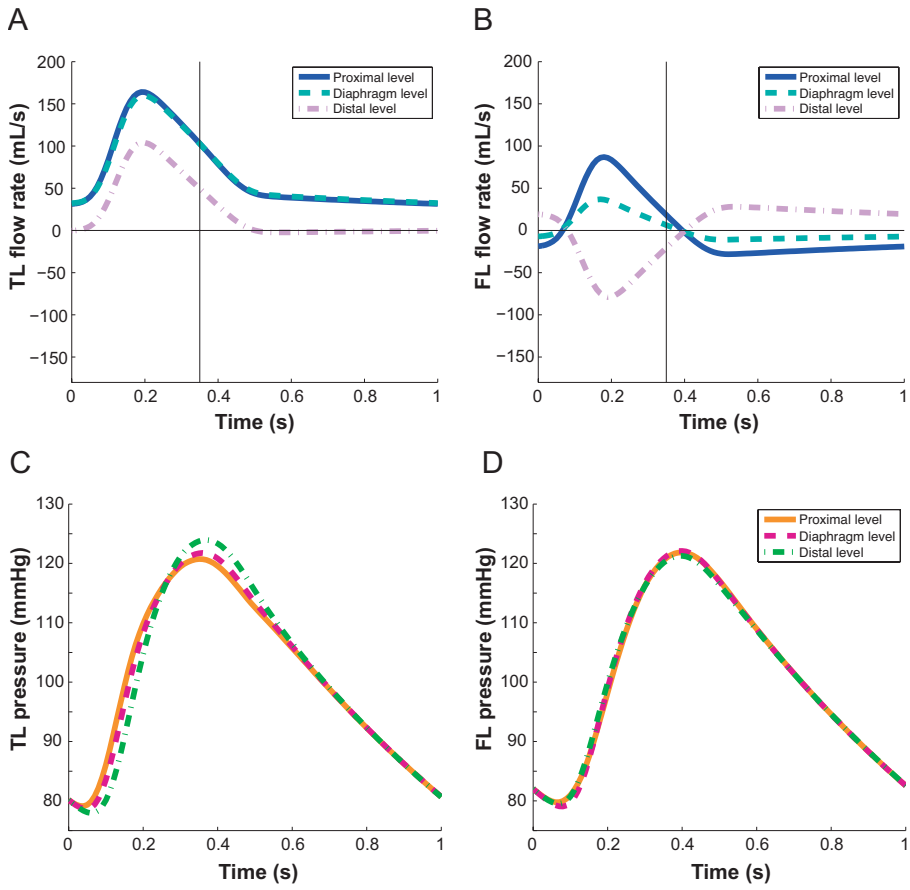

Figure 6.4: Flow (A-B) and pressure profiles (C-D) in the true lumen (TL) and the false lumen (FL; including TL side branches), assessed at the proximal, diaphragm and distal levels, for the reference case of a chronic aortic dissection. Antegrade flows are positive and retrograde flows are negative.

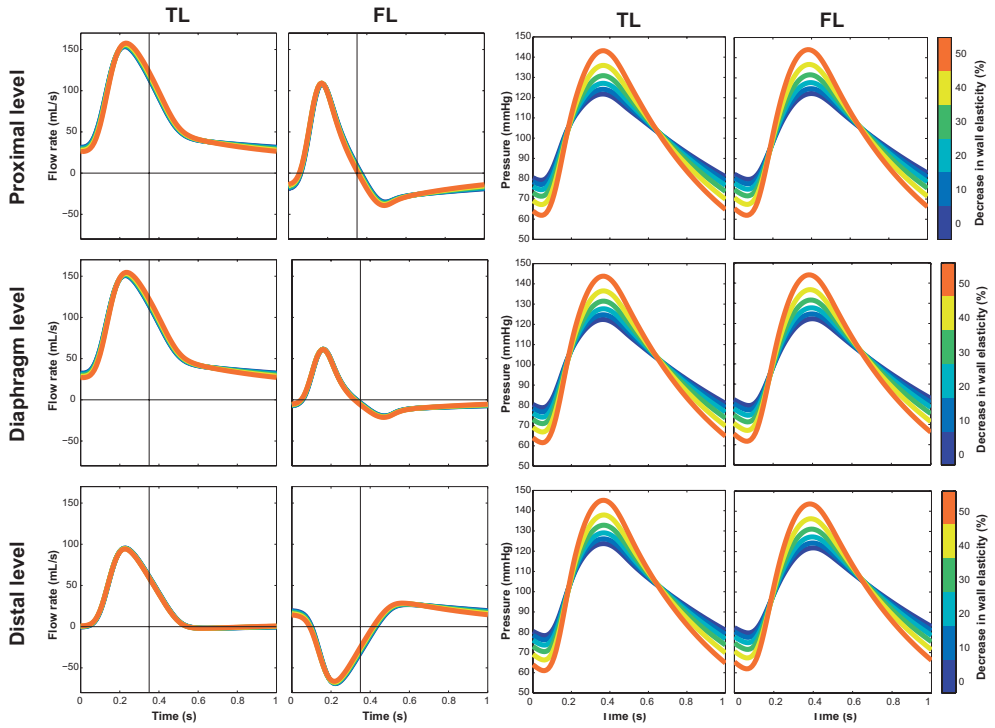

Figure 6.5: Changes in flow patterns (Left) and pressure profiles (Right) with changes in wall stiffness of the whole dissected segment. Antegrade flows are positive and retrograde flows are negative. TL, True lumen; FL, False lumen.

6.3.3 Changes in the Incidence of Visceral Side Branches Originating from the FL

Visceral arteries, with 65% of flow going into them, were distributed between the TL and the FL, in order to evaluate a different amount of visceral side branches connected to the FL. The main effect of an increase in visceral side branches from the FL was an apparently uniform vertical shift in the TL and FL flow patterns at all levels (Fig. 6.6, Left). This affected the diastolic FL flow, especially at the diaphragm and distal levels. An increase in FL visceral side branches flattened the diastolic flow, thus decreasing the flow reversal after systole.

The presence of visceral side branches at the FL seemed not to significantly affect intraluminal pressures (Fig. 6.6, Right).

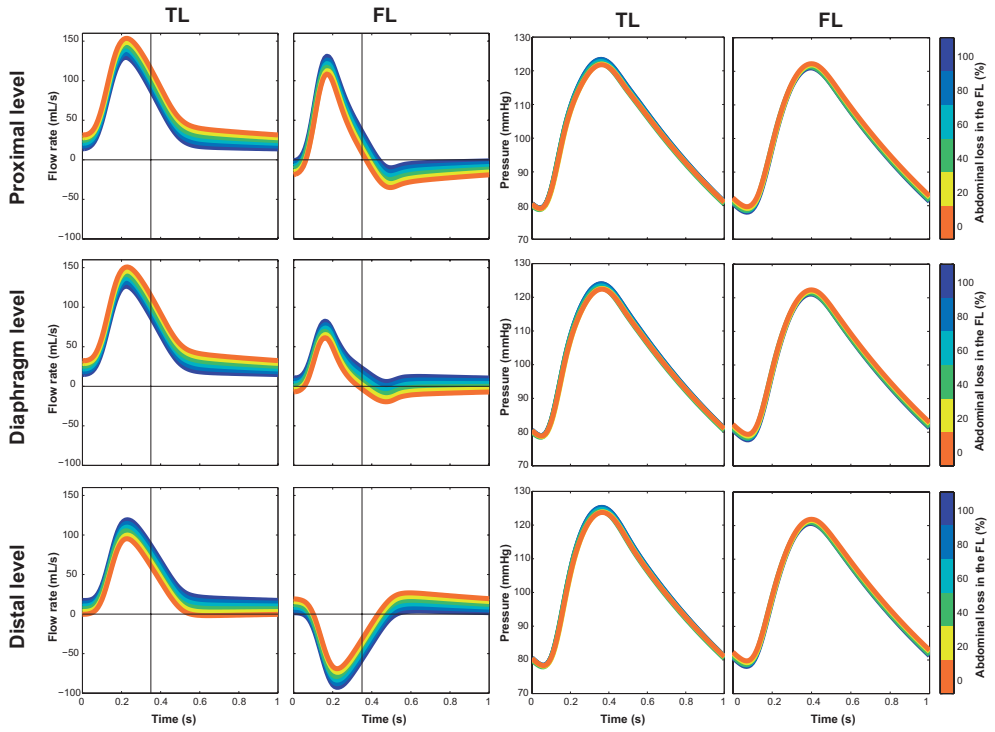

Figure 6.6: Changes in flow patterns (Left) and pressure profiles (Right) with changes in the percentage of side branches connected to the false lumen (FL). Antegrade flows are positive and retrograde flows are negative. *TL*, True lumen.

6.3.4 Changes in Cumulative Tear Size

For this part of the study, proximal and distal tear sizes (equally sized) were simultaneously changed (in the reference case, without changing luminal geometry and properties) to obtain different cumulative tear areas (from 25 to 300 mm^2 - equivalent to a tear of 5.64 mm and 19.55 mm diameter, respectively). However, in reality, both the aorta, as well as the peripheral vessels, change diameter and thus resistance and compliance (mainly through vaso dilatation/constriction) to maintain pressures within physiological limits. When changing tear sizes over a wide range, without this adaptive response, TL pressures rose above normal range when decreasing the interluminal communication (Fig. 6.7).

Therefore, in an attempt to be much closer to clinical reality, we evaluated the effect of tear size by on the one hand, starting from a chronically large tear that was acutely partially occluded (for example, after endovascular treatment) and on the other hand, from a chronically stable small tear that acutely would tear and increase its size. In

these scenarios, we simulated the homeostatic response by TL vasodilatation or constriction (by changing diameter by 20%).

For the change from large to small tear size, we used the reference case, decreased the tear size from 300 to 25 mm^2 and dilated the TL diameter by 20% (Fig. 6.8). For the increase from 25 to 300 mm^2, the model was firstly recalibrated (E = 0.125 MPa; $R_{PT} = R_{DT} = 1.9927$ mm Hg ml s) to approach the same inlet pressure as the reference case and next, with the increase in tear size, the TL diameter was decreased by 20 % (Figure 6.9).

In both scenarios, the flow patterns changed similarly (Fig. 6.8 and 6.9, Left). Smaller tear size was associated to a more damped and shifted FL flow with a significant delay in the time-to-peak flow compared to the TL. Regarding diastolic FL flow, larger tear sizes had more retrograde flow in the proximal site and more antegrade flow at the distal site.

As expected, the TL pulse pressure importantly increased when acutely going to a smaller communication (acute hypertension with therapy) and decreased when tear size increased suddenly (acute hypotension with further dissection) (Fig. 6.8 and 6.9, Right)

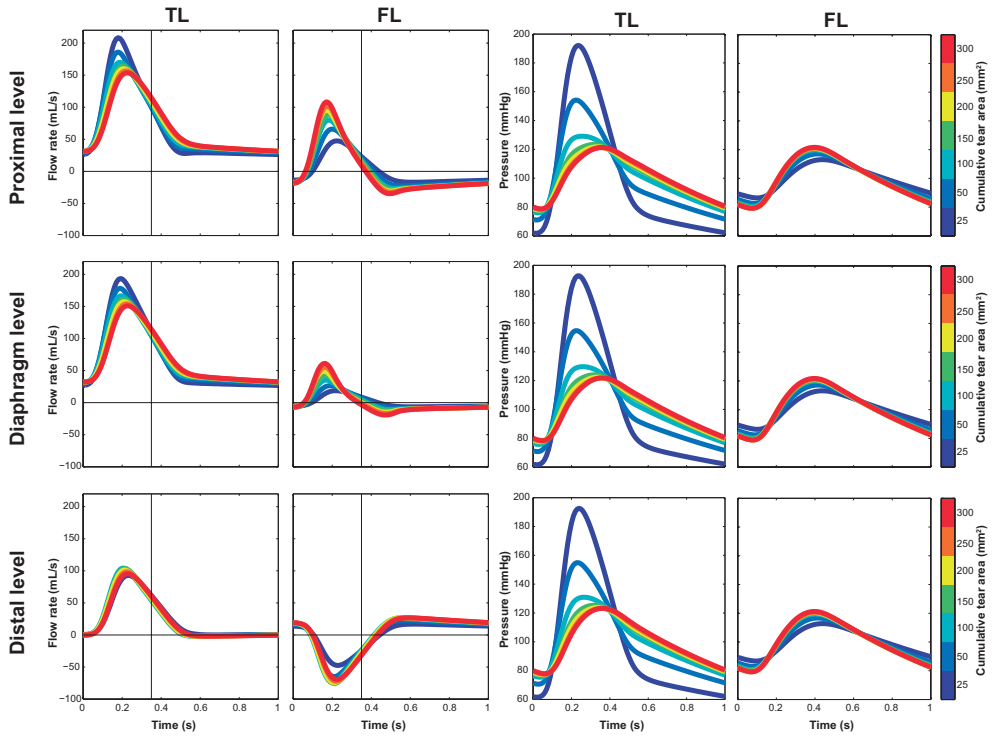

Figure 6.7: Changes in flow patterns (Left) and pressure profiles (Right) with variations in the cumulative tear area, without changing luminal geometry and properties. Antegrade flows are positive and retrograde flows are negative. *TL*, True lumen; *FL*, False lumen.

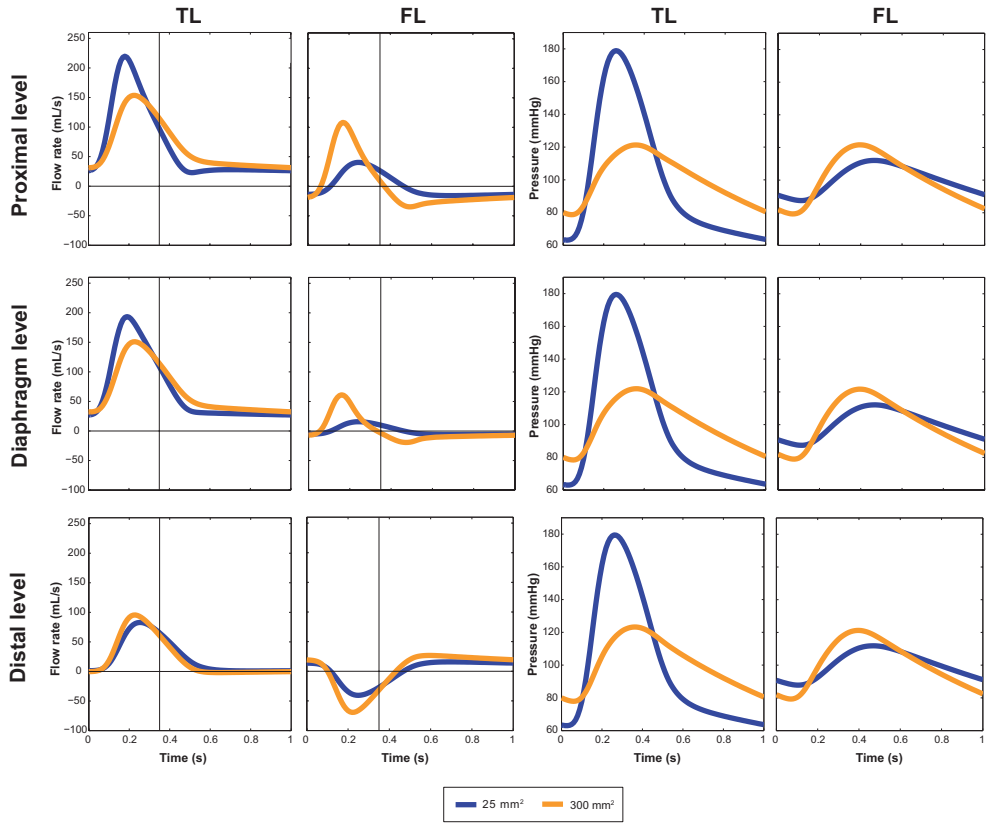

Figure 6.8: Variations in flow patterns (Left) and pressure profiles (Right) for a decrease in the cumulative tear area (from 300 mm^2 to 25 mm^2) and resultant true lumen (TL) vasodilatation. Antegrade flows are positive and retrograde flows are negative. *FL*, False lumen.

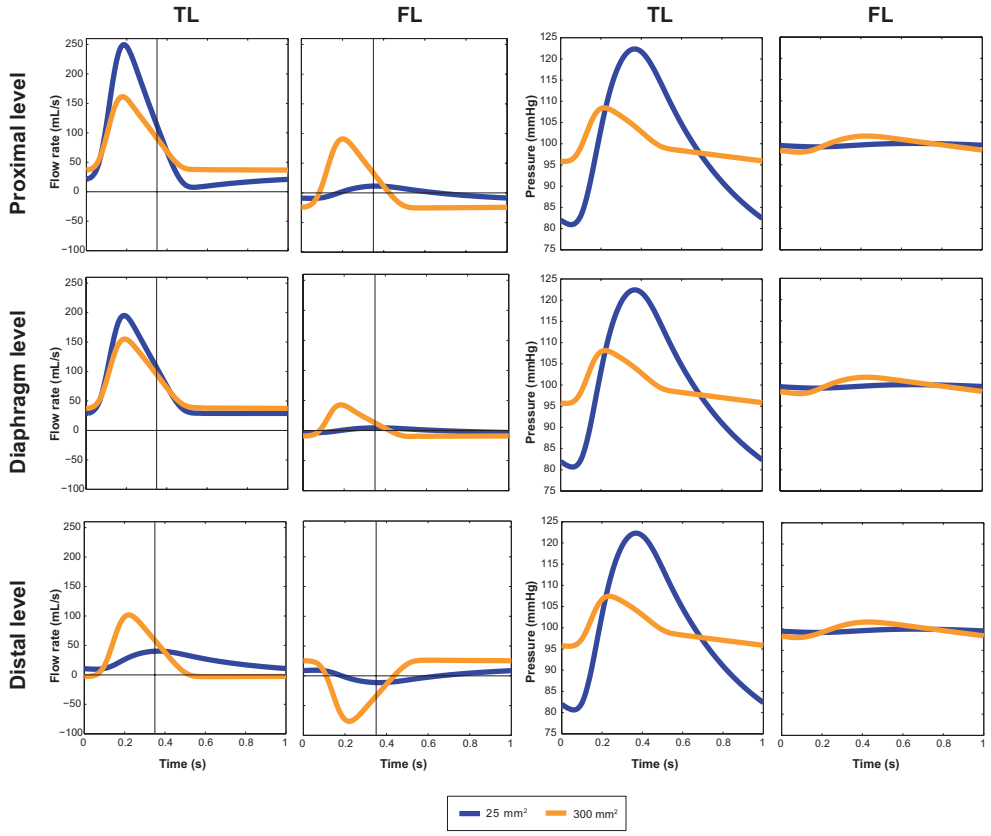

Figure 6.9: Variations in flow patterns (Left) and pressure profiles (Right) for an increase in the cumulative tear area (from 25 mm^2 to 300 mm^2) and resultant true lumen (TL) vasoconstriction. Antegrade flows are positive and retrograde flows are negative. *FL*, False lumen.

6.3.5 Altered Spatial Distribution of Tear Size along the Dissection

A total tear area of approximately 302.57 mm^2 (reference case) was differently distributed between the proximal and distal tears of the segment.

The local tear size determined the local proportion of flow going into the FL (Fig. 6.10, Left). Thus when increasing distal tear area at the expense of the proximal, the local flow pattern scaled proportionally, decreasing flow in the proximal site and increasing it at the distal, without affecting the shape of the profile much. However, this also made that the place along the dissection where the inversion of the flow patterns from predominantly antegrade to predominantly retrograde in systole shifted from being proximal towards being distal (Fig. 3C-E). The flow inversion point was distal to the diaphragm in the presence of a larger proximal tear and proximal to the diaphragm when the larger tear was at the distal part of the dissections. Thus, when more than

50% of total tear area was located distally, the profile at the (fixed) diaphragm started to show a clear systolic biphasic pattern with an increase in systolic FL reverse flow and mostly antegrade diastolic flows. Instead, systolic FL flows turn to be more monophasic in the presence of a large proximal tear and small distal tear, with a decrease in systolic reverse flow and an increase in diastolic retrograde flows.

Intraluminal pressures along the whole dissection were not significantly affected by redistribution of tear size (Fig. 6.10, Right).

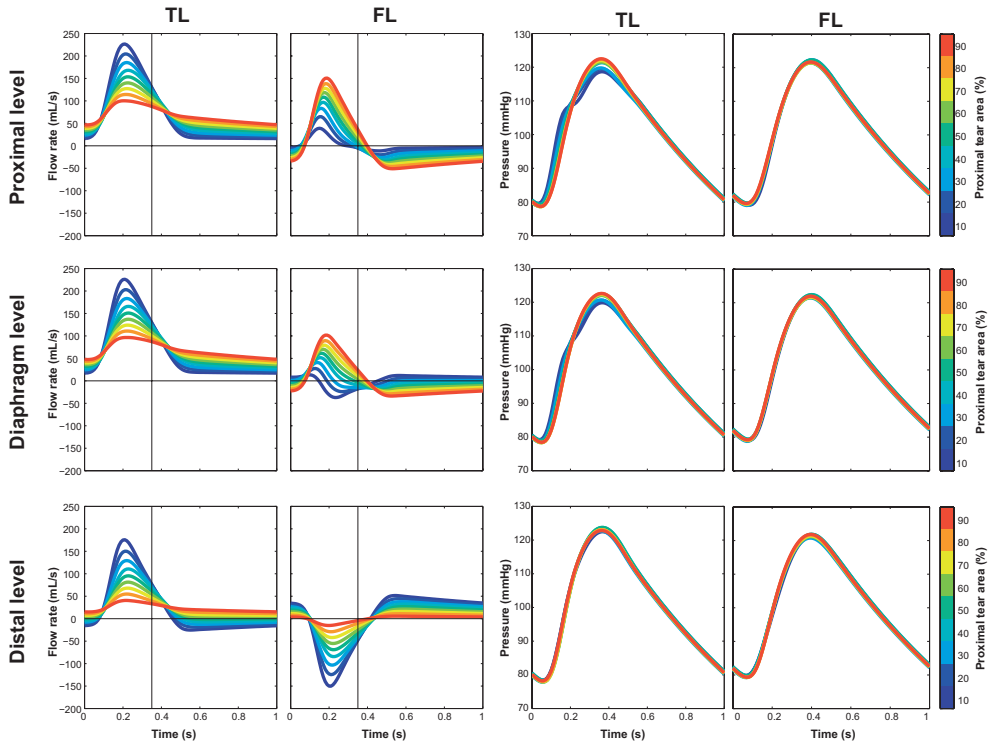

Figure 6.10: Changes in flow patterns (Left) and pressure profiles (Right) with changes in the distribution of total tear area between the proximal and distal tear. The color scale represents the percentage of total area distributed at the proximal site. Antegrade flows are positive and retrograde flows are negative. *TL*, True lumen; *FL*, False lumen.

6.3.6 Derived Parameters

Figure 6.11 shows how the quantitative parameters extracted from the flow profiles are influenced by the above described changes.

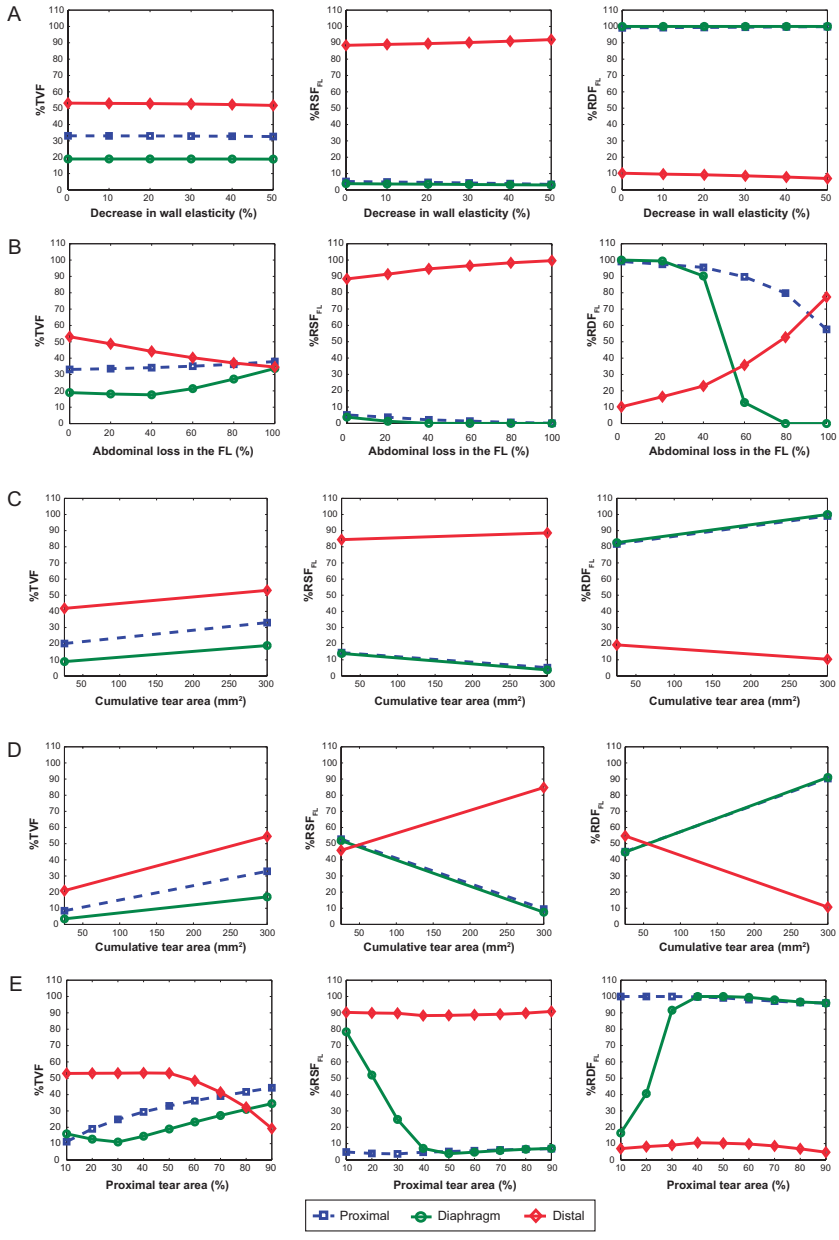

Figure 6.11: Percentage of total volume flow into the FL (%TVF), percentage of systolic (%RSF_{FL}) and diastolic (%RDF_{FL}) retrograde flow in the false lumen for changes in (A) wall stiffness of the dissected segment; (B) percentage of side branches connected to the FL; (C) decrease and (D) increase in cumulative tear area; (E) distribution of total area between the proximal and distal tear.

Changes in wall stiffness (Fig. 6.11A) do not change the percentage of total volume flow into the FL (%TVF) nor the percentage of retrograde systolic ($\%RSF_{FL}$) of diastolic flow ($\%RDF_{FL}$) in the FL.

However, all other changes had a clear influence. Visceral side branches from the FL resulted in a dramatic change in the $\%RDF_{FL}$, especially at the diaphragm (Fig. 6.11B).

Increasing the cumulative tear size increased the volume flow into the FL at all levels and gradually changed the flow reversal at all sites (Fig. 6.11C-D).

Changing the spatial distribution of the tear size had important and non-linear changes in all parameters, especially at the level of the diaphragm (Fig. 6.11E). Larger proximal tears compared to distal ones resulted in overall more flow into the FL and a reversal of the flow profiles at the diaphragm.

6.3.7 Comparison with In-vivo Data

Figure 6.1 shows the 4 most prevalent instantaneous flow profiles (at the level of the diaphragm) as measured with phase-contrast MRI in patient population. The 4 patients were in chronic follow-up after a type A dissection and had a graft at the ascending aorta and a patent dissection extending along the ThAo and the AbAo (see Table 6.1 for details).

While these flow profiles look complex and very different, the above described modelling results have clearly shown that each of the changes in flow directions, especially at the diaphragm level, can be explained. From the Figures 6.5-10, most of the variability in FL flow profiles can be attributed to changes in the spatial distribution of the tear sizes and the presence or absence of visceral side branches to the FL.

Table 6.2 shows the quantitative flow results as well as a description of the geometry of the dissection of our 4 representative cases. When comparing between patients with systolic monophasic and biphasic FL flow patterns, patients with a systolic monophasic flow profile at the diaphragm had large proximal communications between the lumina and small distal tears while patients with a systolic biphasic pattern showed small proximal tears and larger distal tears (as predicted from Figure 6.10 Left). In all the cases, there was no restricted communication between the lumina, which would have been evidenced from later FL time-to-peak flow compared to the TL (as predicted from Fig. 6.8-9 Left). When comparing between patients with the same systolic flow pattern, the patients with diastolic retrograde patterns did not show major visceral side branches in the FL while the patient with diastolic antegrade patterns did have major visceral side branches in the FL (as predicted from Fig. 6.6).

Therefore, a clear overall correspondence exists between the observed patient profiles at the level of the diaphragm and the simulation results, illustrating the capability of the lumped-parameter computational model to explain and interpret clinical flow profiles in aortic dissections.

Table 6.2: Quantitative flow assessment at the level of the diaphragm for the 4 patients selected.

	Patient – Flow pattern			
	1 - BA	2 - BR	3 - MA	4 - MR
$\lvert TVF_{TL} \rvert$ *(mL/cycle)*	5377	4343	3627	4620
$\lvert TVF_{FL} \rvert$ *(mL/cycle)*	3534	3460	3137	3851
%TVF	39.66	44.35	46.38	45.46
$\%RSF_{FL}$	9.31	4.47	0	1.48
$\%RDF_{FL}$	21.28	98.87	0	100
TTP_{TL} *flow (s)*	0.18	0.20	0.23	0.22
TTP_{FL} *flow (s)*	0.11	0.11	0.11	0.11
Communication between the lumina	Absence of tears of significant size at the ThAo. Presence of tears at the renal and infra-renal levels.	Multiple small tears at the aortic arch, ThAo and AbAo Not significant large proximal tears.	Main proximal tear with multiple small tears at the ThAo. Absence of significant tears at the AbAo.	Large proximal tear of 3.2 cm2 area. Absence of additional significant tears at the ThAo and AbAo.
Incidence of visceral side branches in the FL	Left-renal artery and celiac trunk.	Right-renal artery.	Left-renal artery and inferior mesenteric artery.	Right-renal artery.

TL, True lumen; *FL*, False lumen; *TVF*, Total volume flow; *%TVF*, proportion of total flow that goes into the FL; *RSF*, Retrograde systolic flow; *RDF*, Retrograde diastolic flow; *TTP*, Time-to-peak flow; *ThAo*, Thoracic aorta; *AbAo*, Abdominal aorta

6.4 Discussion

The current study demonstrates that intraluminal flow patterns in aortic dissections, especially in the FL, are predominantly determined by the abdominal arteries communicating with the FL and the spatial distribution of the size of the interluminal communications. Moreover, the local changes of the flow during the cardiac cycle are extremely dependent on the position along the dissection with an inversion of the profiles in between tears.

Progressive aortic dilatation and potential subsequent rupture are one of the main concerns for the long-term evolution of patients with chronic aortic dissections. Besides the influence of increased pressures, aneurysmal growth of the descending aorta in these patients has been linked to the amount of communication between the lumina and to FL patency (Inoue et al. 2000; Evangelista et al. 2012). Therefore, imaging-based assessment of the flow in individual patients, together with a better understanding of the determinant mechanisms, may be useful for predicting enlargement and future complications.

The main goal of the present study was to elucidate on the probable causes of the most prevalent haemodynamic patterns observed in patients with chronic aortic dissections. For this, we used a computational lumped-parameter model able to assess realistic local flow patterns in a diverse range of geometric and biophysical variations. To the extent of our knowledge, it is also the only computational lumped-parameter model of an aortic dissection that can capture a wide variety of influencing factors, including e.g. the presence of visceral side branches from the dissected lumina. This model was previously validated and compared to in-vitro measurements (see Chapter 5 for details).

In order to draw clinically relevant conclusions, we also selected 4 patients in follow up for chronic aortic dissections in our centre, that represented the most prevalent flow patterns that we observe in our practice. The MRI flow measurements in these patients could be reproduced by our model and the predicted dominant factors determining the temporal profile during the cardiac cycle were indeed present in these patients with characteristic changes in the direction of the flow in the FL that could be attributed to changes in the presence of visceral side branches in the FL and the position and size of the interluminal communication.

Table 6.3: Quantitative flow assessment at the proximal, diaphragm and distal levels of the dissected segment for the reference case of a chronic dissection.

	Proximal level		*Diaphragm level*		*Distal level*	
	TL	FL	TL	FL	TL	FL
Total flow (mL/cycle)	6742.2	3295.5	6740.6	1532.7	2435.5	2759.0
Peak flow rate (mL/s)	154.32	106.39	151.69	59.56	96.44	70.35
Time to peak flow (s)	0.22	0.17	0.23	0.16	0.23	0.22

TL, True lumen; *FL*, False lumen

Looking at our simulated reference case of a chronic dissection, flow characteristics (Table 6.3) had a number of similarities with MRI measurements reported from patients, in concordance with our clinical observations and François et al. 2012. Total flow volume in the TL was generally larger than in the FL and TL flows were mostly antegrade over the whole length of the dissection, with time-to-peak flow rate in the TL that was delayed compared to the FL. However, FL flows were retrograde either depending on the position along the length of the dissection or the time point in the cardiac cycle. Reversed FL flow occurred in late systole or diastole in ThAo, as also observed by Chang et al. 1991 and Strotzer et al. 2000. Only close to the distal part of the dissected segment systolic flow in the FL was always predominantly retrograde.

The impact of tear size and location in determining haemodynamics has already been the subject of several experimental and clinical studies (Tsai et al. 2008; Evangelista et al. 2012; Rudenick et al. 2013a). However, a more systematic and thorough

analysis of tears and their correlation with flow phenomena was still lacking. We found that a large area of communication between the lumina increased the proportion of FL flow volume and affected systolic and diastolic FL flow reversal at the proximal and distal sites of the dissection. Moreover, a decrease in total area of communication resulted in a more damped FL flow curve and delayed time-to-peak flow compared to the TL, which is due to the damping effect of the tears, inhibiting fast changes in flow. Additionally, in agreement with our previous experimental studies (Rudenick et al. 2013a), the cumulative size of tears significantly determined intraluminal pressures and the exact anatomic configuration where the tears were located (large tear in the proximal or distal site) played a secondary role. But although the spatial location of the size of the tears did not influence the intraluminal pressures, it did importantly determine the intraluminal flow profiles, mostly around the centre of the dissection (and thus at the level of the diaphragm, which is currently a standard position to acquire MRI based flows). When the proximal communication was sufficiently smaller than the distal one, flows at the diaphragm showed a characteristic systolic biphasic pattern with an increase in systolic retrograde FL flow and mainly diastolic antegrade flow. When the proximal tear turned larger than the distal one, systolic FL flow patterns turned more monophasic with a decrease in systolic retrograde FL flow together with predominantly diastolic retrograde flow. As expected, the local size of communication was directly related to local amount of flow.

Since many patients with aortic dissections have visceral side branches (including important ones such as the celiac trunk) originating from the FL and this has been reported to be significant related to aortic enlargement (Inoue et al. 2000), we have also assessed their influence on flow profiles. Our results showed that the incidence of FL visceral side branches increased the amount of FL flow volume and affected FL flow direction, so that FL flows became more unidirectional (mostly antegrade or retrograde depending on the level of the dissection), primarily affecting the percentage of retrograde FL flow in diastole. This is consistent with the findings of Inoue et al. 2000 (taking into account that their measurements were done at the central part of the FL) where patients with mostly antegrade and retrograde patterns showed a higher incidence of abdominal arteries originating from the FL than those with bidirectional flows, and patients with antegrade patterns had more flow in the FL. On the other hand, visceral side branches connected to the FL did not significantly affect intraluminal pressures, which suggests that visceral side branches might be associated to aortic expansion because of their effects on flows rather than pressures, considering the fact that the total amount of flow and complexity of flow patterns in the FL have been previously related to aortic enlargement (Inoue et al. 2000; Amano et al. 2011; Clough et al. 2012).

Changes in wall stiffness have been also reported as a potential factor in the determination of pressures and wall shear stress (WSS) (Evangelista and González-Alujas 2006; Nienaber et al. 2006b) and might play an important role in haemodynamics and FL enlargement in aortic dissections. This parameter is altered in most of the patients, since the majority of them have abnormal elastic properties of the aorta as a consequence of the natural aging process or other underlying factors, such as hypertension,

genetic disorders (e.g. Marfan syndrome) and atherosclerosis. In our model, the effects of variations in wall stiffness were not influencing local flow patterns but were very important for determining pressure, with a significant increase of the systolic pressure and pulse pressure in stiffer arteries. The intraluminal pulse pressure was increased by a 61% and 92%, with a 40% and 50% compliance decrease respectively, which was consistent with the findings of Reymond et al. 2012 and Johnson et al. 2010, who have assessed the effects of local stiffening on aortic pressures.

In conclusion, the current study gives novel insights into the potential causes of both spatial and temporal variations in FL flow patterns observed in patients with chronic aortic dissections and is the first to favourably compare computational predictions with clinical cases.

6.4.1 Clinical Implications

Progressive aortic enlargement is mostly the result of the effect of high intraluminal pressures as well as complex flow patterns and associated WSSs. Our results demonstrated the high complexity and variation in FL flow patterns compared to the TL and its relation to geometrical and biophysical properties of the dissected aortas, implying that measurements of flows could help in the assessment and prognosis of patients with chronic aortic dissection.

Most of the information seems to be in the FL flow profile, but the assessment of TL flows is also important to compute the proportion of volume going into the FL, which is an index already suggested to predict aortic enlargement (Inoue et al 2000).

Although TL and FL pressures show no large changes depending on where they are assessed, in all variations of the determining parameters of the FL flow that we have studied, there was a very important influence of the point along the dissection where the flow was assessed. This implies that measuring FL flows at only one level of the dissection (e.g. the diaphragms or the centre of the dissection) will not enable the understanding of the whole complex flow variation, especially since there is an inversion of the flow profiles along the length present in most cases. A comprehensive imaging study to assess flow should therefore measure them at several places along the dissection.

Nevertheless, in our study, FL flow patterns at the level of the diaphragm were able to depict changes in the distribution of interluminal communication along the dissected segment and the presence of visceral side branches in the FL. Based on this, a measurement of the FL patterns at the level of the diaphragm could give a first general insight in the individual patient. With regards to pressures, on the one hand, wall stiffness only influenced intraluminal pressures and its effects could not be noticed from the mere analysis of flow patterns. On the other hand, the presence of visceral side branches in the FL or the spatial distribution of total area of the tears only determined flows. Therefore, since all of these mechanisms coexist in a patient, they need to be carefully addressed when assessing haemodynamics for prognosis in aortic dissections.

6.4.2 Study Limitations

The model used is a simplification of the anatomical reality. Aortic dissections can be very complex with the presence of aortic tortuosity; irregularities of the lumina diameter along the dissected segment; a helicoidal intimal flap; complex communication between the lumina where iliac arteries can be involved at the end of the dissection; partial FL thrombosis; flap mobility, among a few others. Additionally, a lumped-parameter model does not account for wave propagation phenomena. These aspects could be important in exact flow (and pressure) determination. Nevertheless, the simplifications are justified for the current purpose of characterizing overall flow profiles depending on changes in different key parameters.

6.5 Conclusions

Intraluminal flow patterns in chronic aortic dissections, especially their time course with directional changes of the flow, depend on the position of assessment and on the size and spatial distribution of the tears and visceral side branches. Therefore, a standardized imaging protocol measuring the local flow patterns can give useful insights in individual patients and might aid with their clinical management and assessment of their prognosis.

CHAPTER 7

General Conclusions and Perspectives

7.1 The Integrated Multi-disciplinary Approach towards Understanding Aortic Dissections

Experimental approaches, to study and evaluate both cardiovascular diseases and new therapeutic ways, have been for a long time the first and only step before the in-vivo translation. With the availability of computational techniques and the steady increase in computational power, the use of computational simulations for studying cardiovascular diseases is emerging and becoming established.

One of the most interesting, fascinating and challenging aspect of this thesis has been the integration of in-vitro, in-silico and in-vivo approaches to understand aortic dilatation and the associated complex flow phenomena in the setting of chronic aortic dissections.

In current clinical practice, because of the absence of clear markers, maximum aortic diameter alone is mostly used to estimate the degree of risk of a patient. However, this approach has important limitations. The individual and isolated measurement does not provide a full description of the whole aortic morphology and is operator dependent; several parameters such as haemodynamics and wall stiffness are not taken into account and thus not integrated during the assessment; follow-up of patients is not standardised and the quantification of their evolution is not straightforward. Moreover, current medical imaging modalities have their technical limitations, such as the inevitable presence of noise; the inadequate spatial and temporal resolution to evaluate haemodynamic or morphologic characteristics in aortic dissections; and the incapability of some techniques for monitoring the whole (3D) dissected aortic segment. Therefore, the in-vivo approach alone has its drawbacks and consequently, there is little knowledge on the (isolated) determinants and relevance of the haemodynamic and prognostic variations detected among patients. Thus, the optimal way to assess and interpret them with imaging is neither established.

On the other hand, our in-vitro approach could closely recreate the real setting and allowed the assessment of intraluminal pressures and flows in several anatomic configurations often seen in clinical practice, in addition to the possibility of applying imaging and measurement techniques, such as ultrasound imaging or catheterization, that

might be translated to the clinical practice afterwards. In-vitro experiments were also an essential step in the course of this thesis to obtain the necessary data for the construction and validation of the computational models afterwards developed, because of the absence of enough in-vivo data available for these tasks. And last but not least, they provided questions and hypotheses to further assess in-silico. Nevertheless, in-vitro approaches are very complex and expensive to build and they are limited with regards to the number of different scenarios that could be studied, making that this approach alone was also not adequate and had to be complemented with others.

Finally, the in-silico approach was the most cost-effective and flexible option in comparison to in-vivo and in-vitro approaches. It allowed performing a wide parametric study of the possible variables associated to flow phenomena in chronic aortic dissections, based on the knowledge resulting from the previous in-vivo and in-vitro approaches. In particular, one of the main contributions at this point of the study has been the creation of a lumped-parameter model of an aortic dissection. With the use of this simplified model, it was possible to elucidate the parameters that might influence intraluminal pressures and flows in patients.

Summarising, the integrated multi-disciplinary approach made use of the strengths of each methodology, combining and comparing the varied and complementary information retrieved from each one. As expected, the integrated approach indeed provided superior insight than each methodology alone, which in turn might aid to improve the assessment and subsequent management of patients.

7.2 Main Take-home Messages Arisen from this Thesis Project

7.2.1 Intraluminal Pressures and Tear Size/Location

Intraluminal pressures are determined by the global cumulative size of tears and not by local tear size. Average pressure seems not to vary along the lumina of the dissection, so that local aortic dilatation should be the result of not only intraluminal pressures, but also its combination with other parameters.

7.2.2 Importance of Wall Compliance on Intraluminal Haemodynamics

Wall compliance is a key parameter in the determination of intraluminal haemodynamics in aortic dissections. In this regard, some aspects should be highlighted:

Rigid-wall simulations seem to be a good approach when studying intraluminal pressures in the existence of a large enough interluminal area of communication, but it turns not suitable if the study focuses on the assessment of either flow patterns or intraluminal pressures in the presence of diminished interluminal communication.

Therefore, in general, a computational rigid-wall simulation might not be the right computational approach to study aortic dissections, even if it was suggested as such in the majority of computational studies performed in this field. Not only does it overestimate pressures (primarily within the FL), but it also cannot approximate the complex flow patterns resulting from the presence of elastic, and thus cyclically expanding, walls.

Additionally, from the observations of, and comparisons between, clinical data and rigid-wall computational predictions, even patients with a stiffer aortic wall (e.g. Marfan patients) show flow patterns matching those resultant from an elastic-wall simulation, which means that even at those cases, a fully rigid-wall simulation is not a good approximation of reality.

Eventually, wall compliance is a key determinant of intraluminal pressures, so that an increase in wall stiffness is directly related to an important augmentation in systolic pressure and pulse pressure amplification in the TL and FL. Whereas its effects cannot be noticed from the mere evaluation of flow patterns and it cannot be locally measured in a non-invasive way in patients. Therefore, wall stiffness should be kept in the mind during the clinical follow-up.

7.2.3 Temporal and Spatial Flow Pattern Variations

Flow patterns have a high variability, both temporal as well as spatial along the lumina, which means that the assessment of flows could help in the assessment and prognosis of patients. This also contradicts the typical clinical assumption that measuring flow patterns at the middle section of the dissected segment will reflect the mean flow within it. The study has also elucidated that the size and spatial distribution of the tears and the presence of side branches originating from the FL are the most probable determinants of the flow pattern variations observed in patients. In particular, the presence of visceral side branches originating from the FL did significantly affect FL flows making them more unidirectional whereas it did not significantly affect intraluminal pressures. This suggests that diminished discharge of the FL through abdominal side branches might play a relevant role in aortic dilatation because of their impact on intraluminal flows rather than pressures, taking into account that complex flows have been previously associated to aortic dilatation in aortic dissections.

7.2.4 Coexistence of Different Mechanisms in the Determination of Intraluminal Haemodynamics

In the setting of aortic dissections, flow phenomena and thus the resulting aortic dilatation, are complex and the result of several coexistent morphological and biomechanical variables. Therefore, the assessment of changes in aortic diameter alone has serious limitations for optimal clinical management and additional geometrical and biomechanical changes should also be integrated in the clinical pipeline.

7.3 Future Perspectives

Future research should mainly focus on a further validation of the results arising from this thesis by specifically investigating the proposed mechanisms in our large population of patients with chronic aortic dissections. Therefore, the next step is to carefully correlate the clinically observed FL flow patterns with other key clinical parameters suggested by our predictions, such as the presence of communicating side branches from the FL and the cumulative size and spatial distribution of the communicating tears. This information should be fully integrated during the follow-up and correlated with the long-term evolution of the patients, in order to assess its prognostic value.

Now, given the evidence that an elastic (even clinically abnormally rigid) wall is a key determinant of intraluminal flow patterns in aortic dissections and, in most cases, essential to be included in the modelling approach used, three-dimensional fluid structure interaction simulations would be useful to obtain more detailed information on blood flow on both, synthetic and patient-specific geometries. This way, clinical parameters of importance can be quantified, such as wall and shear stresses, that cannot be easily and precisely computed from current medical imaging techniques. This could give a more detailed vision on the possible causes of the very local or tortuous aortic dilatation observed in patients.

For the objectives of our study, of giving an overall characterisation of flow phenomena in aortic dissections, all the simulations have been performed under the assumption that a unique proximal and distal tear size well approximate the cumulative proximal and distal tear areas, respectively, without the need for discriminating into local tears and analysing in detail every local point along the dissected segment. However, given the evidence of the high complexity of flow patterns along the dissected segment and the way that they change depending on the relative tear location, a more specific and precise computational study should incorporate, as much as possible, all the present tears and ideally be based on the geometrical assessment of the individual patient.

Bibliography

Akin I, Kische S, Ince H, Nienaber CA. Indication, timing and results of endovascular treatment of type B dissection. *Eur J VascEndovasc Surg*. 2009;37:289 –296.

Amano Y, Sekine T, Suzuki Y, Tanaka K, Takagi R, Kumita S. Time-resolved three-dimensional magnetic resonance velocity mapping of chronic thoracic aortic dissection: a preliminary investigation. *Magn Reson Med Sci*. 2011;10(2):93-99.

Anagnostopoulos CE, Prabhakar MJ, Kittle CF. Aortic dissections and dissecting aneurysms. *Am J Cardiol*. 1972;30(3):263-273.

Asakura T, Kamino T. Flow patterns and spatial distribution of atherosclerotic lesions in human coronary arteries. *Circ Res*. 1990;66:1045-1066.

Barrett R, Berry M, Chan TF, Demmel J, Donato JM, Dongarra J, Eijkhout V, Pozo R, Romine C, Van der Vorst H. Templates for the Solution of Linear Systems: Building Blocks for Iterative Methods, 2nd ed, Philadelphia, PA: *SIAM*. 1994.

Bernard Y, Zimmermann H, Chocron S, Litzler JF, Kastler B, Etievent JP, Meneveau N, Schiele F, Bassand JP. False lumen patency as a predictor of late outcome in aortic dissection. *Am J Cardiol*. 2001;87(12):1378-1382.

Bordone M, Oñate E, Rudenick PA, Bijnens BH, Soudah E. Study of flow phenomena in aortic dissection, GiD Congress, Barcelona. 2010.

Borghi A, Wood NB, Mohiaddin RH, Xu XY. Fluid-solid interaction simulation of flow and stress pattern in thoracoabdominal aneurysms: a patient-specific study. *J Fluids Struct*. 2008;24:270-280.

Chang CP, Liu JC, Liou YM, Chang SS, Chen JY.The role of false lumen size in prediction of in-hospital complications after acute type B aortic dissection. *J Am Coll Cardiol*. 2008;52(14):1170-1176.

Chang JM, Friese K, Caputo GR, Kondo C, Higgins CB. MR measurement of blood flow in the true and false channel in chronic aortic dissection. *J Comput Assist Tomogr*. 1991;15(3):418-423.

Cheng C, Tempel D, van Haperen R, van der Baan A, Grosveld F, Daemen MJ, et al. Atherosclerotic lesion size and vulnerability are determined by patterns of fluid shear stress. *Circulation*. 2006;113:2744–2753.

Cheng Z, Tan FP, Riga CV, Bicknell CD, Hamady MS, Gibbs RG, Wood NB, Xu XY. Analysis of flow patterns in a patient-specific aortic dissection model. *J Biomech Eng*. 2010;132(5):051007-1 - 051007-9.

Cheng Z, Riga C, Chan J, Hamady M, Wood NB, Cheshire NJ, Xu Y, Gibbs RG. Initial findings and potential applicability of computational simulation of the aorta in acute type B dissection. *J Vasc Surg*. 2013;57(2 Suppl):35S-43S.

Chung JW, Elkins C, Sakai T, Kato N, Vestring T, Semba CP, et al. True-lumen collapse in aortic dissection: part I. Evaluation of causative factors in phantoms with pulsatile flow. *Radiology*. 2000;214(1):87-98.

Clough RE, Waltham M, Giese D, Taylor PR, Schaeffter T.A new imaging method for assessment of aortic dissection using four-dimensional phase contrast magnetic resonance imaging. *J Vasc Surg*. 2012;55(4):914-923.

Coady MA, Rizzo JA, Goldstein LJ, Elefteriades JA. Natural history, pathogenesis, and etiology of thoracic aortic aneurysms and dissections. *Cardiol Clin*. 1999;17:615–635.

Compass website: TDYN: http://www.compassis.com

Davies PF, Spaan JA, Krams R. Shear stress biology of the endothelium. *Ann Biomed Eng*. 2005;33:1714-1718.

Erbel R, Oelert H, Meyer J, Puth M, Mohr-Katoly S, Hausmann D, Daniel W, Maffei S, Caruso A, Covino FE, et al. Effect of medical and surgical therapy on aortic dissection evaluated by transesophageal echocardiography. Implications for prognosis and therapy. The European Cooperative Study Group on Echocardiography. *Circulation*. 1993;87(5):1604-1615.

Erbel R, Alfonso F, Boileau C, Dirsch O, Eber B, Haverich A, Rakowski H, Struyven J, Radegran K, Sechtem U, Taylor J, Zollikofer C, Klein WW, Mulder B, Providencia LA; Task Force on Aortic Dissection, European Society of Cardiology. Diagnosis and management of aortic dissection. *Eur Heart J*. 2001;22(18):1642-1681.

Evangelista A, González-Alujas T. Pathophysiology of aortic dissection. In: Rosseau, H., Verhoye, J-P.,Heautot, J-F. (Eds). *Thoracic aortic diseases*. 2006. Springer, Berlin/Heidelberg, pp. 33-53.

Evangelista A, Flachskampf FA, Erbel R, Antonini-Canterin F, Vlachopoulos C, Rocchi G, et al; European Association of Echocardiography; Document Reviewers: Pepi M, Breithardt OA, Plonska-Gosciniak E. Echocardiography in aortic diseases: EAE recommendations for clinical practice. *Eur J Echocardiogr*. 2010;11(8):645-658.

Evangelista A, Salas A, Ribera A, Ferreira-González I, Cuellar H, Pineda V, González-Alujas T, Bijnens B, Permanyer-Miralda G, Garcia-Dorado D. Long-term outcome of aortic dissection with patent false lumen: predictive role of entry tear size and location. *Circulation*. 2012;125(25):3133-3141.

Fattori R, Mineo G, Di Eusanio M. Acute type B aortic dissection: current management strategies. *Curr Opin Cardiol*. 2011;26(6):488-93.

Formaggia L, Veneziani A. Reduced and multiscale models for the human cardiovascular system. 2003. Politecnico di Milano.

François CJ, Markl M, Schiebler ML, Niespodzany E, Landgraf BR, Schlensak C, Frydrychowicz A. Four-dimensional, flow-sensitive magnetic resonance imaging of blood flow patterns in thoracic aortic dissections. *J Thorac Cardiovasc Surg*. 2013;145(5):1359-1366.

GiD website - The personal pre and postprocessor, http://www.gidhome.com/, CIMNE (2006).

Gimbrone MA Jr, Topper JN, Nagel T, Anderson KR, Garcia-Cardeña G. Endothelial dysfunction, hemodynamic forces, and atherogenesis. *Ann N Y Acad Sci*. 2000;902:230-40.

Glower DD, Fann JI, Speier RH, Morrison L, White WD, Smith LR, Rankin JS, Miller DC, Wolfe WG. Comparison of medical and surgical therapy for uncomplicated descending aortic dissection. *Circulation*. 1990;82(5 Suppl):IV39-46.

Gusic RJ, Myung R, Petko M, Gaynor JW, Gooch KJ. Shear stress and pressure modulate saphenous vein remodeling ex vivo. *J Biomech*. 2005; 38(9):1760-1769.

Hagan PG, Nienaber CA, Isselbacher EM, Bruckman D, Karavite DJ, Russman PL, Evangelista A, Fattori R, Suzuki T, Oh JK, Moore AG, Malouf JF, Pape LA, Gaca C, Sechtem U, Lenferink S, Deutsch HJ, Diedrichs H, Marcos y Robles J, Llovet A,

Gilon D, Das SK, Armstrong WF, Deeb GM, Eagle KA. The International Registry of Acute Aortic Dissection (IRAD): new insights into an old disease. *JAMA*. 2000;283(7):897-903.

Hoshina K, Sho E, Sho M, Nakahashi TK, Dalman RL. Wall shear stress and strain modulate experimental aneurysm cellularity. *J Vasc Surg*. 2003;37(5):1067–1074.

Wikipedia website - http://en.wikipedia.org/wiki/Aorta

Iguchi A, Tabayashi K. Outcome of medically treated Stanford type B aortic dissection. *Jpn Circ J*. 1998;62(2):102-5.

Inoue T, Watanabe S, Sakurada H, Ono K, Urano M, Hijikata Y, Saito I, Masuda Y. Evaluation of flow volume and flow patterns in the patent false lumen of chronic aortic dissections using velocity-encoded cine magnetic resonance imaging. *Jpn Circ J*. 2000;64(10):760-764.

Iwai F, Sostman HD, Evans AJ, Nadel SN, Hedlund LW, Beam CA, et al. Cine phase-contrast magnetic resonance imaging for analysis of flow phenomena in experimental aortic dissection. *Invest Radiol*. 1991;26(12):1071-1078.

Johnson DA, Rose WC, Edwards JW, Naik UP, Beris AN. Application of 1D blood flow models of the human arterial network to differential pressure predictions. *J Biomech*. 2011;44(5):869-876.

Juvonen T, Ergin MA, Galla JD, Lansman SL, McCullough JN, Nguyen K, Bodian CA, Ehrlich MP, Spielvogel D, Klein JJ, Griepp RB. Risk factors for rupture of chronic type B dissections. *J Thorac Cardiovasc Surg*. 1999;117(4):776-786.

Kamiya A, Togawa T. Adaptive regulation of wall shear stress to flow change in the canine carotid artery. *Am J Physiol Heart Circ Physiol*. 1980;239:H14–H21.

Karmonik C, Bismuth J, Davies MG, Shah DJ, Younes HK, Lumsden AB. A computational fluid dynamics study pre- and post-stent graft placement in an acute type B aortic dissection. *Vasc Endovascular Surg*. 2011;45(2):157-64.

Karmonik C, Partovi S, Müller-Eschner M, Bismuth J, Davies MG, Shah DJ, Loebe M, Böck-ler D, Lumsden AB, von Tengg-Kobligk H. Longitudinal computational fluid dynamics study of aneurysmal dilatation in a chronic DeBakey type III aortic dissection. *J Vasc Surg*. 2012;56(1):260-263.

Karmonik C, Partovi S, Davies MG, Bismuth J, Shah DJ, Bilecen D, Staub D, Noon GP, Loebe M, Bongartz G, Lumsden AB. Integration of the computational fluid

dynamics technique with MRI in aortic dissections. *Magn Reson Med*. 2013;69:1438-42.

Kato M, Bai H, Sato K, Kawamoto S, Kaneko M, Ueda T, Kishi D, Ohnishi K. Determining surgical indications for acute type B dissection based on enlargement of aortic diameter during the chronic phase. *Circulation*. 1995;92(9 Suppl):II107-12.

Khan IA, Nair CK. Clinical, diagnostic, and management perspectives of aortic dissection. *Chest*. 2002;122:311-328.

Learoyd BM, Taylor MG. Alterations with age in the viscoelastic properties of human arterial walls. *Circ Res*. 1966;18:278–292

LePage MA, Quint LE, Sonnad SS, Deeb GM, Williams DM. Aortic dissection: CT features that distinguish true lumen from false lumen. *AJR Am J Roentgenol*. 2001;177(1):207-211.

Leung JH, Wright AR, Cheshire N, Crane J, Thom SA, Hughes AD, Xu Y. Fluid structure interaction of patient specific abdominal aortic aneurysms: a comparison with solid stress models. *Biomed Eng Online*. 2006;5:1-15.

Levesque MJ, Liepsch D, Moravec S, Nerem RM. Correlation of endothelial cell shape and wall shear stress in a stenosed dog aorta. *Arteriosclerosis*. 1986;6(2):220-229.

Malayeri AA, Natori S, Bahrami H, Bertoni AG, Kronmal R, Lima JA, et al. Relation of aortic wall thickness and distensibility to cardiovascular risk factors (from the Multi-Ethnic Study of Atherosclerosis [MESA]). *Am J Cardiol*. 2008;102(4):491-496.

Malek AM, Alper SL, Izumo S. Hemodynamics shear stress and its role in atherosclerosis. *JAMA*. 1999;282:2035:2042.

Marui A, Mochizuki T, Mitsui N, Koyama T, Kimura F, Horibe M. Toward the best treatment for uncomplicated patients with type B acute aortic dissection: A consideration for sound surgical indication. *Circulation*. 1999;100(19 Suppl):II275-80.

Massabuau P. Transesophageal echocardiography for diagnosis and treatment of aortic diseases. In: Rosseau H, Verhoye J-P, Heautot J-F, editors. *Thoracic aortic diseases*. 2006. 1st ed. Berlin/Heidelberg: Springer. p. 33-53.

Masuda Y, Yamada Z, Morooka N, Watanabe S, Inagaki Y. Prognosis of patients with medically treated aortic dissections. *Circulation*. 1991;84(5 Suppl):III7-13.

Mehta RH, Bossone E, Evangelista A, O'Gara PT, Smith DE, Cooper JV, Oh JK, Januzzi JL, Hutchison S, Gilon D, Pape LA, Nienaber CA, Isselbacher EM, Eagle KA; International Registry of Acute Aortic Dissection Investigators. Acute type B aortic dissection in elderly patients: clinical features, outcomes, and simple risk stratification rule. *Ann Thorac Surg.* 2004;77(5):1622-1628.

Mensel B, Kühn JP, Schneider T, Quadrat A, Hegenscheid K. Mean thoracic aortic wall thickness determination by cine MRI with steady-state free precession: validation with dark blood imaging. *Acad Radiol*. 2013;20(8):1004-1008.

Mészáros I, Mórocz J, Szlávi J, Schmidt J, Tornóci L, Nagy L, et al. Epidemiology and clinicopathology of aortic dissection. *Chest*. 2000;117(5):1271-1278.

Milisic V, Quarteroni A. Analysis of lumped parameter models for blood flow simulations and their relation with 1D models. *ESAIM-Mathematical Modelling and Numerical Analysis*. 2004;38:613-632.

Miller DC, Stinson EB, Oyer PE, Rossiter SJ, Reitz BA, Griepp RB, Shumway NE. Operative treatment of aortic dissections. Experience with 125 patients over a sixteen-year period. *J Thorac Cardiovasc Surg*. 1979;78(3):365-382.

Miyahara S, Mukohara N, Fukuzumi M, Morimoto N, Murakami H, Nakagiri K, Yoshida M. Long-term follow-up of acute type B aortic dissection: ulcer-like projections in thrombosed false lumen play a role in late aortic events. *J ThoracCardiovasc Surg*. 2011;142(2):e25-31.

Mohr-Kahaly S, Erbel R, Rennollet H, Wittlich N, Drexler M, Oelert H, et al. Ambulatory follow-up of aortic dissection by transesophageal two-dimensional and color-coded Doppler echocardiography. *Circulation*. 1989;80(1):24-33.

Müller-Eschner M, Rengier F, Partovi S, Unterhinninghofen R, Böckler D, Ley S, von Tengg-Kobligk H. Tridirectional phase-contrast magnetic resonance velocity mapping depicts severe hemodynamic alterations in a patient with aortic dissection type Stanford B. *J Vasc Surg*. 2011;54(2):559-562.

Murgo JP, Westerhof N, Giolma JP, Altobelli SA. Aortic input impedance in normal man: relationship to pressure wave forms. *Circulation*. 1980;62:105–116.

Neri E, Barabesi L, Buklas D, Vricella LA, Benvenuti A, Tucci E, Sassi C, Massetti M. Limited role of aortic size in the genesis of acute type A aortic dissection. *Eur J Cardiothorac Surg*. 2005;28(6):857-863.

Neya K, Omoto R, Kyo S, Kimura S, Yokote Y, Takamoto S, Adachi H. Outcome of Stanford type B acute aortic dissection. *Circulation*. 1992;86(5 Suppl):II1-7.

Nichols WW, O'Rourke MF, Charalambos V. Properties of the arterial wall: practice. In: Nichols, W.W., O'Rourke, M.F., Charalambos, V. (Eds). *McDonald's blood flow in arteries: theoretical, experimental, and clinical principles*. 2011a. CRC Press, pp. 77-109.

Nichols WW, O'Rourke MF, Charalambos V. The nature of flow of a liquid. In: Nichols WW, O'Rourke MF, Charalambos V (Eds). *McDonald's blood flow in arteries: Theoretical, experimental, and clinical principles*. 2011b. CRC Press; pp. 13-54.

Nienaber CA. Medical Treatment or Endovascular Stent-Graft Treatment for Acute Aortic Syndrome. In: Rosseau, H., Verhoye, J-P.,Heautot, J-F. (Eds). *Thoracic aortic diseases*. 2006a. Springer, Berlin/Heidelberg, pp. 223-237.

Nienaber CA, Haverich A, Erbel R, 2006b.Diseases of the aorta and trauma to the aorta and the heart. In: Camm, J., Lüscher, T.F., Serruys, P. (Eds). *The ESC textbook of cardiovascular medicine*. Blackwell Publishing, Oxfors, pp. 993-1031.

Nollen GJ, Groenink M, Tijssen JG, Van Der Wall EE, Mulder BJ. Aortic stiffness and diameter predict progressive aortic dilatation in patients with Marfan syndrome. *Eur Heart J*. 2004;25:1146-1152.

Pape LA, Tsai TT, Isselbacher EM, Oh JK, O'gara PT, Evangelista A, et al. Aortic diameter > or = 5.5 cm is not a good predictor of type A aortic dissection: observations from the International Registry of Acute Aortic Dissection (IRAD). *Circulation*. 2007;116(10):1120-1127.

Quint LE, Platt JF, Sonnad SS, Deeb GM, Williams DM. Aortic intimal tears: detection with spiral computed tomography. *J Endovasc Ther*. 2003;10(3):505-510.

Raghavan ML, Vorp DA, Federle MP, Makaroun MS, Webster MW. Wall stress distribution on three-dimensionally reconstructed models of human abdominal aortic aneurysm. *J Vasc Surg*. 2000; 31:760-769.

Reymond P, Merenda F, Perren F, Rüfenacht D, Stergiopulos N. Validation of a one-dimensional model of the systemic arterial tree. *Am J Physiol Heart Circ Physiol*. 2009;297:H208-222.

Reymond P, Westerhof N, Stergiopulos N. Systolic hypertension mechanisms: effect of global and local proximal aorta stiffening on pulse pressure. *Ann Biomed Eng*. 2012; 40(3):742-749.

Reymond P, Crosetto P, Deparis S, Quarteroni A, Stergiopulos N. Physiological simulation of blood flow in the aorta: comparison of hemodynamic indices as predicted by 3-D FSI, 3-D rigid wall and 1-D models. *Med Eng Phys*. 2013; 35(6):784-791

Roberts WC. Aortic dissection: anatomy, consequences and causes. *Am Heart J*. 1981;101:195–214.

Roccabianca S, Figueroa CA, Tellides G, Humphrey JD. Quantification of regional differences in aortic stiffness in the aging human. *J Mech Behav Biomed Mater*. 2014;29:618-634.

Rubin S, Bayle A, Poncet A, Baehrel B. Retrograde aortic dissection after a stent graft repair of a type B dissection: how to improve the endovascular technique. *Interact Cardiovasc Thorac Surg*. 2006;5(6):746-748.

Rudenick PA, Bijnens BH, García-Dorado D, Evangelista A. An in-vitro phantom study on the influence of tear size and configuration on the haemodynamics of the lumina in chronic type B aortic dissections. *J Vasc Surg*. 2013a;57(2):464-474.

Rudenick PA, Bijnens BH, Butakoff C, García-Dorado D, Evangelista A. Understanding haemodynamics and its determinant factors in type B aortic dissections using an equivalent lumped model. In: Camara, O., Pop, M., Rhode, K., Sermesant, M., Smith, N., Young, A. (Eds). *Statistical Atlases and Computational Models of the Heart 2012. Lecture Notes in Computer Science*. 2013b;7746:375-382.

Rudenick PA, Bordone M, Bijnens BH, Soudah E, Oñate E, Garcia-Dorado D, Evangelista A. A multi-method approach towards understanding the pathophysiology of aortic dissections – The complementary role of in-silico, in-vitro and in-vivo information. In: Camara, O., Pop, M., Rhode, K., Sermesant, M., Smith, N., Young, A. (Eds). *Statistical Atlases and Computational Models of the Heart 2010. Lecture Notes in Computer Science*. 2010b;6364:114-123.

Sans S, Kesteloot H, Kromhout D on behalf of the Task Force. Task Force of the European Society of Cardiology on Eur Heart J, Vol. 22, issue 18, September 2001 Task Force Report 1675 cardiovascular mortality and morbidity statistics. Europe. *Eur Heart J*. 1997; 18: 1231–1248.

Schoder M, Czerny M, Cejna M, Rand T, Stadler A, Sodeck GH, et al. Endovascular repair of acute type B aortic dissection: long-term follow-up of true and false lumen diameter changes. *Ann Thorac Surg*. 2007;83(3):1059-1066.

Schor JS, Yerlioglu ME, Galla JD, Lansman SL, Ergin MA, Griepp RB. Selective management of acute type B aortic dissection: long-term follow-up. *Ann Thorac Surg*. 1996;61(5):1339-1341.

Shaaban AM, Duerinckx AJ. Wall shear stress and early atherosclerosis: a review. *AJR Am J Roentgenol*. 2000;174(6):1657-1665.

Shi Y, Lawford P, Hose R. Review of zero-D and 1-D models of blood flow in the cardiovascular system. *Biomed Eng Online*. 2011;10:1-33.

Shirali AS, Bischoff MS, Lin HM, Oyfe I, Lookstein R, Griepp RB, Di Luozzo G. Predicting the risk for acute type B aortic dissection in hypertensive patients using anatomic variables. *JACC Cardiovasc Imaging*. 2013;6(3):349-357.

Song JM, Kim SD, Kim JH, Kim MJ, Kang DH, Seo JB, et al. Long-term predictors of descending aorta aneurysmal change in patients with aortic dissection. *J Am Coll Cardiol*. 2007;50(8):799-804.

Soudah E, Rudenick PA, Bordone M, Bijnens BH, García-Dorado D, Evangelista A, Oñate E. Validation of numerical flow simulations against in-vitro phantom measurements in different type-B aortic dissection scenarios. *Comput Methods Biomech Biomed Engin*. 2013. In Press.

Spalart PR. Strategies for turbulence modelling and simulations. International Journal of Heat and Fluid Flow. 2000;21(3):252-263.

Strotzer M, Aebert H, Lenhart M, Nitz W, Wild T, Manke C, Völk M, Feuerbach S. Morphology and hemodynamics in dissection of the descending aorta. Assessment with MR imaging. *Acta Radiol*. 2000;41:594-600.

Sueyoshi E, Sakamoto I, Uetani M. Growth rate of affected aorta in patients with type B partially closed aortic dissection. *Ann Thorac Surg*. 2009;88(4):1251-1257.

Suzuki T, Mehta RH, Ince H, Nagai R, Sakomura Y, Weber F, et al. Clinical profiles and outcomes of acute type B aortic dissection in the current era: lessons from the International Registry of Aortic Dissection (IRAD). *Circulation*. 2003;108 Suppl 1:II312-317.

Tan FPP, Torii R, Borghi A, Moiaddin RH, Wood NB, Xu XY. Fluid-Structure Interaction Analysis of Wall Stress and Flow Patterns in a Thoracic Aortic Aneurysm. *Int. J. Appl. Mechanics*. 2009;1:179-199.

Trimarchi S, Tolenaar JL, Jonker FH, Murray B, Tsai TT, Eagle KA, Rampoldi V, Verhagen HJ, van Herwaarden JA, Moll FL, Muhs BE, Elefteriades JA.Importance

of false lumen thrombosis in type B aortic dissection prognosis. *J ThoracCardiovasc Surg*. 2013;145(3 Suppl):S208-212.

Tsai TT, Fattori R, Trimarchi S, Isselbacher E, Myrmel T, Evengelista A, Hutchinson S, Sechtem U, Cooper JV, Smith DE, Pape L, Froehlich J, Raghupathy A, Januzzi JL, Eagle KA, Nienaber CA; International Registry of Acute Aortic Dissection. Long-term survival in patients presenting with type B acute aortic dissection: insights from the International Registry of Acute Aortic Dissection. *Circulation*. 2006;114:2226–2231.

Tsai TT, Evangelista A, Nienaber CA, Myrmel T, Meinhardt G, Cooper JV, Smith DE, Suzuki T, Fattori R, Llovet A, Froehlich J, Hutchison S, Distante A, Sundt T, Beckman J, Januzzi JL Jr, Isselbacher EM, Eagle KA; International Registry of Acute Aortic Dissection.Partial thrombosis of the false lumen in patients with acute type B aortic dissection. *N Engl J Med*. 2007;357(4):349-359.

Tsai TT, Schlicht MS, Khanafer K, Bull JL, Valassis DT, Williams DM, Berguer R, Eagle KA. Tear size and location impacts false lumen pressure in an ex vivo model of chronic type B aortic dissection. *J Vasc Surg*. 2008;47(4):844-851.

Tse KM, Chiu P, Lee HP, Ho P. Investigation of hemodynamics in the development of dissecting aneurysm within patient-specific dissecting aneurismal aortas using computational fluid dynamics (CFD) simulations. *J Biomech*. 2011;44(5):827-36.

Westerhof N, Stergiopulos N, Noble MIM. *Snapshots of Hemodynamics. An aid for clinical research and graduate education*. 2010. 2nd ed. Springer, 192 p.

Williams DM, Andrews JC, Marx MV, Abrams GD. Creation of reentry tears in aortic dissection by means of percutaneous balloon fenestration: gross anatomic and histologic considerations. *J Vasc Interv Radiol*. 1993;4(1):75-83.

Williams DM, LePage MA, Lee DY. The dissected aorta: part I. Early anatomic changes in an in vitro model. *Radiology*. 1997;203:23-31.

Wolak A, Gransar H, Thomson LE, Friedman JD, Hachamovitch R, Gutstein A, et al. Aortic size assessment by noncontrast cardiac computed tomography: normal limits by age, gender, and body surface area. *JACC Cardiovasc Imaging*. 2008;1(2):200-209.

Publications

Peer reviewed papers in international journals

Rudenick PA, Segers P, Pineda V, García-Dorado D, Evangelista A, Bijnens BH. False lumen flow patterns as a resultant of morphological and biomechanical characteristics of chronic aortic dissections. Implications for MRI evaluation. 2014. Submitted.

Rudenick PA, Bijnens BH, Segers P, García-Dorado D, Evangelista A. Assessment of wall elasticity variations on intraluminal haemodynamics in type B aortic dissections. 2014. Submitted.

Rudenick P, Bijnens B, García-Dorado D, Evangelista A. An in-vitro phantom study on the influence of tear size and configuration on the haemodynamics of the lumina in chronic type B aortic dissections. *J Vasc Surg*. 2013;57(2):46-474.

Soudah E, Rudenick PA, Bordone M, Bijnens B, García-Dorado D, Evangelista A, Oñate E. Validation of numerical flow simulations against in vitro phantom measurements in different type B aortic dissection scenarios. *Comput Methods Biomech Biomed Engin*. 2013; In press.

Peer reviewed papers in conferences proceedings

Rudenick PA, Bijnens BH, Butakoff C, García-Dorado D, Evangelista A. Understanding haemodynamics and its determinat factors in type B aortic dissections using an equivalent lumped model. Lecture Notes in Computer Science. 7746, pp. 375 - 382. Springer, 2013. ISBN 978-3-642-36960-5

Garcia-Canadilla P, Rudenick PA, Crispi F, Cruz-Lemini M, Palau-Caballero G, Gratacos E, Bijnens BH. Understanding prenatal brain sparing by flow redistribution based on a lumped model of the fetal circulation. *Lecture Notes in Computer Science*. 7945, pp. 123 - 131. Springer-Verlag (Germany), 2013. ISBN 978-3-642-38898-9

Rudenick PA, Bijnens BH, García-Dorado D, Evangelista A. In-vitro assessment of flow patterns and velocities in different anatomic configurations of descending chronic aortic dissections. *7th International Symposium on Image and Signal Processing and Analysis (ISPA 2011)*. pp. 733 - 738. Institute of Electrical and Electronics Engineers (

IEEE), 2011. ISBN 978-1-4577-0841-1.

Rudenick PA, Bordone M, Bijnens BH, Soudah E, Oñate E, García-Dorado D, Evangelista A. A multi-method approach towards understanding the pathophysiology of aortic dissections - The complementary role of in-silico, in-vitro and in-vivo information. *Lecture Notes in Computer Science*. 6364, pp. 114 - 123. Springer (Germany), 2010. ISSN 0302-9743.

Rudenick PA, Bordone M, Bijnens BH, Soudah E, Oñate E, García-Dorado D, Evangelista A. Influence of tear configuration on false and true lumen haemodynamics in type B aortic dissection. *Conference Proceedings: Annual International Conference of the IEEE Engineering in Medicine and Biology Society*. 1. pp. 2509 - 2512. IEEE, 2010. ISSN 1557-170X.

Bordone M, Oñate E, Rudenick P, Bijnens B, Soudah E. Study of flow phenomena in aortic dissection. *5th Conference On Advances And Applications Of GiD & 1st Kratos Workshop*, Barcelona (Spain).

Abstracts in conferences proceedings

Rudenick P, Bijnens B, Segers P, García-Dorado D, Evangelista A. Haemodynamic-mechanical interaction in type-B aortic dissections: experimental and computer model study. In *ARTERY 2013*, London – United Kingdom, 2013.

Teixido Tura G, Pineda V, Bijnens B, Rodriguez-Palomares J, Cuellar H, Rudenick P, Carro A, Moral S, García-Dorado D, Evangelista A. Predictive value of flow volumen and flow patterns in the patent FL of descending aorta dissection by magnetic resonance imaging. *European Heart Journal*. 2012; 33:508-508.

Rudenick P; M Bordone; B Bijnens; E Soudah; E Oñate; D García-Dorado; A Evangelista. Understanding different haemodynamic patterns in chronic aortic dissections and the relation to tear position and size - a modelling study. European Journal of Echocardiography. 1 - 2, pp. 43 - 43. Oxford Journals, 2010. ISSN 1525-2167.

Funding Sources

This thesis study has received funding from:

- Subprograma de Proyectos de Investigación en Salud (FIS), Instituto de Salud Carlos III, (ref. PI108/0608, PI11/01709), Spain.

- Programa de ayudas destinadas a universidades, centros de investigación y fundaciones hospitalarias para la contratación de personal investigador novel (FI-DGR 2011), Spain.

- Seventh Framework Programme (FP7/2007-2013) under grant agreement No. 611823.